Report No. 113-30
Part II

TWO PHASE FLOW AND HEAT TRANSFER IN POROUS BEDS UNDER VARIABLE BODY FORCES

Final Report
Part II

By James L. Evers and Harold R. Henry

Project Director:

Harold R. Henry, Ph.D.
Professor of Engineering Mechanics
University of Alabama

Submitted to

George C. Marshall Space Flight Center
National Aeronautics and Space Administration
Huntsville, Alabama

Contract No. NAS8-21143
University of Alabama No. 22-6560

November 1969
Bureau of Engineering Research
University of Alabama

Report No. 113-30
Part II

TWO PHASE FLOW AND HEAT TRANSFER IN POROUS BEDS UNDER VARIABLE BODY FORCES

Final Report
Part II
By James L. Evers and Harold R. Henry

Project Director:

Harold R. Henry, Ph.D.
Professor of Engineering Mechanics
University of Alabama

Submitted to

George C. Marshall Space Flight Center
National Aeronautics and Space Administration
Huntsville, Alabama

Contract No. NAS8-21143
University of Alabama No. 22-6560

November 1969
Bureau of Engineering Research
University of Alabama

TABLE OF CONTENTS

TABLE OF CONTENTS (Continued)

LIST OF TABLES

LIST OF FIGURES

LIST OF FIGURES (Continued)

LIST OF FIGURES (Continued)

LIST OF SYMBOLS

A	area
a	viscous constant
b	inertial constant
C_D	drag coefficient
c_v	specific heat at constant volume
d	diameter of a particle comprising the porous bed
D	width of channel
Da	Darcy number (equation II-21)
E	energy
F	force
f( )	a function of ( )
Gr	Grashof number (equation A-12)
Gv	Gravity-Viscous number (equation A-6) (equation II-22)
H	modified pressure (equation II-17)
K	absolute permeability (equations II-1 & II-2)
k	specific permeability
L	length of the channel
M	coefficient in equation II-42

m	mass
N	number of bubble breaks per unit time
P	pressure
Q	heat transferred to the system
q	volumetric flowrate
R	radius of curvature
Re	Reynolds number
r	spherical bubble radius
Sg	volumetric quality
St	Surface Tension-Viscous number (equation A-2)
T	temperature
V	velocity
v	specific volume
W	work
x	distance along flow direction
z	distance oriented opposite to gravitational force
α	viscous constant
β	inertial constant
Γ	ratio of radii
γ	ratio of specific heats
$\gamma_{\ell, g}$	liquid and gas body forces
μ	viscosity, absolute
ν	viscosity, kinematic

ρ	density
σ	surface tension

Subscripts

f	final
g	gas
i	initial
k	kinetic
ℓ	liquid
p	potential
s	surface
t	turbulent
v	viscous

PREFACE

This is Part II of a seven (7) part final report under contract No. NAS8-21143 between the George C. Marshall Space Flight Center and the University of Alabama. This report includes the results of analytical and experimental studies conducted on a laboratory pilot model of a channel for the study of two-phase flow under low or zero gravity. It includes the formulation of dimensionless parameters to indicate the relative magnitude of the effects of capillarity, gravity, pressure gradient, viscosity, and inertia. The investigation is based on the basic equations of fluid mechanics and thermodynamics. The dimensional analysis and analytical work provide a framework for the presentation of experimental results which are put into a form allowing extrapolation of the ground-based experimental data to reduced gravity situations.

The range of parameters utilized in the experiments were such as to allow the evaluation and selection of porous materials, liquid, gas and other parameters necessary for the design of a flight experiment. Details of these selections are included in Part VII of this Final Report. Gas injector configurations were also developed.

Extensive computations were made to determine dissolved gas content. The results indicated that use of nitrogen and the Cargille fluid employed herein caused a negligible amount of dissolved gas for the pressures under consideration. Therefore it was not necessary to develop instrumentation to determine the amount of gas content of the fluid.

Techniques were investigated by using a laser velocimeter for measuring point velocities of the fluid within the porous material without disturbing the flow. These efforts were unfruitful and a scheme to obtain separate bulk velocities of the liquid and gas was substituted.

I. INTRODUCTION

A description of the behavior of gas bubbles in a liquid flowing through a porous bed is essential in many physical and chemical processes involving interaction between the liquid and gaseous systems. In some operations the transfer of mass between a foreign gas or a gaseous phase of the liquid and the liquid is the essential part of the problem, while in others the kinetic behavior of foreign gas bubbles represents the principal area of interest. Often the presence of the gaseous phase is undesirable but unavoidable thus requiring alterations to conventional flow theory to account for the presence of the gas.

In principle, two immiscible Newtonian fluids flowing through a porous bed could be completely described by a suitable solution of the Navier-Stokes equation if the boundary conditions could be correctly formulated. However, this is quite an ambitious task when one considers the high degree of complexity of a mathematical description of a randomly packed granular porous bed. Perhaps these general equations could not be solved even if they could be set up. These difficulties have been dealt with in

basically two ways. First, porous media have been represented by models which contain some characteristics of porous beds while being simple enough to allow their mathematical description (11) (34) (8). Second, experimental results correlated with the use of pertinent parameters have been used to establish the quantitative characteristics of flow. The validity of these models is established by experimentation showing which models exhibit the characteristic phenomena taking place in the porous media and which do not.

A. Single Phase Flow

Both of these methods have been applied to single fluids flowing through granular beds with varying degrees of success. For example, one of the earliest known empirical descriptions of the flow of a liquid through a packed bed was made by Darcy (6). His equation was based on measurements of the flow of water through sands and sandstones and expressed the fact that the rate of flow of the liquid through unit cube of the sand was proportional to the differential pressure head. This conclusion was later altered by Dupuit (7) to include the effect of viscosity and porosity on the rate of flow and has been thoroughly substantiated by subsequent tests (13) (4) (5), so that the resulting expression known as Darcy's law forms the basis for the current

theory of flow through porous media at low Reynolds numbers (i.e. Re $<$ 1).

However, one of the shortcomings of this law rests in the fact that the constant of proportionality, called the permeability, must be determined experimentally instead of being derivable from a knowledge of the geometry of the porous bed. Kozeny (14) sought to deal with this deficiency by assuming that the granular bed was equivalent to a group of parallel, similar channels, such that the total internal surface and the total internal volume are equal to the particle surface and to the pore volume, respectively, in the bed itself. He furthermore considered that, owing to the tortuous character of the flow through a granular bed, the length of the equivalent channels should be greater than the length of the bed. These considerations led Kozeny to an expression for permeability in terms of surface area, porosity, and rock texture. However, experimental verification of this development has not been entirely satisfactory, and consequently this method has not been generally accepted by other investigators in this field.

The simplest models that have been given a more rigorous analytical treatment have depicted the porous bed as a bundle of capillary tubes (30) (31) (26). Their solutions have, for the most part, resulted in further verification of Darcy's law. In fact, it

is clear that one can confidently use this law within its range of validity to predict the flow of a single fluid through a porous medium provided one is able to determine the permeability of the bed.

For higher Reynolds numbers where inertial effects are known to be significant, Forchheimer (9) was among the first to propose that instead of the pressure gradient being proportional to the first power of the velocity, as is the case for Darcy flow, it is the sum of two terms, one of which is proportional to the first power and the other to the second power of the velocity. Blick (2) arrived at the same conclusion by considering the porous bed to be made up of bundles of capillary tubes with orifice plates spaced throughout the tubes at a distance equal to the tube diameter. The pressure drop for fluid flowing through a porous medium was obtained by applying the laws of conservation of mass and momentum. Rose (27) has asserted that the expression proposed by Forchheimer and Blick implies that the energy dissipated at any flow rate is the sum of the energy dissipated in laminar friction and in turbulence. It is his opinion that laminar and turbulent flow cannot each exist unaffected by the other in the same flow system, and consequently an expression of this kind is incorrect. Rose was not able to express his experimental data in the simple two term form, but required an additional term proportional to the three-halves power

FIGURE I-1

PERMEABILITY vs QUALITY
FOR UNCONSOLIDATED SAND
(REF. 33)

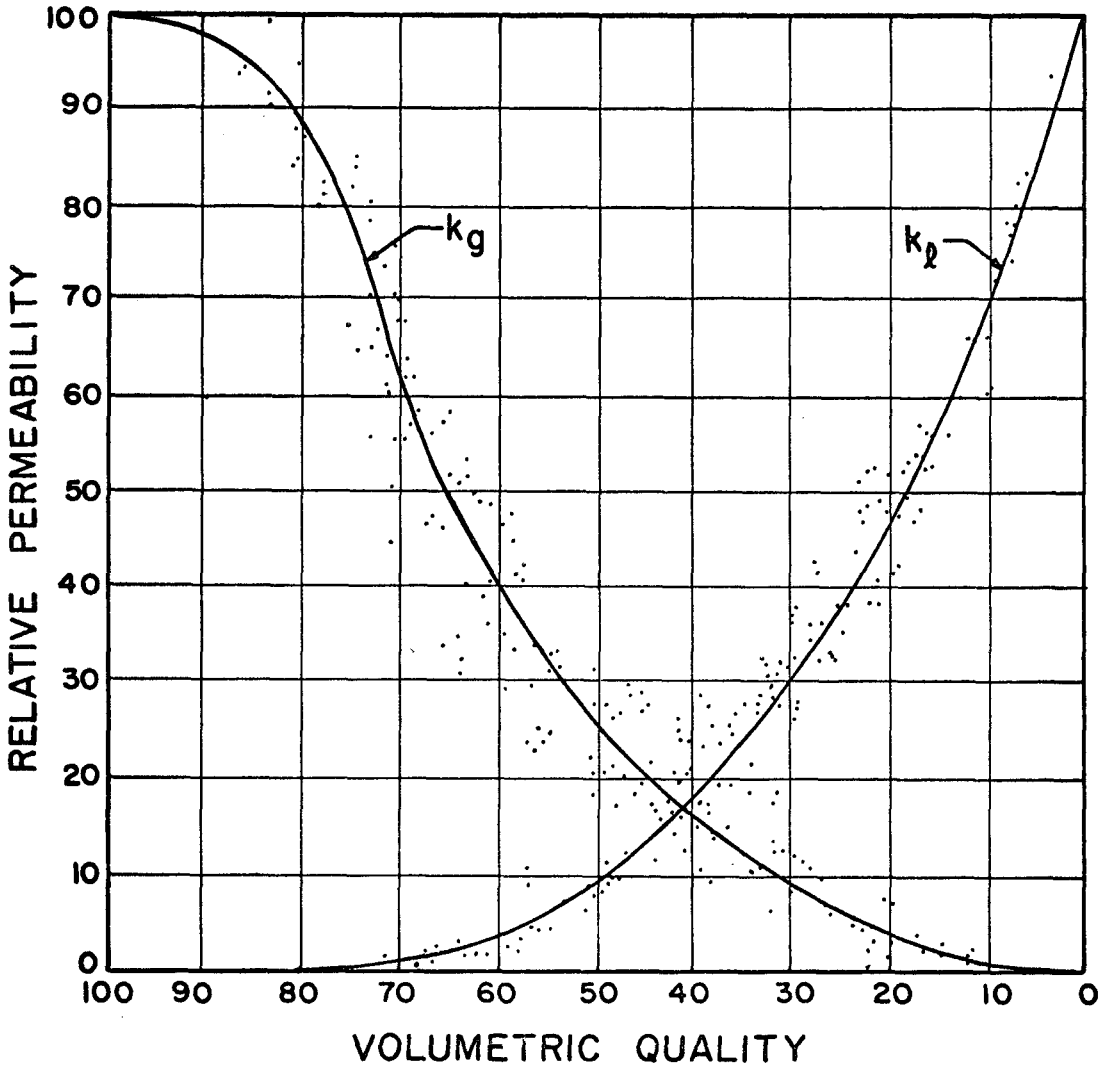

of velocity to give reasonable agreement in the transition range. This additive term is presented as merely an empirical correction to allow for the fact that the energies are not simple additive. Morcom (23), however, found that the two term expression relating the pressure drop to the fluid velocity may be used provided the value of the coefficient of the velocity squared term is varied according to the shape of the material forming the bed.

B. Two Phase Flow

Past investigations of two phase flow through porous media have resulted from the study of displacement of oil by gas or water from sandstone and unconsolidated sand (12) (20) (33). The results are expressed in terms of the relative permeability of each phase as a function of the volumetric quality (ratio of the volume of gas to pore volume). This method of presentation, of course, indicates that the results are only valid for Darcy flow since the use of permeability implies that the pressure gradient is proportional to the first power of velocity. In addition, the resulting curves (Figure I-1) are not to be considered fundamental and only apply to the range of beds tested. This places a serious limitation on one's ability to predict the pressure drop of a gas-liquid mixture flowing through a packed bed. This becomes especially significant when it is discovered that many commercial

operations for two phase flow through porous beds are conducted well outside the Darcy flow regime (3). Therefore, in order to complete the picture of two phase flow, a general correlation for intermediate and high Reynolds number is needed to supplement or replace the permeability versus volumetric quality studies.

C. Purpose of Present Investigation

The purpose of the present investigation was to study experimentally the dynamics of bubble flow through a porous channel. The principal data taken were flow rates of liquid and gas, pressure drops across the bed, volumetric quality, and high speed photographs of the bubble flow patterns. Analysis of the photographs indicated that the gas flow occurred as individual bubbles throughout the channel length. This led to a phenomenological description of the various forces involved in the flow, particularly the drag forces on the bubbles. The data were generalized by utilizing dimensionless parameters, which were fitted into the framework of the approximate analysis for the various forces and used to obtain empirical values of the drag coefficients.

One of the more important aspects of this study dealt with an investigation of the effect of gravity on the flow of a gas-liquid mixture, the goal being an expression that would predict

the pressure drop along a packed bed with a gas-liquid mixture flowing through it in any gravity field.

In spite of the fact that this analysis was not a rigorous theoretical treatment of the problem, it has been extremely useful in correlating the data taken from beds packed with different size media. For instance, a proper application of the forces on the fluid due to the relative velocity between the gas and liquid allows common curves to be used for upward and downward flow of the mixture.

II. THEORY OF TWO-PHASE POROUS MEDIA FLOW

A. Darcy Regime

For the flow of multi-phase systems, Muskat and Meres (22) have proposed that Darcy's equations should be valid for each flowing phase and have speculated that relative permeabilities of each phase, k_g and k_ℓ, might be obtained which would allow the two components of flow to be described by:

$$V_\ell = -K \frac{k_\ell}{\mu_\ell} \text{ grad } (P \pm \gamma_\ell z) \qquad \text{II-1}$$

$$V_g = -K \frac{k_g}{\mu_g} \text{ grad } (P \pm \gamma_g z) \qquad \text{II-2}$$

Scheidegger (30) reviewed these results and commented that "These deductions of Darcy's law for multiple phase flow is, so far, only a theoretical speculation. It is of course always possible to define relative permeabilities as in the above equations, but these equations make sense only if the relative permeability is independent of pressure and velocity, i.e. if

it is a function of the saturation* only. From a great number of investigations it appears that the relative permeabilities of immiscible fluids are indeed, within limits, such functions of saturation only."

Experimental data correlated from this point of view (22) and graphically presented as in Figure I-1 for different porous beds illustrate the validity of this assumption. This is especially significant when one considers that the permeabilities of the sands comprising the separate experiments ranged from 17.8 to 262 darcys (1400 percent variation). However, questions immediately arise regarding the generality of such results. Would these curves be identical if the fluid and gas flowed upward or downward instead of horizontally through the sand packed column? And for what Reynolds number ranges would these results be valid? In the case of single fluids flowing through porous beds the Darcy concept is inadequate for Reynold numbers greater than one. In addition, it can be shown experimentally that for porous beds composed of large particle sizes, the three flow configurations (horizontal, upward and downward) yield data which cannot be correlated by use of the permeability concept. The reasons for this will become clearer after the flow model pro-

---

*Scheidegger's definition of saturation is identical to the definition of volumetric quality given herein.

posed by this investigation is analyzed. At the present we can state that the relative permeability concept is expected to be applicable only when the ratio of the velocity of liquid to gas is very small or when this ratio approaches one. More specifically, the driving force on the gaseous phase is the pressure gradient plus or minus the body force which is negligible for gases. This is in agreement with the Muskat and Meres proposal. However, it is shown herein that this pressure gradient is a function of the relative velocity of the gas with respect to the liquid as well as the absolute velocity of the gas. When the relative magnitudes of these two effects were analyzed in light of the conditions tested in the present study, the data indicated that the dominant effect was due to the relative velocity when the bulk Reynolds number was greater than one. On the other hand, conditions can exist in which the liquid velocity is small compared to that of the gas, resulting in a pressure gradient which is a function of the gas velocity alone. This is also true when the velocities of the two phases become equal because the relative velocity is zero, and the gas velocity term must dominate.

B. Non-Darcy Flow Regime

In this analysis, the forces exerted on the fluid by the

granular particles comprising the porous medium and the gaseous phase are represented by drag coefficients multiplied by the dynamic pressures. If we recall that the drag coefficient for a single obstacle in a flowing stream varies with the Reynolds number as shown for instance, for a sphere in Figure II-1, then in order to use a force representation as described above it is obvious that the value of the drag coefficient must be considered to be a variable quantity at low and intermediate Reynolds numbers. In fact, at low Reynolds numbers where the viscous forces are known to be dominant, the drag coefficient of an obstacle is inversely proportional to the Reynolds number. On the other hand, when the inertial forces are dominant (i.e. $Re \gg 1$), the drag coefficient has a constant value. At Reynolds number values between the above extremes where both viscous and inertial forces are significant, it is possible that the force on an obstacle in a flowing stream can best be represented by a combination of the two types of drag forces. For instance, under streamline flow conditions where the viscous forces F_v contribute the only significant force terms, we can write the equation as follows (15)

$$F_v = \frac{C_D}{2} \rho V^2 \frac{\Pi d^2}{4} = \frac{\alpha_1}{8} \mu \Pi d V \qquad \text{II-3}$$

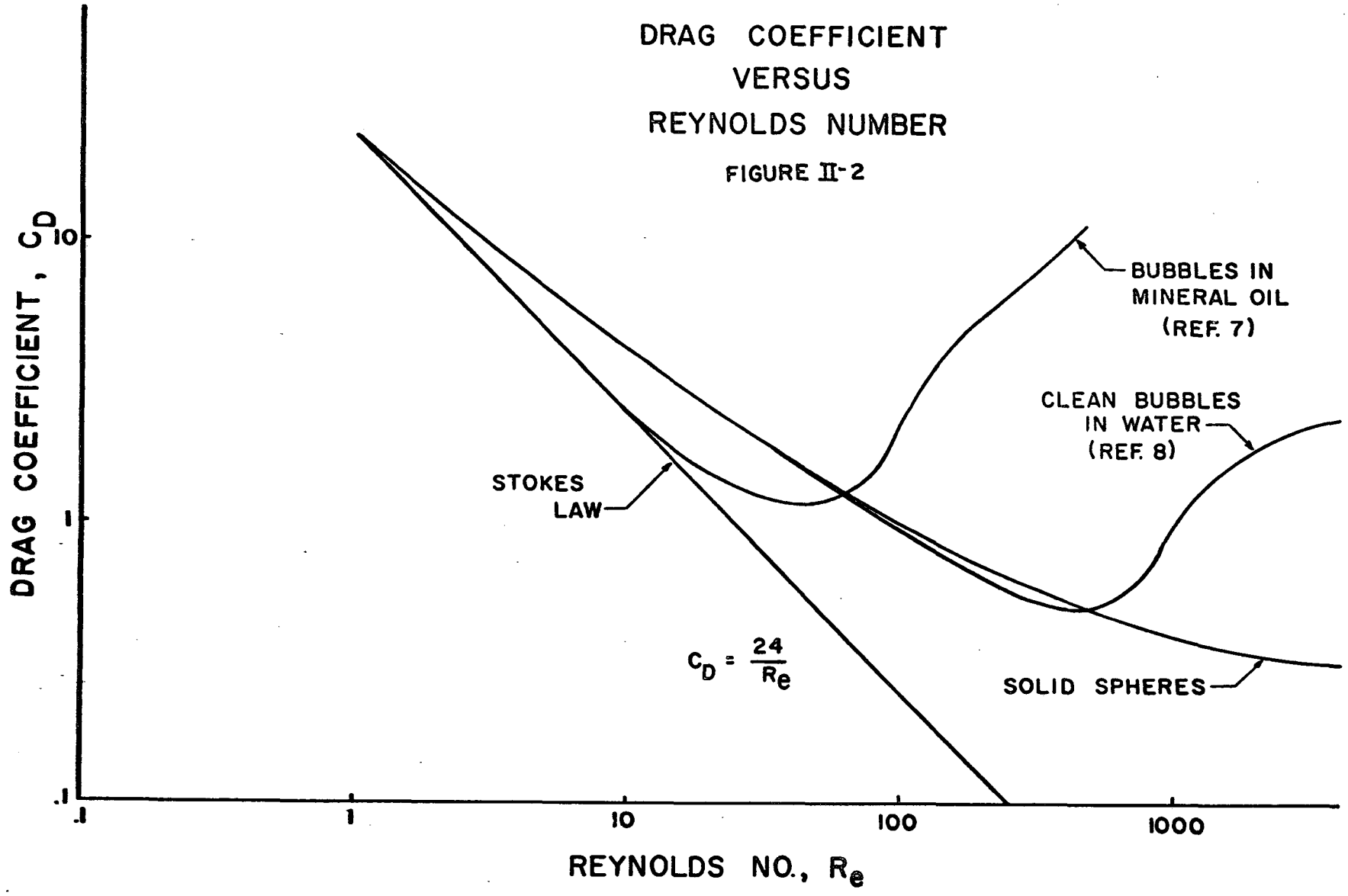
DRAG COEFFICIENT
VERSUS
REYNOLDS NUMBER
FIGURE II-2
DRAG COEFFICIENT, C_D
10
1
.1
.1
1
10
100
1000
REYNOLDS NO., R_e
BUBBLES IN MINERAL OIL (REF. 7)
CLEAN BUBBLES IN WATER (REF. 8)
STOKES LAW
$C_D = \frac{24}{Re}$
SOLID SPHERES

where

$$C_D = \frac{\alpha_1}{R_e} \qquad \text{II-4}$$

For the equations developed here the granular particles are considered to be spherical for the sake of simplicity.

Now if the driving force on a unit volume of liquid (the pressure gradient plus or minus the liquid body force) is equated to the resisting forces produced by the drag of a unit volume of particles making up the porous bed, the following equation results.

$$-\left(\frac{\partial P}{\partial x} \pm \gamma_\ell\right) = \frac{3}{4}(1-\varphi)\,\alpha_1 \frac{\mu}{d^2}\,V \qquad \text{II-5}$$

This is equivalent to the relationship known as Darcy's law for single phase flow which was developed from empirical considerations.

Similarly, for completely turbulent flow, the force F_T that a obstacle exerts on a flowing stream can be written as

$$F_T = \frac{C_D}{2}\,\rho V^2\,\frac{\Pi d^2}{4} = \frac{\beta_1}{8}\,\Pi \rho d^2 V^2 \qquad \text{II-6}$$

where

$$C_D = \beta_1 \qquad \text{II-7}$$

When both viscous and inertial forces play a significant role, it has been generally accepted (9) (2) that the total force can be represented by the sum of inertial and viscous forces in the following manner:

$$F = \frac{\alpha_1}{8} \mu \Pi d V + \frac{\beta_1}{8} \Pi \rho d^2 V^2 \qquad \text{II-8}$$

Again, if the driving force of a unit volume of liquid is equated to the drag force produced by a unit volume of particles the following expression is obtained in which the particles were again considered to be spherical.

$$-\left(\frac{\partial P}{\partial x} + \gamma_\ell\right) = \frac{3}{4}(1-\varphi) \left[\frac{\alpha_1 \mu_\ell V_\ell}{d^2} + \frac{\beta_1 \rho_\ell V_\ell^2}{d} \right] \qquad \text{II-9}$$

An equation of this form for a single fluid flowing through a porous bed at high Reynolds numbers has been proposed by other investigators based on entirely different premises. For example, in the introduction it was pointed out that Forchheimer (9) proposed an expression for the pressure gradient through a porous bed proportional to the first and second powers of the velocity in order to extend the Darcy equations to higher Reynolds numbers. A similar result was also obtained by Blick's (2) analysis of the capillary tube model with orifice plates. This

formulation is used for convenience of presentation throughout this thesis. However, the validity of the principal contribution herein does not depend upon the validity of this formulation. For instance, drag force terms which will be used in the equations to follow could be expressed as other functions of velocity without altering the basic concepts being proposed in this study. When the final correlations were made, however, this assumption was shown to be valid for the packed beds tested in this investigation.

Since the drag coefficients in this analysis will be applied to closely packed particles rather than to a single obstacle in a uniform stream, the numerical values of C_D are not expected to coincide with those for a single obstacle. For example, two spheres, one directly behind the other would not exert a force on the stream twice as large as one standing along in the stream. However, one might expect the shape of the drag coefficient curves to be similar for the two cases.

In combining all terms responsible for the energy loss (pressure drop) accompanying the flow of the liquid-gas mixture through a porous bed, the equation is written as the rate of work per unit volume that each phase produces. This is done to facilitate the inclusion of the energy loss due to the surface tension forces of the gas-liquid interface.

For one dimensional upward or downward flow, the driving

force on a unit volume of liquid is $(\frac{\partial P}{\partial x} \pm \gamma_\ell)$. When this driving force is multiplied by the bulk liquid velocity, the rate of work produced by this force is obtained. The effects combining to dissipate this energy are composed of the energy that the drag force of the solid particles extracts from the fluid, the energy required to break the gas bubbles, and the energy absorbed by the fluid due to the relative velocities of the gas bubbles and fluid stream. These effects are indicated in the following equation:

$$-(\frac{\partial P}{\partial x} \pm \gamma_\ell)V_\ell = \left\{\frac{1}{2} C_{D_1} \rho_\ell V_\ell^2 \left[\frac{(1-\varphi)6}{\Pi d^3}\right]\frac{\Pi d^2}{4} + \frac{1}{2} C_{D_2} \rho\, V_\ell^2\, \frac{6(1-\varphi)}{\Pi d^3}\frac{\Pi d^2}{4}\right\} V_\ell$$

$$-\left\{\frac{1}{2} C'_{D_3} \rho_\ell (V_g - V_\ell)^2 \left[\frac{6\varphi S_g}{\Pi d^3}\right]\frac{\Pi d^2}{4}\right\} V_\ell + \sum_{i=1}^{n} \frac{W_i}{AL} \qquad \text{II-10}$$

where the constants in this equation are again for spherical particles.

In equation (II-10) C_D is a drag coefficient, ρ is the density of the liquid phase, φ is the porosity of the porous bed, S_g is the volumetric quality, γ_ℓ is the body force of the liquid, d is the diameter of the solid particles, L is the length of the channel, W_i is the energy required to break a gas bubble, and N is the number of breaks occurring in a unit time per unit volume.

Replacing the drag coefficients C_{D_1} and C_{D_2} by the relation-

ships given in equations II-4 and II-7 to account for the presence of both viscous and inertial forces and considering for illustrative purposes both the solid particles and gasous bubbles to be spherical we obtain,

$$-\left(\frac{\partial P}{\partial x} \pm \gamma_\ell\right) = \frac{3}{4}(1-\varphi)\frac{\alpha'_1}{d^2}\mu_\ell V_\ell + \frac{3}{4}(1-\varphi)\frac{\beta_1}{d}\rho_\ell V_\ell^2 - \frac{3}{4}S_g\frac{C'_{D_3}}{d}\varphi\rho_\ell(V_g-V_\ell)^2 + \sum_{i=1}^{n}\frac{W_i}{V_\ell AL} \qquad \text{II-11}$$

Rendering this equation dimensionless yields

$$-\left(\frac{\partial P}{\partial x} \pm \gamma_\ell\right)\frac{d^2}{\mu_\ell V_\ell} = \alpha_1 + \beta_1 Re_\ell - S_g C_{D_3}\left(\frac{V_g-V_\ell}{V_\ell}\right)\frac{(V_g-V_\ell)d\rho_\ell}{\mu_\ell} + \sum_{i=1}^{n}\frac{W_i d^2}{AL\mu_\ell V_\ell^2} \qquad \text{II-12}$$

In a similar treatment of the gaseous phase, the driving force is the pressure gradient since the body force on the gas is of negligible magnitude. The rate of work on a unit volume of bubbles can be expressed as

$$-\left(\frac{\partial P}{\partial x}\right)\left(\frac{\Pi d^3}{6}\right)\left(\frac{6\varphi S_g}{\Pi d^3}\right)V_g = C'_{D_3}\frac{\rho_\ell}{2}(V_g-V_\ell)^2\left(\frac{\Pi d^2}{4}\right)\left(\frac{6\varphi S_g}{\Pi d^3}\right)V_g + C_{D_4}\rho_g V_g^2\left(\frac{\Pi d^2}{4}\right)\left(\frac{6\varphi S_g}{\Pi d^3}\right)V_g + \sum_{i=1}^{n}\frac{W_i}{AL} \qquad \text{II-13}$$

A diminsionless form of this equation can be written as

$$-\left(\frac{\partial P}{\partial x}\right)\frac{d^2}{\mu_\ell V_\ell}=C'_{D_3}\frac{\rho_\ell d}{\mu_\ell}\left(\frac{V_g-V_\ell}{V_\ell}\right)+C_{D_4}\left(\frac{d\rho_g V_g}{\mu_g}\right)\frac{\mu_g}{\mu_\ell}\frac{V_g}{V_\ell}$$

$$+\sum_{i=1}^{n}\frac{W_i d^2}{AL\mu_\ell V_g V_\ell} \qquad \text{II-14}$$

Observations of bubble flow have indicated that when a bubble is large enough to be greatly deformed as it passes through the pores, it very early breaks into smaller sizes, thus minimizing the solid to gas contact. Therefore, the second term on the right hand side of equation II-14 is negligible except at flow conditions where the liquid and gas velocities are nearly equal.

The last term in equations II-10 and II-14 represents the rate of energy transformation resulting from the breaking of nitrogen bubbles. This effect is discussed more fully in a later portion of this chapter. However, in the conclusion of this discussion, it will be shown that this contribution to energy transfer is also negligible for all the flow conditions studied in this series of tests. Therefore, for the flow regimes where

the drag forces on the gaseous phase due to the solid particles and the rate of energy transformation due to the breaking of gas bubbles can be ignored, the gas equation (equation II-14) can be written as

$$(-\frac{\partial P}{\partial x})\frac{d^2}{\mu_\ell V_\ell} = C'_{D_3}\rho_\ell d\,(\frac{V_g - V_\ell}{\mu_\ell})(\frac{V_g - V_\ell}{V_\ell}) \qquad \text{II-15}$$

When equation II-15 is substituted into equation II-12, the following equation is obtained,

$$-(\frac{\partial P}{\partial x} + \gamma_\ell)\frac{d^2}{\mu_\ell V_\ell} + KS_g(-\frac{\partial P}{\partial x})\frac{d^2}{\mu_\ell V_\ell} = \alpha_1 + \beta_1 Re_\ell \qquad \text{II-16}$$

where α_1 and β_1 are to be determined experimentally, and K is a quantity which accounts for the non-sphericity of the gas bubbles as well as the difference in size between the bubbles and the granular particles.

In an attempt to elucidate the role of the various parameters in the resulting equation, the following expressions (the gradient of which is the liquid driving force) will be termed the modified pressure H,

$$H = P + \gamma_\ell z \qquad \text{II-17}$$

where P is the pressure at a point and z is distance oriented

opposite to the gravitational force. Then the driving force on the liquid can be expressed as

$$\frac{\partial H}{\partial x} = \frac{\partial P}{\partial x} + \gamma_\ell \frac{\partial z}{\partial x} \qquad \text{II-18}$$

where the partial derivative of z with respect to x is plus unity for upward flow and minus unity for downward flow or

$$\frac{\partial H}{\partial x} = \frac{\partial P}{\partial x} \pm \gamma_\ell \qquad \text{II-19}$$

Putting this expression into equation II-16 we obtain

$$-\frac{\partial H}{\partial x}\frac{d^2}{\mu_\ell V_\ell} - KS_g\left[\frac{\partial H}{\partial x} \mp \gamma_\ell\right]\frac{d^2}{\mu_\ell V_\ell} = \alpha_1 + \beta_1 Re_\ell \qquad \text{II-20}$$

Each of the terms in this equation is a dimensionless parameter representing the ratio of various forces existing in the flow. For example, the first term in equation II-20 represents the ratio of the liquid driving force to the viscous forces. Since it was Darcy who first proposed that the ratio of the liquid driving force to the viscous force was a constant for a particular porous bed, we will call this parameter the Darcy number. In particular, the Darcy number will be defined as

$$-\frac{\partial H}{\partial x}\frac{d^2}{\mu_\ell V_\ell} = Da \qquad \text{II-21}$$

The last term on the left side of equation II-20 represents the ratio of the liquid body force to the viscous force. This parameter will be called the "Gravity-Viscous" number and will be designated by the letter Gv, more specifically

$$-\frac{\gamma_\ell d^2}{\mu_\ell V_\ell} = Gv \qquad \text{II-22}$$

so that equation II-20 can now be written in terms of the Darcy number and Gravity-Viscous parameter,

$$Da\,(1+KS_g) \pm KS_g\,Gv = \alpha_1 + \beta_1\,Re_\ell \qquad \text{II-23}$$

This equation relating the pressure gradient resulting from a gas-liquid flow through a porous bed to the liquid Reynolds number was developed on the assumption that the drag forces on the fluid are functions of the sum of two terms, one which is proportional to the liquid velocity and the other proportional to the velocity squared. The validity of this assumption can be checked by plotting the left hand side of equation II-23 versus the liquid Reynolds number. The resulting curves required to substantiate this claim will be straight lines with slopes equal to

β_1 for the region of flow where inertial effects are significant, with α_1 as the zero intercept of these curves. In addition, at lower Reynolds numbers where the viscous effects are dominant, the curves are expected to have a horizontal slope.

When the force-velocity relationship described in equation II-8 assumes some other form, the present analysis has sufficient generality to allow its inclusion. The only difference in the results would be the expectation of a curve having a different shape.

The last term included in the dimensionless pressure gradient equation II-12 is the rate of energy required to break up the gas bubbles. The large pressure gradients associated with "break-through" phenomena are not present in this study since a steady homogeneous flow condition existed in which solid-gas-liquid interfaces did not occur. Therefore, it was concluded that the only contribution of the surface tension forces to the pressure gradient resulted in the break down of larger bubbles to ever smaller sizes. Observations of a bubble being deformed from its equilibrium configuration suggest that a restoring force is present. This has led to the question of whether the deforming forces on a bubble are conservative. For example, as a bubble is forced through a constriction such as an orifice in a thin plate, the surrounding liquid must first

supply work to the bubble until it reaches the unstable equilibrium position where equal volumes of the bubble are on both sides of the plate. Then as the bubble continues to move through the orifice it does net work on the surrounding stream. This behavior leads one to suspect that perhaps all the work supplied to the bubble is recovered. In fact the basic equations of capillarity are derived by assuming that the work required to deform a bubble is equal to the increase in surface energy (16) which implies that the surface forces are conservative.

Suppose, on the other hand, that the bubble breaks during its deformation. The work done on the bubble up to this point is not recovered and the net work results in a pressure gradient. A determination of the magnitude of this contribution to the pressure gradient of the flowing stream will require that the total work necessary to accomplish all breaks per unit length be obtained. This quantity can then be included in the expression for rates of work done by the pressure gradient and drag forces.

In obtaining the work required to break a vapor bubble, it will be helpful to recall the following corollary to the first law of thermodynamics: "There exists a property of a system called energy E, such that a change in its value is equal to the

difference between the heat supplied Q to the system and the work done W by the system, during any change of state."

$$\Delta E = Q - W \qquad \text{II-24}$$

The system to be studied consists of a nitrogen bubble plus an infinitesimal portion of the surrounding liquid. It is analyzed in light of the above corollary as it experiences a division into two bubbles of equal mass. The change in energy E is comprised of the sum of the change in kinetic energy E_k during the bubble break, the change in internal energy E_i, the change in potential energy E_p and the change in the energy associated with the gas-liquid interface E_s. However, the kinetic and potential energies are not expected to change as the bubble breaks. Therefore, the change in energy can be expressed as the sum of the internal and interfacial surface energies,

$$\Delta E = \Delta E_i + \Delta E_s \qquad \text{II-25}$$

Joule demonstrated experimentally that the internal energy for a perfect gas is a function of temperature alone, which can be expressed as

$$\Delta E_i = mC_v dT = - m \int p dv \qquad \text{II-26}$$

where c_v is the specific heat of the nitrogen at constant volume, T is the temperature and m is the mass of gas contained in the bubble. If an isentropic deformation is assumed, then the change in internal energy can also be expressed as the integral of the differential change in specific volume times the pressure.

The change in energy associated with the bubble surface can be evaluated by determining the work required to change the bubble surface. However, since surface tension can be considered as the free energy of the surface per unit area (1) (17) (16), the change in the energy associated with the surface can be expressed as the surface tension times the change in the interfacial area

$$\Delta E_s = \sigma \Delta A \qquad \text{II-27}$$

The work required to break a single nitrogen bubble into two bubbles containing equal masses of gas can now be expressed as

$$W = \Delta E_i = \Delta E_s = \sigma \Delta A - m \int P dv \qquad \text{II-28}$$

where P is the pressure inside the bubble, A is the area of the bubble and v is the specific volume of the nitrogen. The relationship between the specific volume and the pressure

during an isentropic change of state is given by

$$Pv^{\gamma} = \text{constant} = P_o v_o^{\gamma} \qquad \text{II-29}$$

Expressing the pressure in terms of the specific volumes shown above and putting this into equation II-28 yields

$$W = \sigma(8\Pi r_1^2 - 4\Pi r_o^2) - \frac{mRT_o}{1-\gamma}\left[\frac{\rho_1^{\gamma-1}}{\rho_o^{\gamma-1}} - 1\right] \qquad \text{II-30}$$

Equating the mass of the gas before and after the bubble breaks yields

$$\rho_o \frac{4}{3}\Pi r_o^3 = 2\rho_1 \frac{4}{3}\Pi r_1^3 \qquad \text{II-31}$$

or

$$\frac{\rho_o}{\rho_1} = \frac{2r_1^3}{r_o^3} = 2\Gamma^3 \qquad \text{II-32}$$

where

$$\Gamma = \frac{r_1}{r_o} \qquad \text{II-33}$$

Then equation II-30 can be written in terms of the ratio of radii, Γ

$$W = 4\Pi\sigma r_o^2 [2\Gamma^2 - 1] + \frac{mRT_o}{\gamma-1}\left[\left(\frac{1}{2\Gamma^3}\right)^{\gamma-1} - 1\right] \qquad \text{II-34}$$

The radius of a vapor bubble is related to the difference in pressure across the interfacial surface. For example, by equating the pressure forces acting on an element of the bubble interface to the forces of surface tension, the following expression is obtained

$$P_o - P_\ell = \sigma \left(\frac{1}{R_1} + \frac{1}{R_2}\right) \qquad \text{II-35}$$

where P_o is the pressure inside the bubble, P_ℓ is the pressure of the surrounding fluid, σ is the surface tension and R_1 and R_2 are the radii of curvature in two arbitrarily chosen directions of the element of bubble interface.

When the bubble is considered to be spherical, the radii of curvature are equal yielding

$$P_o - P_\ell = \frac{2\sigma}{r_o} \qquad \text{II-36}$$

A similar equation can be written for the two bubbles resulting from the break

$$P_1 - P_\ell = \frac{2\sigma}{r_1} \qquad \text{II-37}$$

Solving for the ratio of internal pressures P_o/P_1 in terms of the pressure in the liquid, the surface tension, and the bubble radii, we get

$$\frac{P_o}{P_1} = \frac{\frac{2\sigma}{r_o} + P_\ell}{\frac{2\sigma}{r_1} + P_\ell} \qquad \text{II-38}$$

The equation of state for an isentropic process yields the pressure ratio P_o/P_1 in terms of the density ratio ρ_o/ρ_1.

$$\frac{P_o}{\rho_o^{\gamma}} = \frac{P_1}{\rho_1^{\gamma}} = \text{constant} \qquad \text{II-39}$$

Combining this equation and equation II-32, yields an expression for the pressure ratio $\frac{P_o}{P_1}$, in terms of the ratio of radii Γ.

$$\frac{P_o}{P_1} = (2\Gamma^3)^{\gamma} \qquad \text{II-40}$$

Substituting this equation into equation II-38 results in the following equality

$$2^{\gamma}\Gamma^{3\gamma} + 2^{\gamma}\Gamma^{3\gamma-1} M = M+1 \qquad \text{II-41}$$

where

$$M = \frac{2\sigma}{\gamma_o P_\ell} \qquad \text{II-42}$$

An estimate of the number of breaks occurring per unit

time was determined in this study by observing the bubble sizes at the inlet and outlet and requiring that continuity of mass exist in the gaseous phase. Therefore, the energy term in equation II-14 can be written as

$$\sum_{i=1}^{n} \frac{W_i d^2}{ALV^2 \mu_\ell} = \frac{3}{4\Pi} \frac{V_g}{V_\ell} \frac{\varphi}{L} \text{Sg Pavg} \left[\frac{1}{r_f^3 p_f} - \frac{1}{r_i^3 P_i} \right] \frac{d^2}{\mu_\ell V_\ell} x$$

$$\left\{ 4\Pi\sigma r_o^2 [2\Gamma^2 - 1] + \frac{mRT_o}{\gamma - 1} \left[\left(\frac{1}{2\Gamma^3} \right)^{\gamma - 1} - 1 \right] \right\} \qquad \text{II-43}$$

An order of magnitude determination of this quantity has shown it to be negligible for the range of parameters studied in these tests.

III. DESCRIPTION OF EXPERIMENTAL APPARATUS AND TESTING PROCEDURE

A. Selection of Porous Media, Liquid and Gas

It was desirable that the porous bed used for these fundamental gas-liquid flow studies be transparent. This property allowed continuous visual measurements that were essential in establishing the action of the gas bubbles as they interact with the liquid and solid while proceeding through the porous bed. In fact, these observations formed the basis for the flow model which is analyzed in a later section of this report. A transparent bed also allowed a simple volumetric quality measurement to be made with photodiodes as will be described under a separate heading. The possibility of measuring point velocities in the pores of the bed with a laser velocimeter has also been studied and is only possible if a transparent bed is obtained.

The first solid that came to mind when considering transparency was glass. However, in spherical shapes or when boken into irregular pieces it was quite apparent that a container of glass was far from being transparent. This

is due to the refractions and reflections of incident light rays as they enter and leave the glass particles. By the time an image being transmitted by light rays has traveled through even one layer of glass particles it has become quite distorted. Such an image is completely obscured when viewed through several layers of glass particles. Therefore, to avoid the complete dispersion of light rays entering the porous bed, the fluid surrounding the glass particles must have the same refractive index as the glass which renders the bed optically homogeneous.

Initially, spherical flint glass beads 3mm in diameter with an index of refraction of 1.51 were selected for the porous bed.

An extensive survey was then conducted to find a suitable liquid phase which could be used safely under laboratory conditions. This fluid was also required to be transparent, non-corrosive, viscous, nonflammable, and available in fairly large quantities and most importantly, to have the same index of refraction as the glass beads. No single component liquid was found satisfying all these conditions so mixtures of liquids were then sought. For instance, two miscible liquids, one with a refractive index higher and the other lower than flint glass could be mixed in suitable proportions to give the

desired optical quality. These combinations were also not in abundance. This search, however, did turn up two such combinations, the first being halowax and mineral oils. These gave satisfactory optical quality, but the halowax oil was found to be highly corrosive and toxic so it was discarded. The liquids finally selected were composed of a straight chain hydrocarbon (code 50) and a halogenated aromatic (code 42) manufactured by the Cargille Laboratories and sold under the name Cargille immersion liquids. The refractive index as a function of the composition of the two immersion liquids was established by mixing the two in different proportions by volume and measuring the resulting refractive index on the Bausch and Lomb, Abbe -3L refractometer shown in Figure III-1. The graphical representation of this variation in refractive index with immersion liquid composition is shown in Figure III-2. It can be seen that a refractive index of 1.51 requires 34 percent code 42 and 66 percent code 50.

The transparency of the mixture of the glass beads and Cargille fluid, although not perfect, seemed adequate for many of the original purposes. However, for measurement which would require a minimum of light scatter, an improvement in the quality of bed transparency was desired. This led to an investigation into the reasons for this imperfection

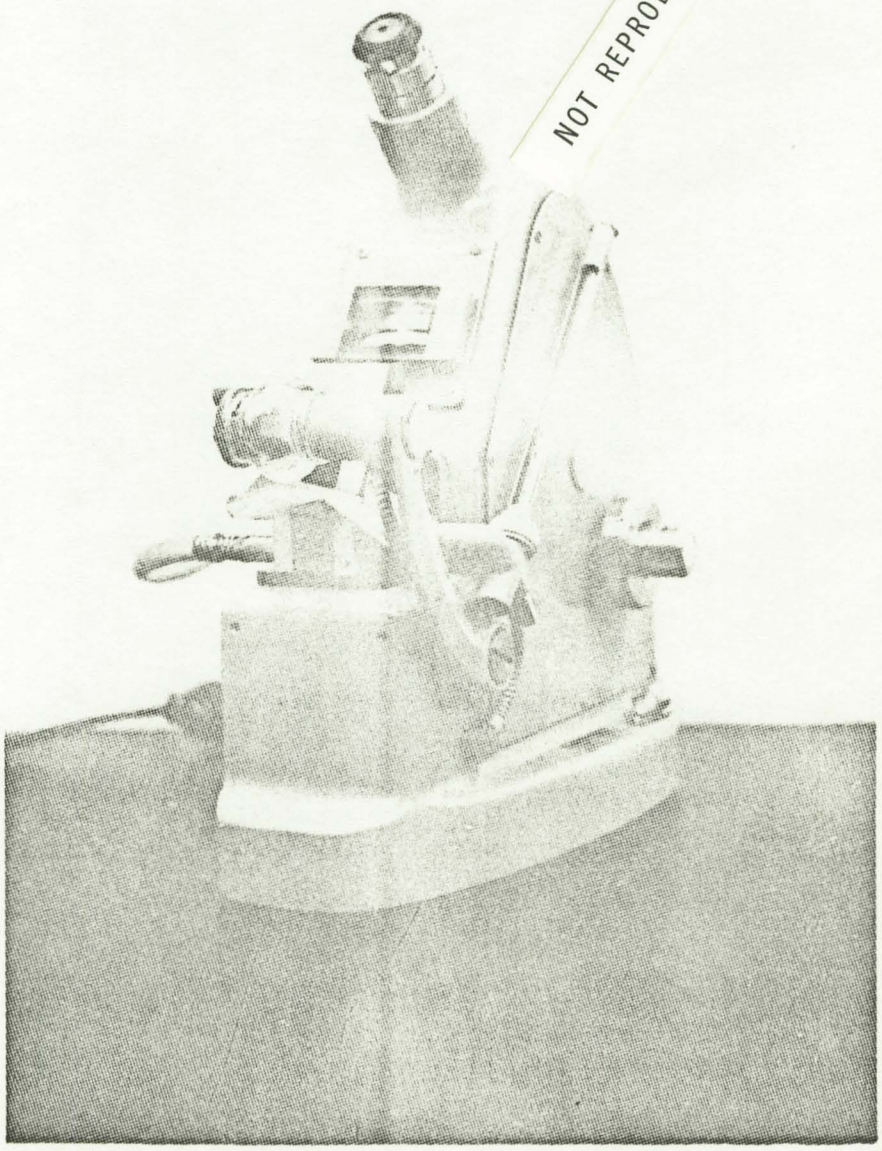

Figure III-1. Bausch and Lomb Refractometer

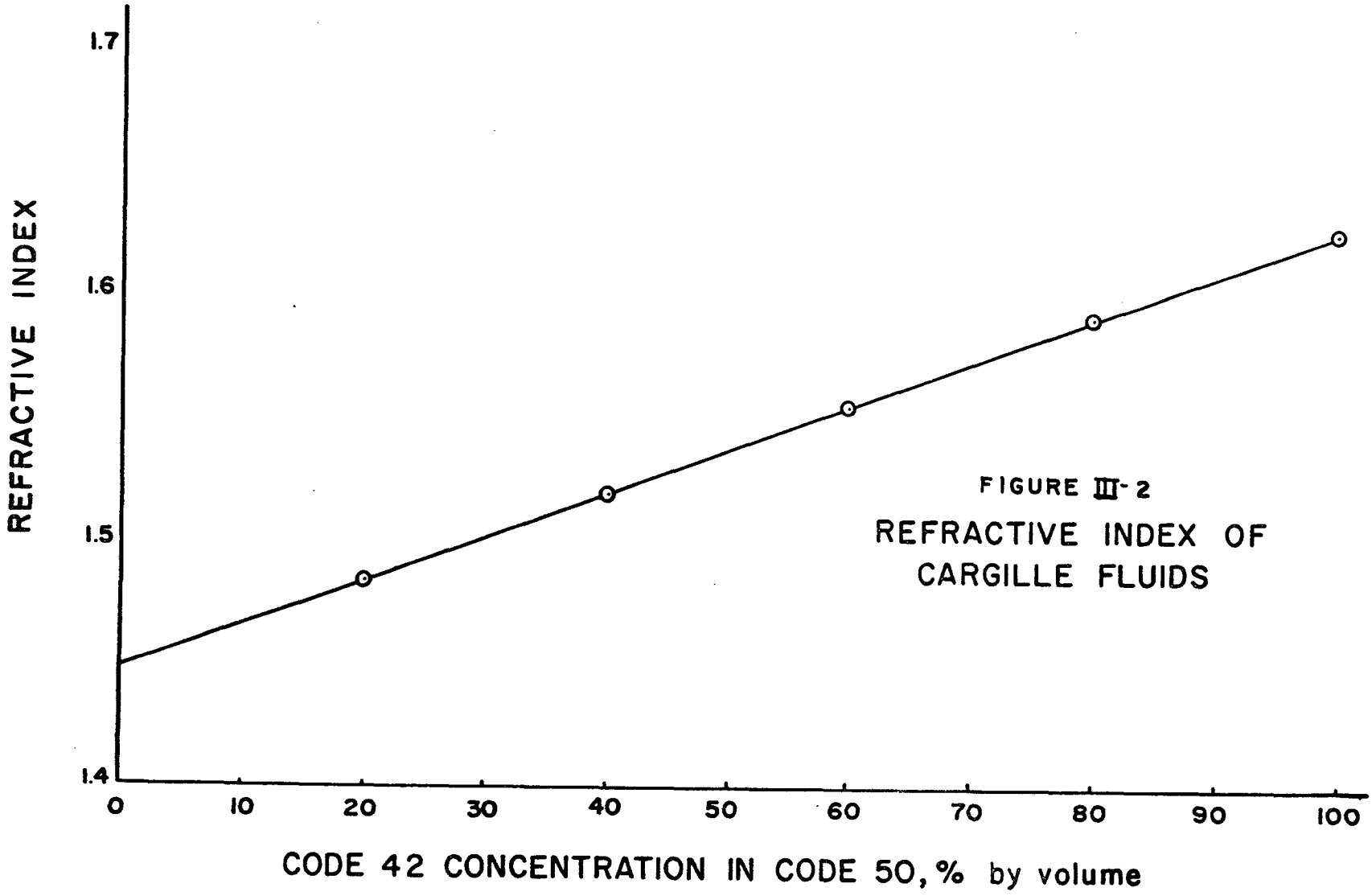

FIGURE III-2

REFRACTIVE INDEX OF CARGILLE FLUIDS

in transparency. The inability to match the indexes of refraction perfectly seemed to be caused by three types of imperfections. First, a large portion of the beads were found to have foreign matter inclusions which were in the form of opague ash particles or gas holes. Secondly, the index of refraction from bead to bead was determined to be somewhat variable. Finally, the fact that white light was used produced the inevitable dispersion, the effect of which appears as a faint color along the edge of each glass particle. The correction of these first two imperfections was ruled out since it would have meant obtaining a new batch of beads manufactured under more carefully controlled conditions and from the standpoint of cost and delivery time, this would have been prohibitive. However, since the index of refraction of a substance is a function of the wave length of the light source, it was thought that perhaps the edge effects could be eliminated by using a monochromatic light source. Therefore a mercury vapor lamp, where the visible radiation is concentrated in two lines: a green line of 5461 Angstroms and a violet line of 4385 Angstroms was used to determine the possibility of improving the transparency with monochromatic light. The violet ray was absorbed by a suitable filter and a strong pure green beam was obtained. The refractive index of the liquid

was then changed in small incremental steps while transparency observations were being made. The results of these tests showed that the transparency was not improved significantly by a monochromatic light source. However, one should recall that these tests were conducted on a sample of beads that had both inclusions and variations in refractive index from bead to bead. Therefore, these imperfections might have been of such a magnitude that any improvement due to monochromatic light was obscured.

Since there were no published data concerning the physical properties of the immersion liquid mixture, these quantities had to be determined by standard methods. For instance, the viscosity versus temperature relations shown in Figure III-3 were determined by the Saybolt Viscometer arrangement shown in Figure III-4 utilizing a universal orifice. The surface tension versus temperature relation graphically illustrated in Figure III-5 was determined with aid of a Cenco Platinum Ring Tensiometer shown in Figure III-6. The liquid density versus temperature curve shown in Figure III-7 was obtained by using a set of Central Scientific Company hydrometers shown in Figure III-8.

A decision on the choice of the gaseous phase was made with the stipulations that it be readily obtainable, common enough so that published thermodynamic properties are available, and

FIGURE III-3

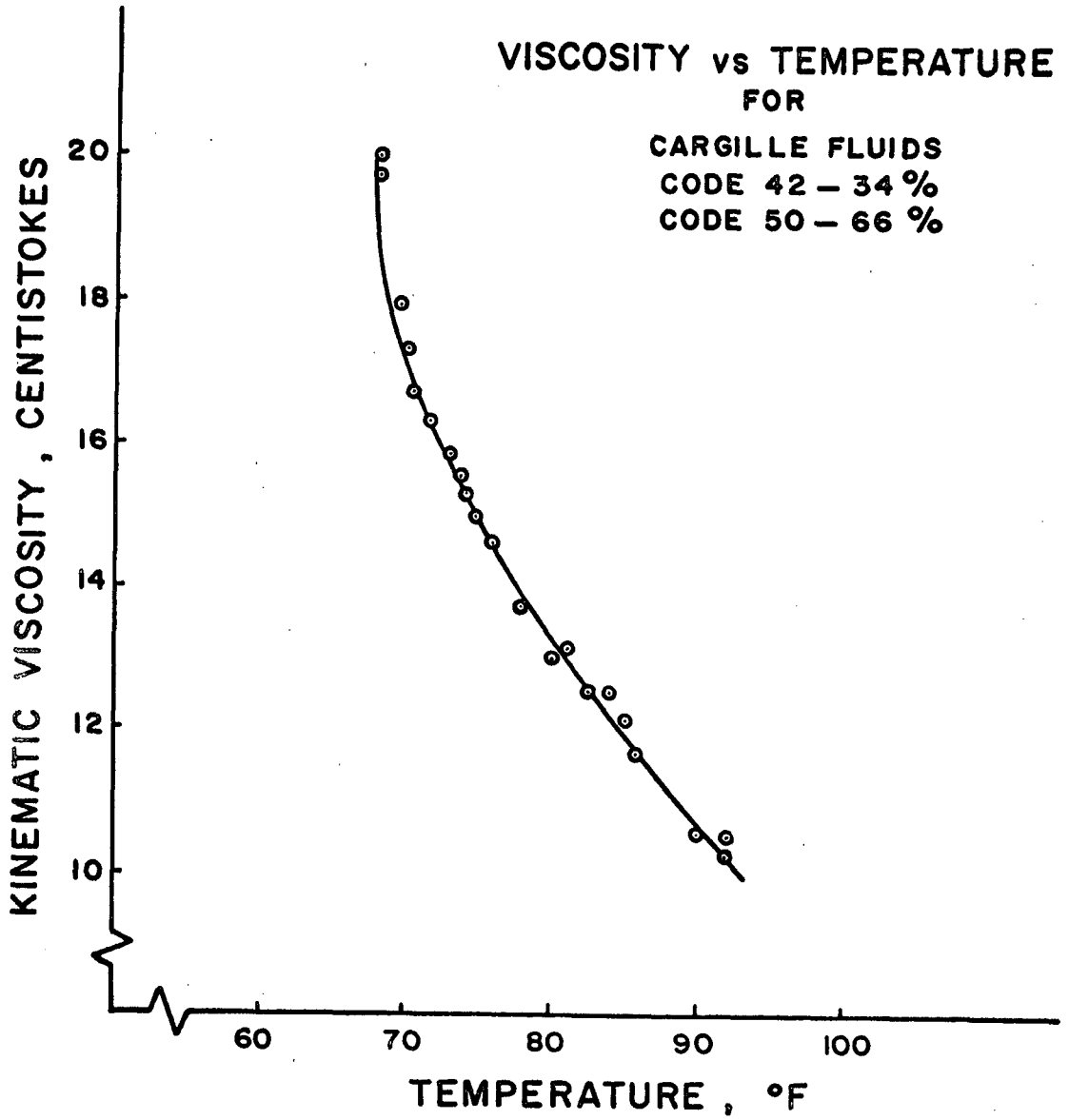
VISCOSITY vs TEMPERATURE
FOR
CARGILLE FLUIDS
CODE 42 – 34 %
CODE 50 – 66 %
KINEMATIC VISCOSITY, CENTISTOKES
20
18
16
14
12
10
60
70
80
90
100
TEMPERATURE, °F

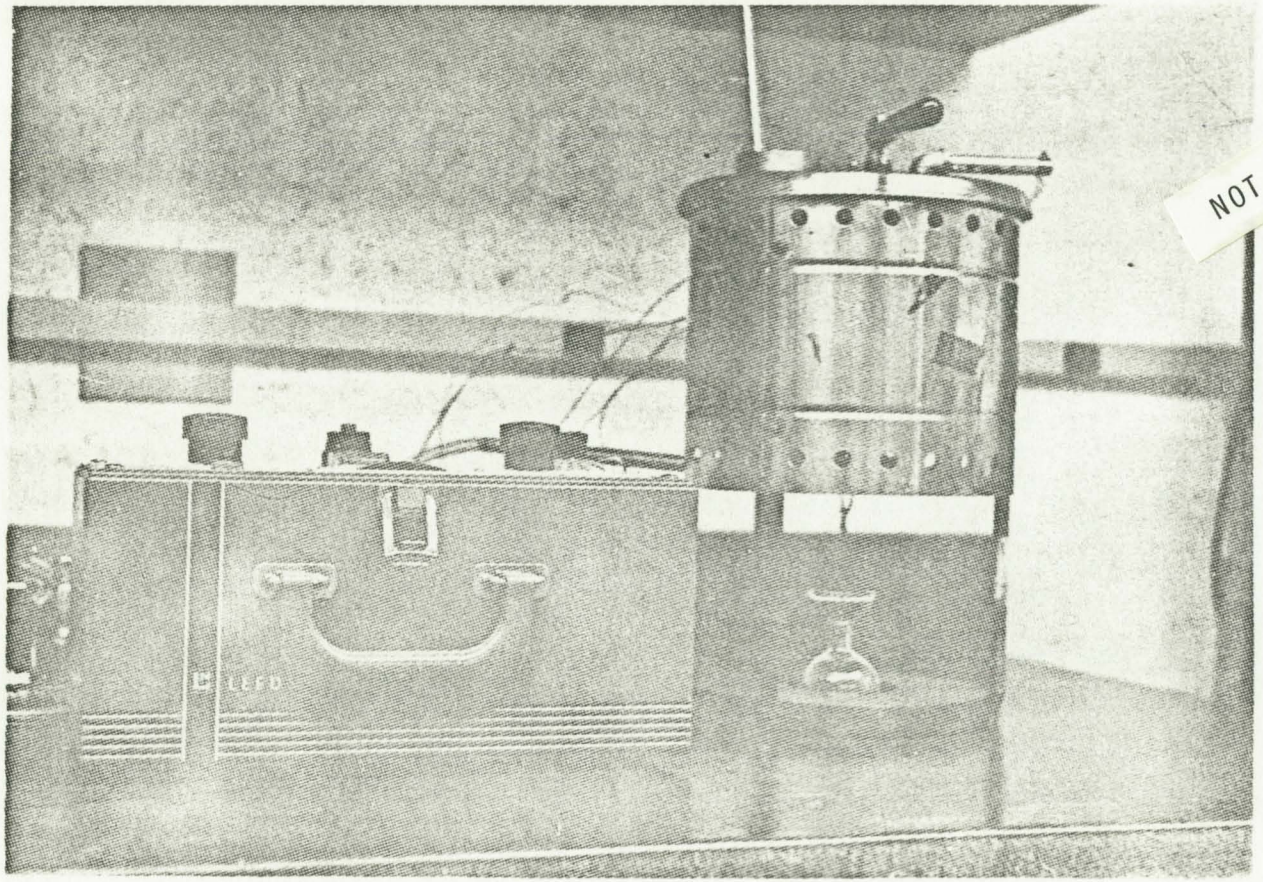

Figure III-4. Saybolt Viscometer

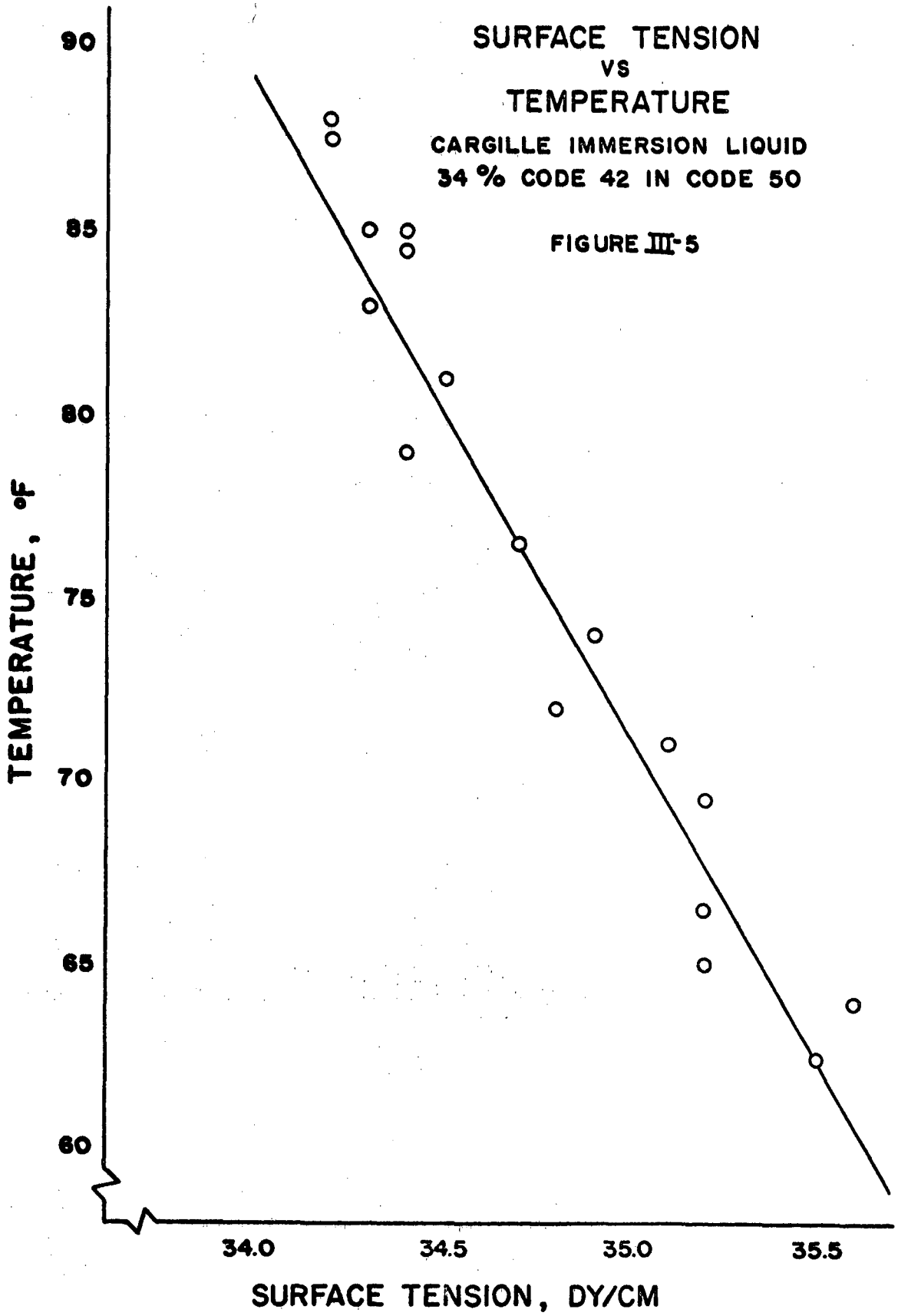
SURFACE TENSION
VS
TEMPERATURE
CARGILLE IMMERSION LIQUID
34 % CODE 42 IN CODE 50
FIGURE III-5
TEMPERATURE, °F
90
85
80
75
70
65
60
34.0
34.5
35.0
35.5
SURFACE TENSION, DY/CM

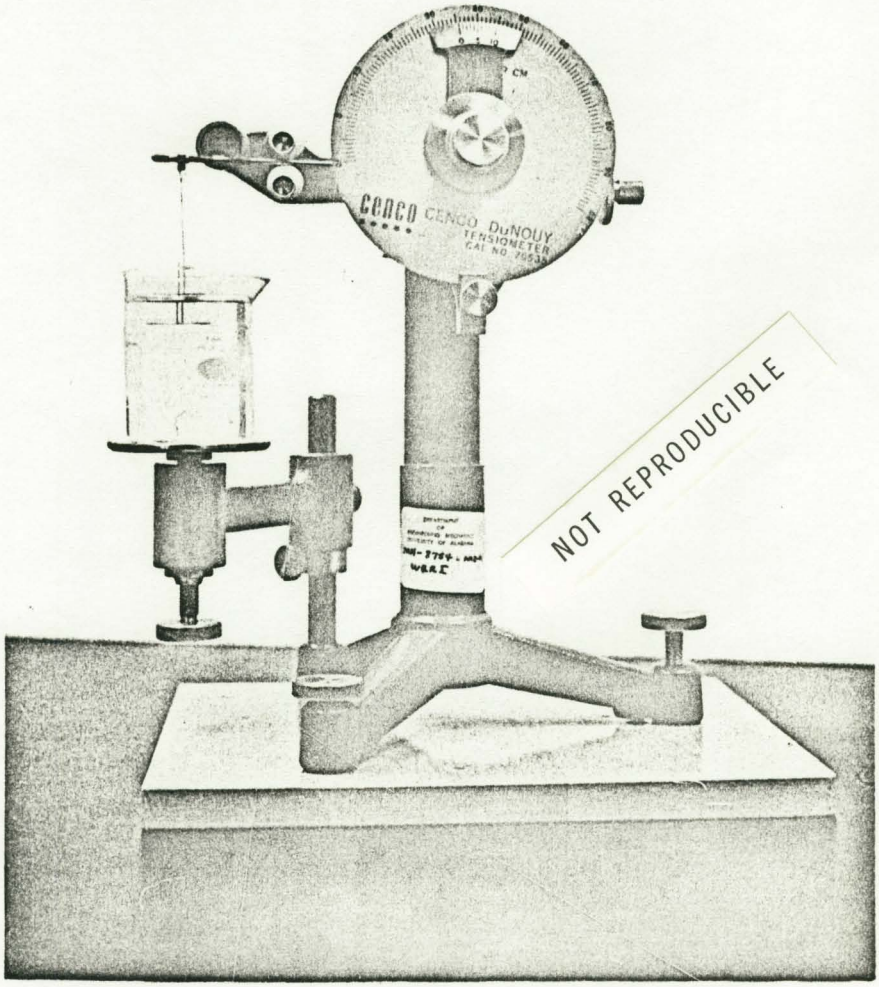

Figure III-6. Tensiometer

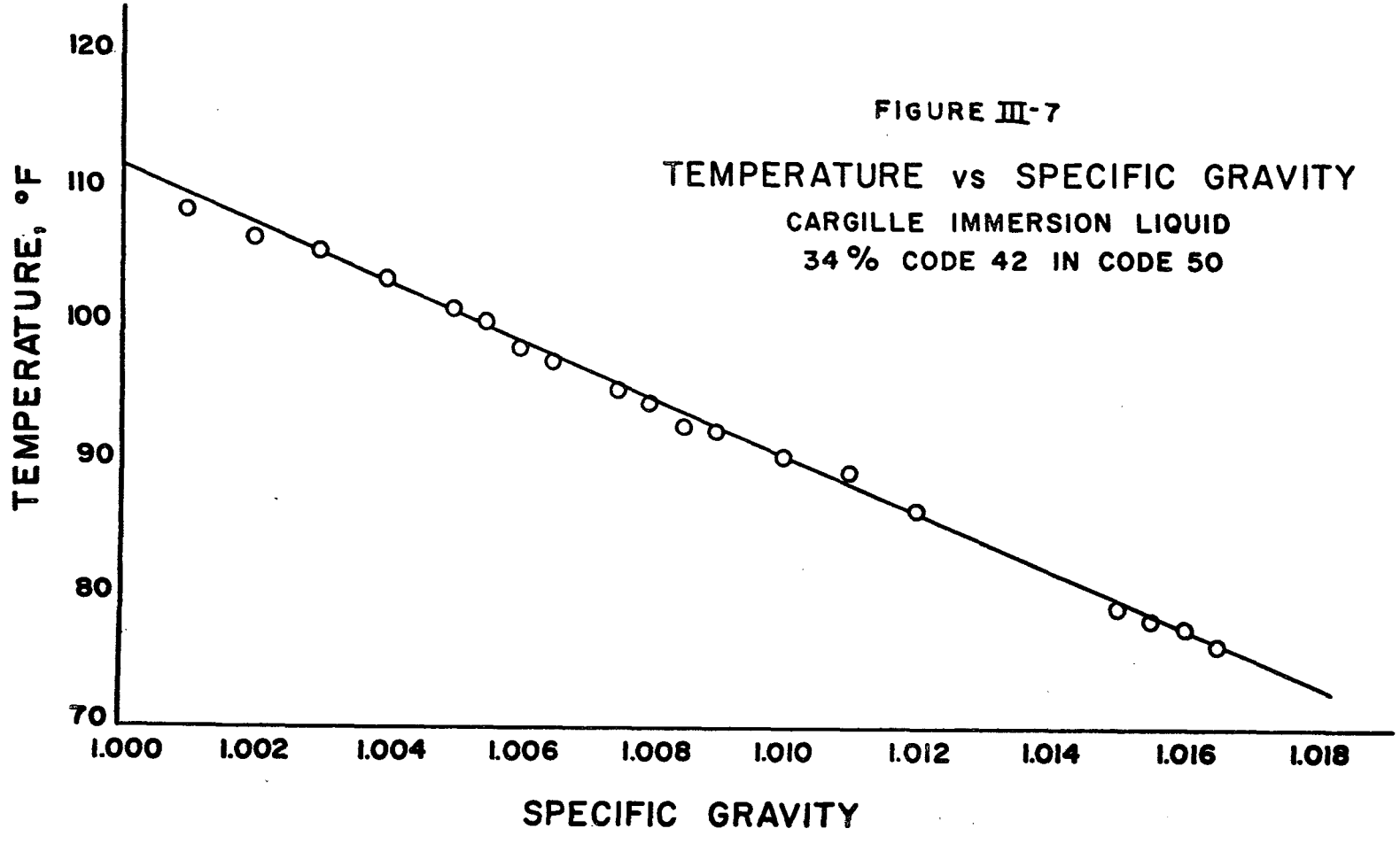

FIGURE III-7

TEMPERATURE vs SPECIFIC GRAVITY

CARGILLE IMMERSION LIQUID

34 % CODE 42 IN CODE 50

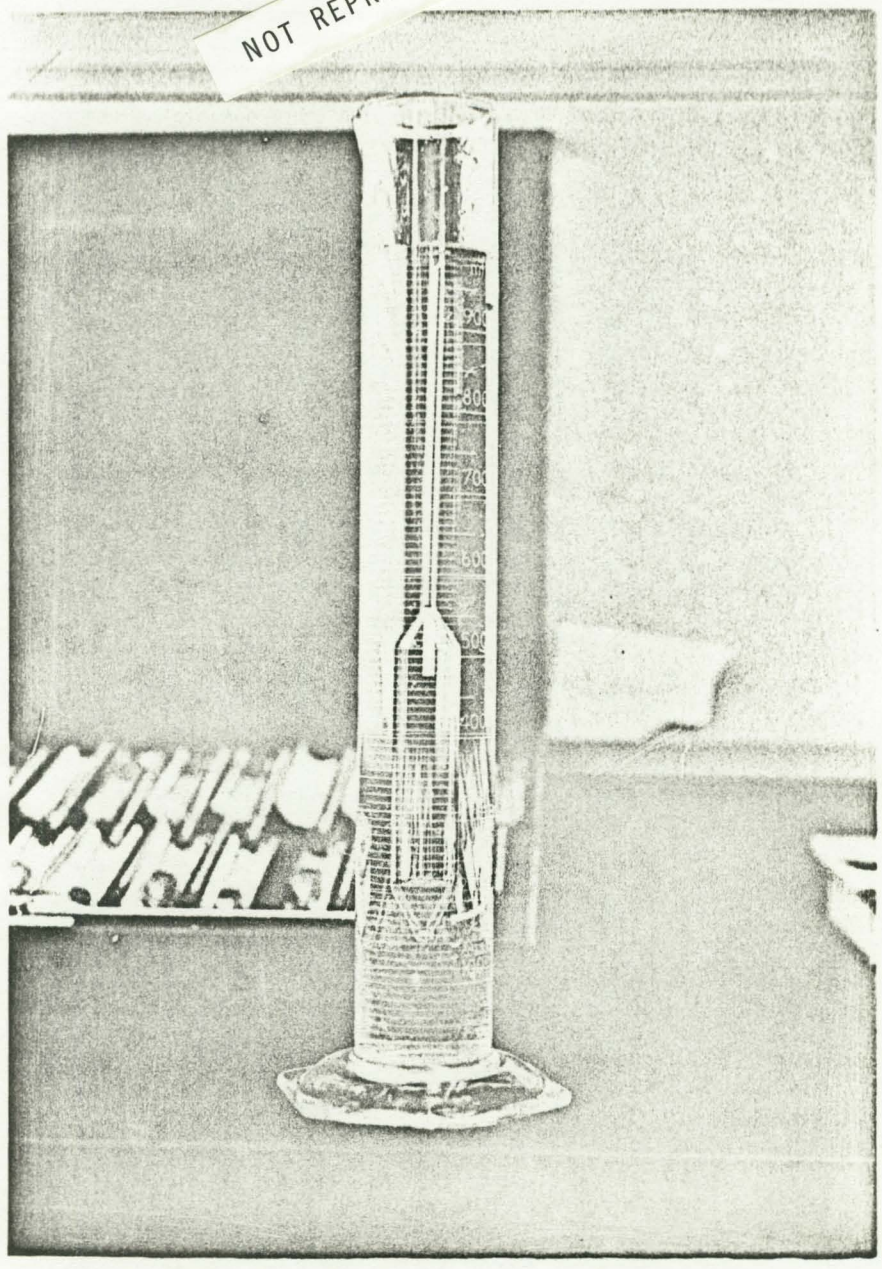

Figure III-8. Specific Gravity Measurements

relatively pure of foreign particles and moisture. Bottled nitrogen, extra dry grade, filled these requirements adequately and was used in all of these studies as the gaseous phase.

B. Channel, Flow Circuit and Instrumentation

The 12.7 mm and 3 mm spherical glass particles which made up the porous bed were packed into a plexiglas channel with a square cross section 4 inches on a side and 44 inches in length (Figure III-9). The 3/8 inch plexiglas sheets used to construct the channel were cemented along all seams and further held together by cap screws, thus forming a test section that could be pressurized up to 25 psi. For tests conducted on the bed composed of .88 mm particles, a shorter channel was used due to the larger pressure gradient produced by this medium. This channel had the same size cross section as that described above. However, the length was 28 inches and channel walls were 1/2 inch plexiglas sheets. All seams were cemented with plexiglas solvent as well as being held together by cap screws. A pressure of 30 psi was possible in this channel due to the increase in wall thickness.

The porous material was held in place by retainer screens stretched across the fluid reservoirs at each end of the channel. These reservoirs were originally intended to allow a visualization of the bubbles before and after going into the porous bed. However,

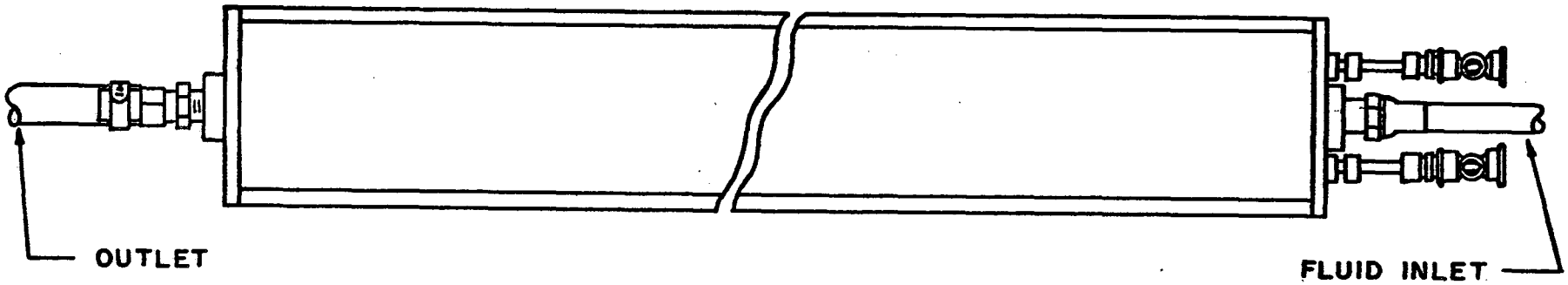

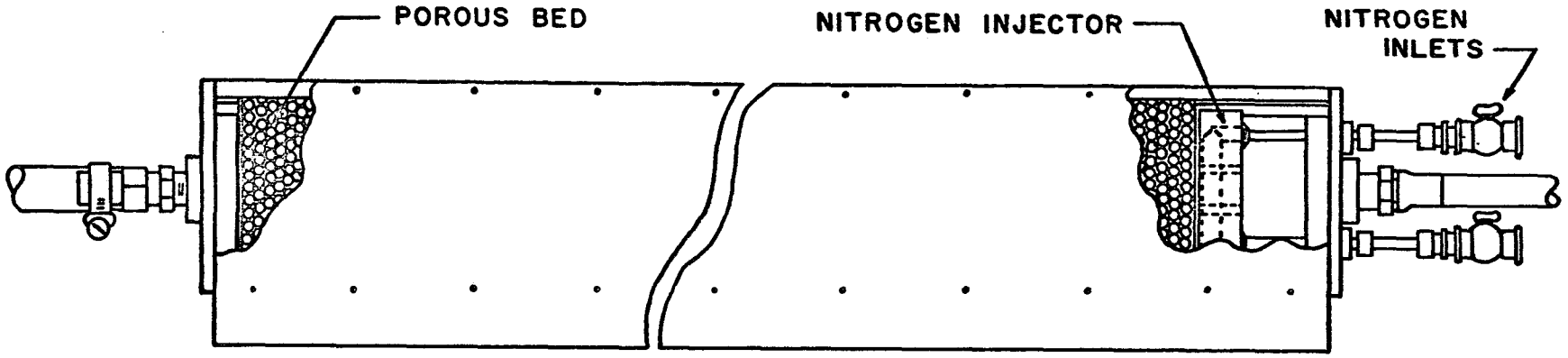

FIGURE III-9

CHANNEL FOR POROUS BED

when volumetric quality measurements were being made by weighing the channel it was necessary to estimate the volume of gas present in these reservoirs.

This estimation was more trouble than the acquired flow visualization could justify. Therefore, the reservoirs were eliminated, and the porous bed was extended from the gas injector to the channel outlet.

The nitrogen phase of the gas-liquid flow was introduced into the porous bed by nine hypodermic needles fitted into the plexiglas injector as shown in Figure III-10. Some initial tests were run before the installation of these needles. However, the need for injecting the gas through long slender tubes was discovered when the channel was placed in a downward flow position. The porous bed in this position packed down about 1/8 inch so that when the gas was being injected before the needles were used, it entered into a clear liquid region rather than the porous bed. The magnitude of the liquid velocity in this area was much smaller than in the porous bed so that gas leaving the injector was not pulled into the bed and thus formed a gas pocket just below the injector. When gas did finally build up to the point that it was forced through the bed, the largest portion of it went down the sides of the channel giving a very uneven flow pattern. This difficulty was eliminated by

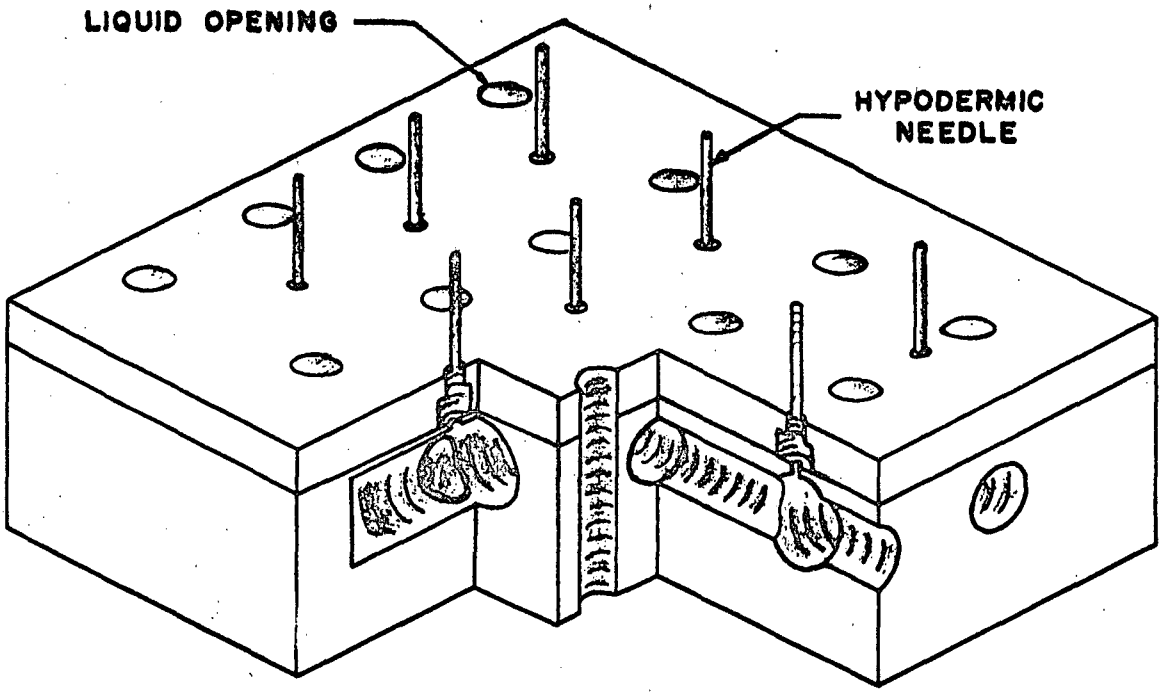

FIGURE III-10

NITROGEN INJECTOR

injecting the gas through the hypodermic tubing inside the packed bed where the local velocities were high enough to overcome the bouyant force of the gas bubbles.

The liquid and gaseous phases were controlled by the flow circuit shown in Figure III-11. The nitrogen gas was supplied to the channel from a high pressure storage bottle regulated to any desired pressure below 2400 psi by an Airco nitrogen two stage regulator. The rate of gas flow was maintained by a needle valve located between the pressure regulator and the gas flow meter. The gas flow rate was monitored with a Fisher Scientific Company variable area type flowmeter with measuring capabilities from .030 cfm to 3.35cfm. The temperature and pressure of the nitrogen was monitored with a thermocouple and an Ametek test guage respectively.

The liquid phase was forced through the packed channel by a Gerotor positive displacement 20 gallons per minute pump. This pump was driven by a Louis Allis Adjusto-Spede drive which would yield a stepless variation in speed from 100 to 1675 rpm. The rate of liquid flow was measured by a Fisher-Portor 1700 series variable area flowmeter which had a fluid measuring capacity ranging from .94 gpm to 9.4 gpm. The temperature was measured in the liquid reservoir with a

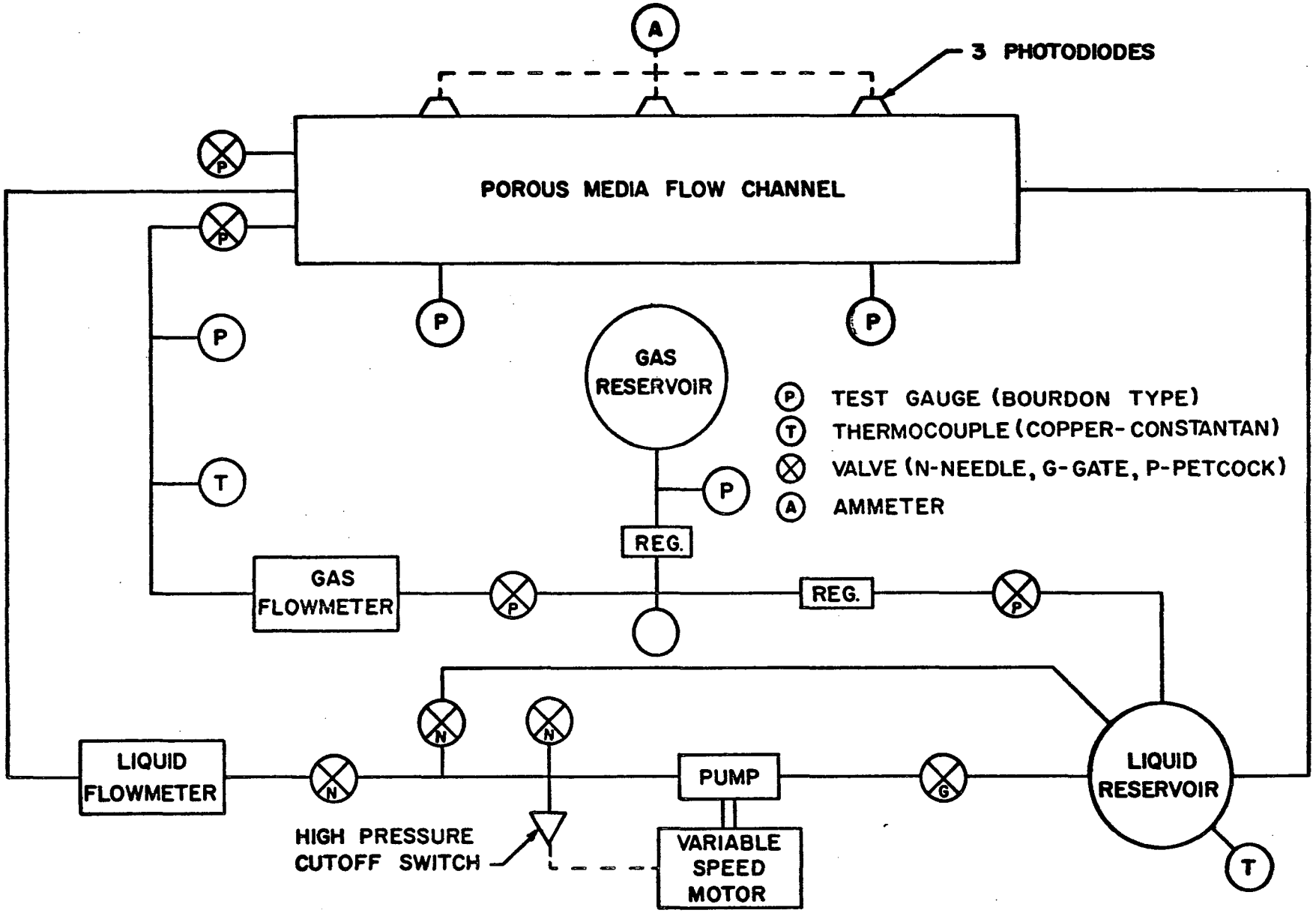

FIGURE III-11 FLOW CIRCUIT FOR TWO-PHASE POROUS MEDIA PILOT TEST APPARATUS

thermocouple. The pressure drop along the channel was measured with Ametek test gauges when the 3 mm and 0.88 mm particles were used. However, when the 12.7 mm particles were being tested the pressure gradient was reduced to the point that a U tube manometer was required to measure the pressure differential with suitable accuracy. In the latter case, an Ametek test gauge was used to determine the absolute pressure level at the channel inlet.

The variable speed motor was found to be necessary in obtaining a steady flow at all flow rates in the range of the flowmeter mentioned above. The original circuit utilized the 20 gpm constant displacement pump driven at a constant speed of 1750 rpm, with two globe valves splitting the flow in any proportions to the packed channel and to the by-pass line which led back to the liquid reservoir. This arrangement produced a flow through the channel with significant amounts of unsteadiness. Plans to alleviate this problem included the installation of two needle valves to replace the globe valves and the replacement of the constant speed motor by a variable speed motor. The resulting flow was considerably improved. In particular, the original flow circuit exhibited flow fluctuations of .2 gpm. The improved system reduced these fluctuations to less than 0,05 gpm. In addition to smoothing out the liquid flow,

the heating of the fluid was also considerably reduced since the entire output of the pump could be directed through the flow channel, and the viscous heating of the fluid through the by-pass line was eliminated.

C. Laser Velocimeter

An investigation was conducted to determine the feasibility of using a laser velocimeter to determine point velocities and volumetric quality in a fluid-gas mixture flowing in a channel packed with 3 mm flint glass beads where the indexes of refraction of the fluid and beads were approximately (see section A) matched. This method of velocity measurement has been successfully accomplished in clear liquids by Welch and Tomme (32) and in gases by Foreman, Lewis and George (10). One of the most attractive features of the laser velocimeter is the absence of devices protruding into the flow stream. These are not necessary because flow velocities are indicated by the frequency shift of a light beam passing through the liquid and scattered from small particles suspended in the fluid. In this study 5 micron latex spheres were used for this purpose.

A beam of coherent light was provided by a helium-neon gas laser and was directed through the plexiglas channel as shown in Figure III-12. The optical components shown in this

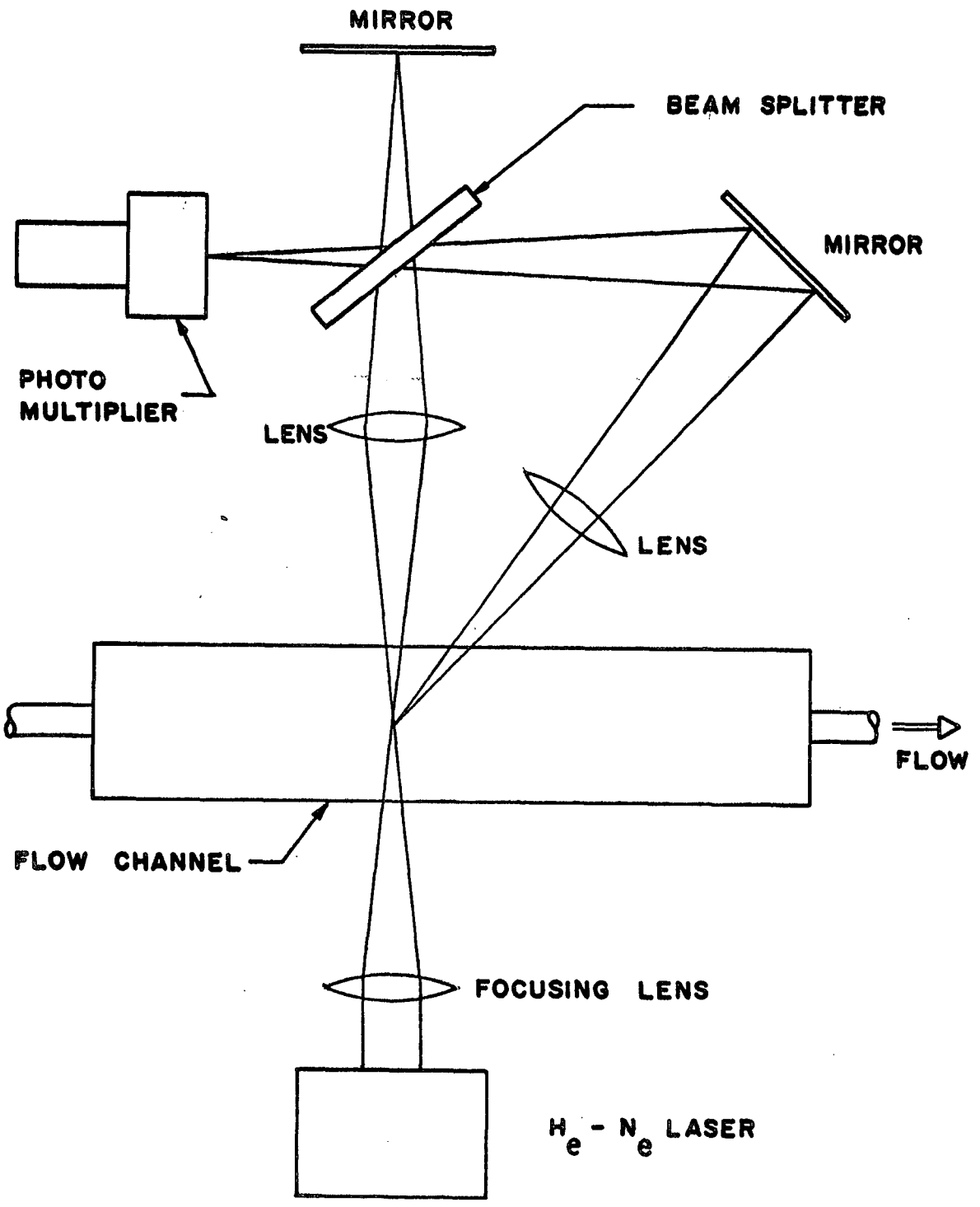

OPTICAL SYSTEM

FIGURE III-12

figure illustrate the manner in which the main beam of light passed through the channel and was directed by the splitter into the photomultiplier tube. The scattered light which has a different frequency due to the Doppler effect produced by the motion of the solids in the fluid was intercepted by a mirror placed at 10 degrees from the main beams and directed along with the main beam into the photomultiplier tube. When these two light beams recombined and entered the photomultiplier, the resulting output was a heterodyne signal that could be correlated to the horizontal component of velocity of the solid particles in the fluid. Since the latex spheres had the same density as the flowing liquid, one could assume their velocity to be that of the liquid.

The initial runs with the laser velocimeter were intended for flow of the liquid phase only. However, very small bubbles were detected in the fluid at all flow rates. It was believed that these bubbles were drawn into the system where negative pressure existed in the pump inlet pipe connections. In order to eliminate this negative pressure on the pump suction side, the system fluid reservoir was pressurized as described in the preceding section, and the bubbles no longer appeared.

In order to determine if the Cargille immersion liquids had enough solid impurities to produce light scatter without the

latex spheres, a test was performed in the clear liquid at one end of the plexiglas channel which contained no glass beads. The results indicated that sufficient impurities were already present in the liquid to produce a distinguishable signal, but the signal was significantly lower than that which had been obtained in earlier glass pipe studies with latex spheres in water. Therefore, it was decided to add 10 milliliters of the latex sphere mixture per 20 gallons of Cargille liquid which resulted in a much improved signal.

The beam was then directed into the porous bed and traverses were made in both horizontal and vertical directions in an attempt to find a spot where the beam was focused in a pore. At certain points in the traverse there occurred maximum output signals which seemed to indicate the location of a pore. However, the signal was very sporadic, occurring at intervals of 2 or 3 seconds superimposed on top of the system noise. To analyze these signals the trigger level on the oscilloscope was set above the noise level, and a polaroid camera was placed over the screen with the shutter open. After the oscilloscope triggered, the film was developed and the length of the wave period was measured and converted to wave frequency. This was repeated for bulk velocities ranging from 10 feet per minute to 25 feet per minute.

The results indicated no correlation between frequency and velocities so it was concluded that this signal was not originating from the velocity dependent heterodyne effect.

The appearance of the laser beam before and after it had passed through the channel was significant. Leaving the laser and entering the face of the plexiglas channel, the beam was about 1 mm in diameter while the exit beam was about 15 mm in diameter. It seems probable that this marked dispersion of the light reduced the intensity of the signal entering the photomultiplier to the same level as the system noise. Many repetitions of these occurrences indicated strongly the futility of obtaining Doppler shift velocities with the present system.

In future attempts to measure velocities in porous beds with a laser velocimeter, it is believed that one or more of the following alterations should be made. (1) The optical quality of the porous bed should be improved by obtaining higher quality glass beads. For instance, the beads should have no bubble or ash inclusions, and there should be more uniformity in index of refraction from bead to bead. (2) The index of refraction of the liquid and glass beads should be carefully matched at the wave length of the helium-neon. (3) The width of the packed bed should be reduced from 4 inches to perhaps 2 inches. (4) A

more powerful laser should be used. (5) The quality of the optical system should be improved in order to obtain a sharper focus point.

D. Data Collection Procedure

For the two cases of greatest pressure drop, the inlet channel pressure was measured 7 inches from the end of the channel by an Ametek bourdon type test gauge with 0 to 30 psi range and an accuracy of 1/4% of the full scale reading. This gauge was mounted on the frame of test equipment as shown in Figure III-13 and was connected to the flow channel through a flexible Tygon tube. The outlet pressure was measured by a 0 to 15 psi Ametek test gauge similar to that mentioned above and connected to the channel 4 inches from the outlet through a flexible Tygon tube. When the 12.7 mm particles were being tested, a U tube manometer was used to measure the differential pressure across the bed. It was possible to read this pressure drop to within one tenth of an inch of the fluid.

The temperature in the liquid reservoir and the gas flowmeter was monitored by Copper-Constantan thermocouples connected to a Leeds and Northrup direct reading potentiometer. The measurement of the temperature of several known standards, such as melting ice and boiling water, indicated that

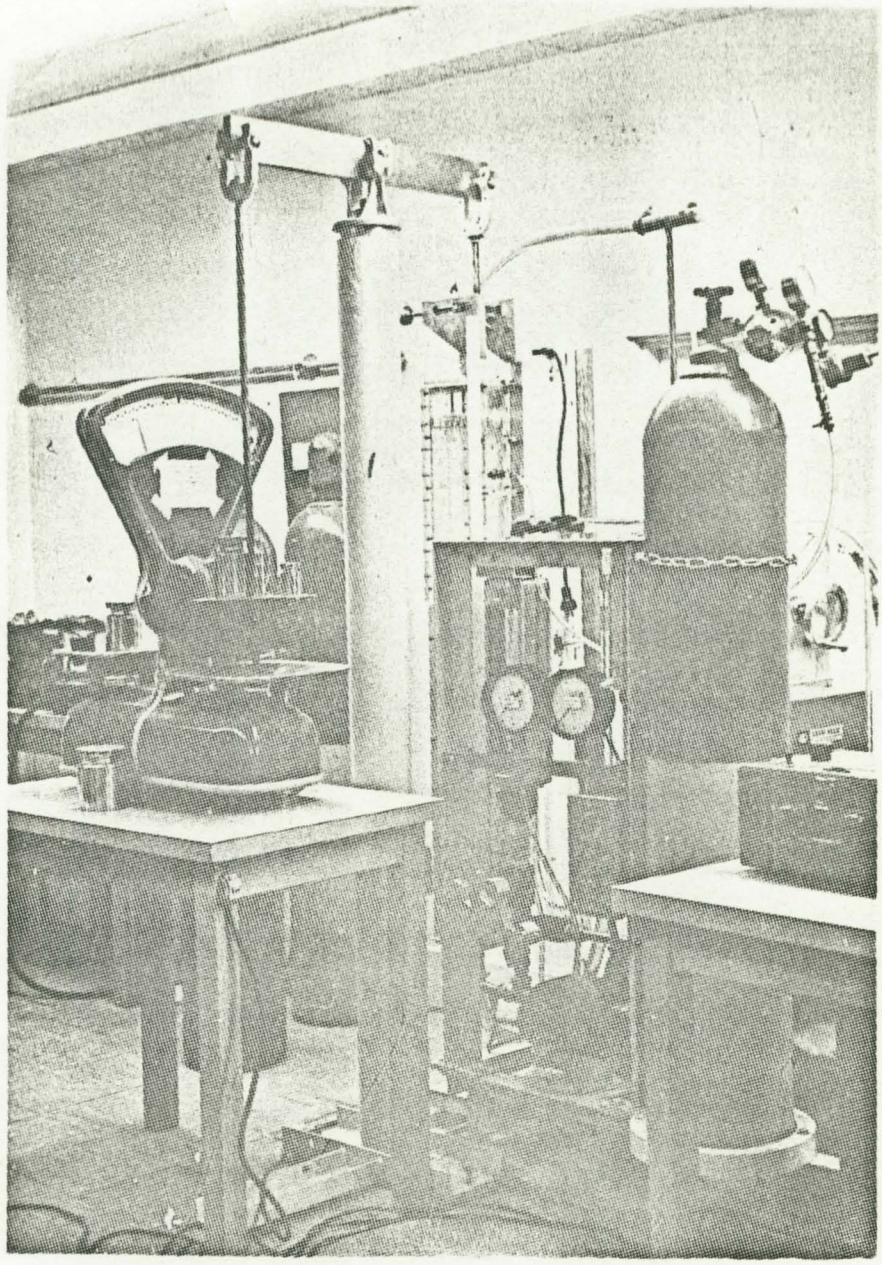

Figure III-13. Experimental Apparatus

this arrangement could be expected to measure temperature to within one degree fahrenheit.

Liquid and gas flow rates were measured by float type flowmeters as described in section B of this chapter. The Fischer and Porter flowmeter used to measure liquid flow rate had a rated accuracy of 2% of the full scale reading while the gas flowmeter manufactured by Fisher Scientific Company was rated to be accurate to within 1% of the full scale reading.

Early in the investigation into the possibility of using the laser velocimeter to measure velocities in the transparent porous bed, it was also suggested that the volumetric quality might be measured by this method. The laser beam must be focused in a pore space. It will then be expected that the beam will scatter completely when gas occupies this pore, and that it will be transmitted when liquid occupies the pore. Therefore, by recording the number of velocity signals being received which were non-zero and comparing this with the number of samples known to be attempted during a given period of time, the volumetric quality is obtained. However, the lack of success in obtaining a strong signal through the bed (see Section C) left this study with the need of a method to measure the volumetric quality.

The large difference in density between the gas and liquid

phases suggested a gravimetric method of determining the fraction of each phase present in the bed at any time. In order to utilize such a method of volumetric quality measurement, a continuous weight of the entire flow channel was required with as much accuracy as possible. Standard spring-type scales with the necessary 50 to 100 pound weight range could not be found with a dial divided in steps of less than 2 ounces or 12.5 hundredths of a pound. Such an arrangement would have been a serious source of inaccuracy especially at very low volumetric quality measurements. Therefore, at the suggestion of Toledo Scale Works, a knife edge counterbalance beam was constructed as shown in Figure III-14. The flow channel was mounted on one side of the counterbalance beam and sufficient weight was added to the other side of the beam to bring the weight being measured into the 0 to 30 pounds range. This could be adequately covered by Toledo balance scales which could measure the change in weight of the flow channel to within one hundredth of a pound.

It was desired to obtain a series of tests at constant volumetric quality (e.g. 0, .04, .08, .12, .16 and .20). Except for the variation in the volume of gas in the outlet tubing, the stiffness of the inlet and outlet fluid lines, and the momentum imparted to the channel by the flowing fluid,

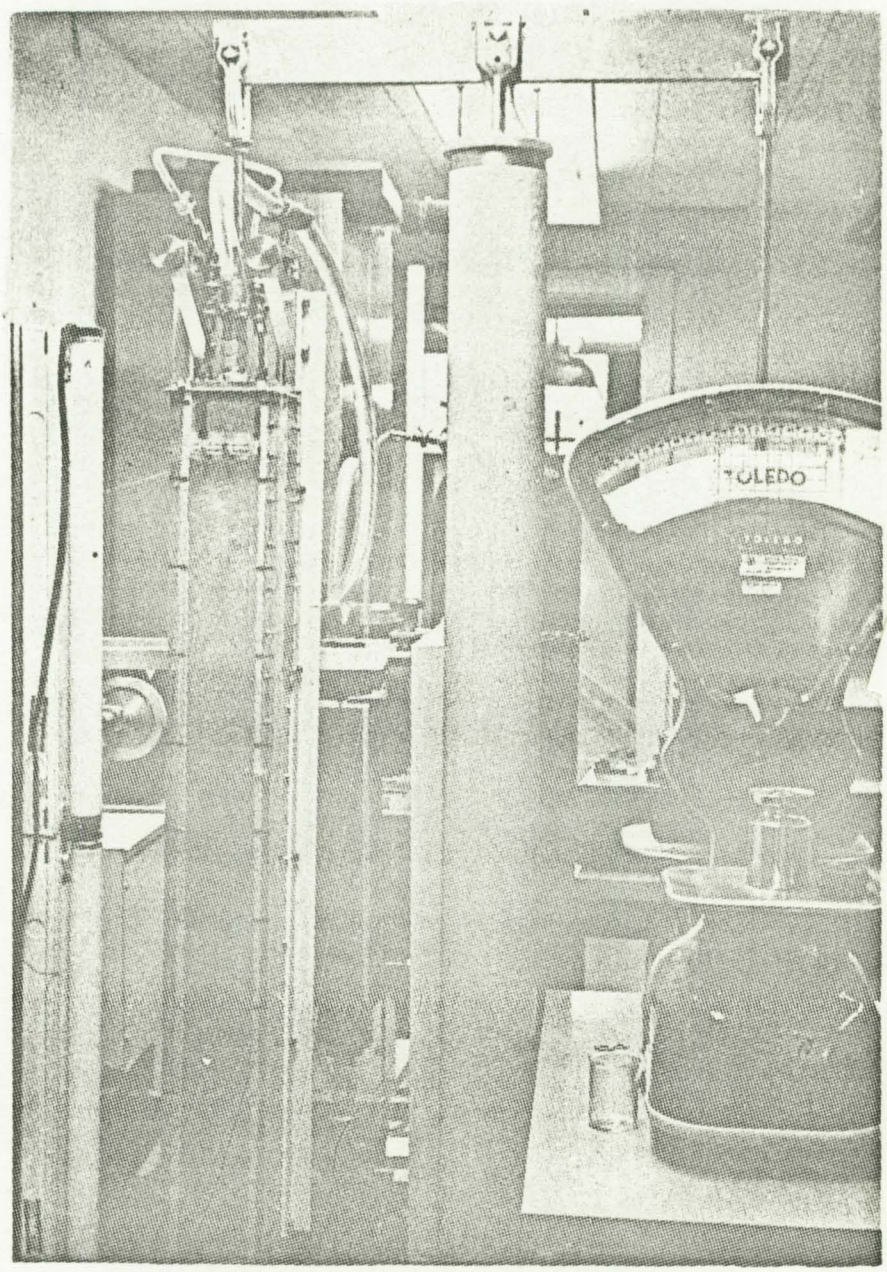

Figure III-14. Counterbalance Arrangement

a specific scale reading would always indicate a certain volumetric quality. These conditions mentioned above which caused deviation from a simple proportionality between the weight decrement and volumetric quality were taken into account by calibrations and are described in the following section. The gas flow was regulated to keep the volumetric quality constant through a series of widely ranging liquid flow rates. When each of the flow rates had reached a stable condition, the liquid and gas flow rates, the pressures at the channel inlet and outlet and at the gas flowmeter, and the temperatures at the liquid reservoir and at the gas flowmeter were all recorded.

E. Calibrations

The liquid flowmeter was calibrated by timing the mass flow collected in a container on a set of balance scales. The resulting calibration curve is shown in Figure III-15. The manufacturer furnished calibration curves with the gas flowmeter so that further attention to the calibration of this instrument was not necessary.

Extensive calibrations were made in connection with the gravimetric measurement of volumetric quality. These were necessary due to the rigidity of the external fluid lines,

FIGURE III-15

CALIBRATION CURVE
9.4 GALLONS / MINUTE
FISHER PORTER ROTAMETER

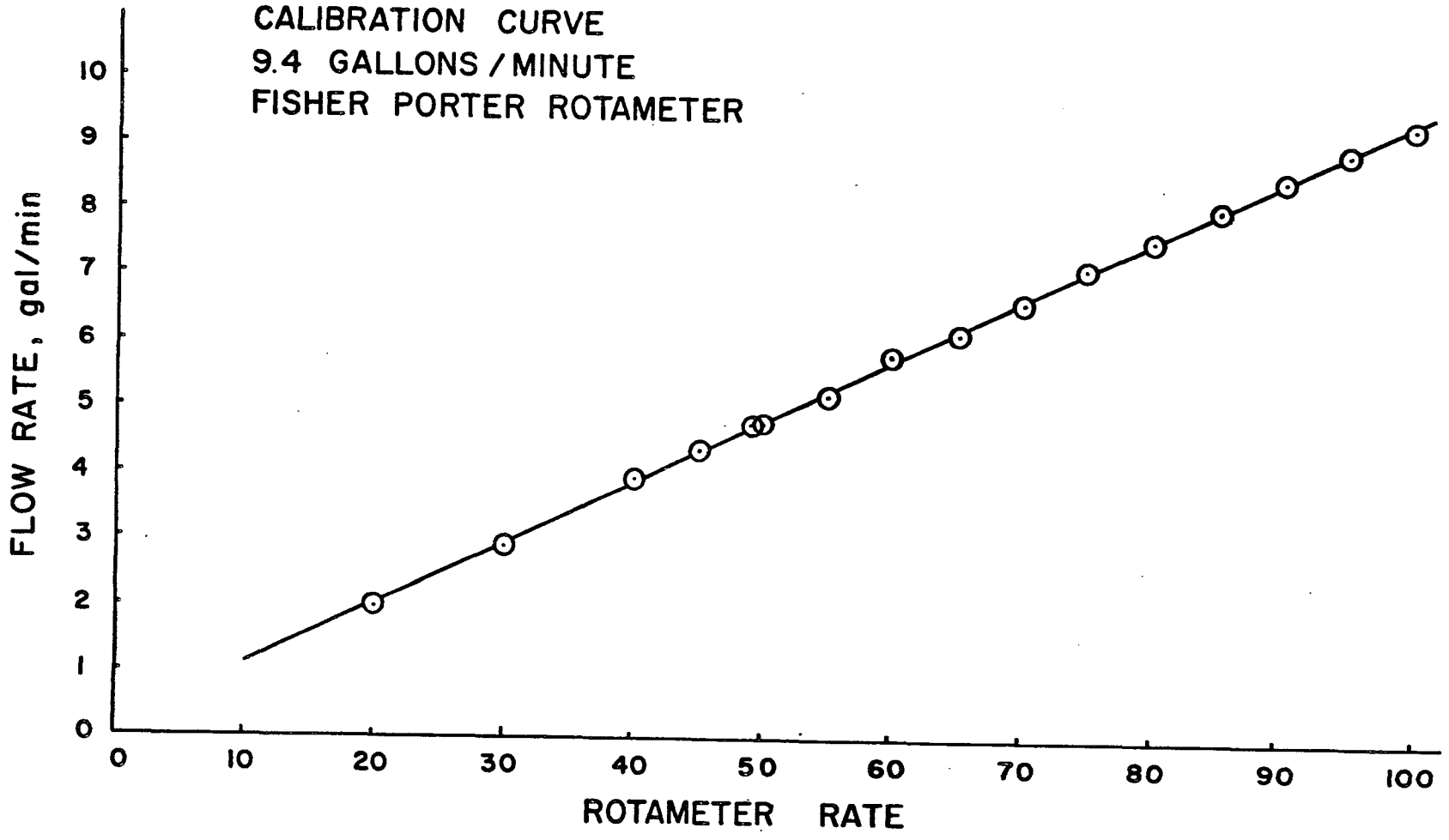

the momentum imparted to the channel by the liquid flow, and bubbles in the exit lines.

Regarding the first of these, the external 1 1/4 inch polyvinyl chloride tubes which delivered the liquid from the pump to the channel and back to the reservoir exhibited some degree of rigidity and consequently required a small force to bend them. The deflection of the tubes is illustrated by the fact that the end of these lines move 3/4 inch from the point where the scale reads 2 lbs. to the point where the scale indicator is on zero. By placing known weights on the flow channel and reading the amount of scale pointer deflection, the error resulting from the fluid lines was recorded. This test was repeated for several liquid flow rates, and the correlation was found to be independent of flow rate. A new calibration was necessary whenever the fluid lines were disturbed so that the curve shown in Figure III-16 is a sample of the many calibrations of this type that were required.

The next calibration accounts for the momentum imparted to the channel by the flowing fluid. When the flow conditions were changed from a steady state, the effect of the momentum change could be measured on the scales. This apparent change in weight was the quantity considered in this calibration. Since the vertical momentum forces considered

FIGURE III-16

CHANNEL WEIGHT CORRECTIONS FOR EXTERNAL FLUID LINES

SYMBOL	q_L IN GPM
⊡	0
⊙	3.00
▽	4.75
△	6.70

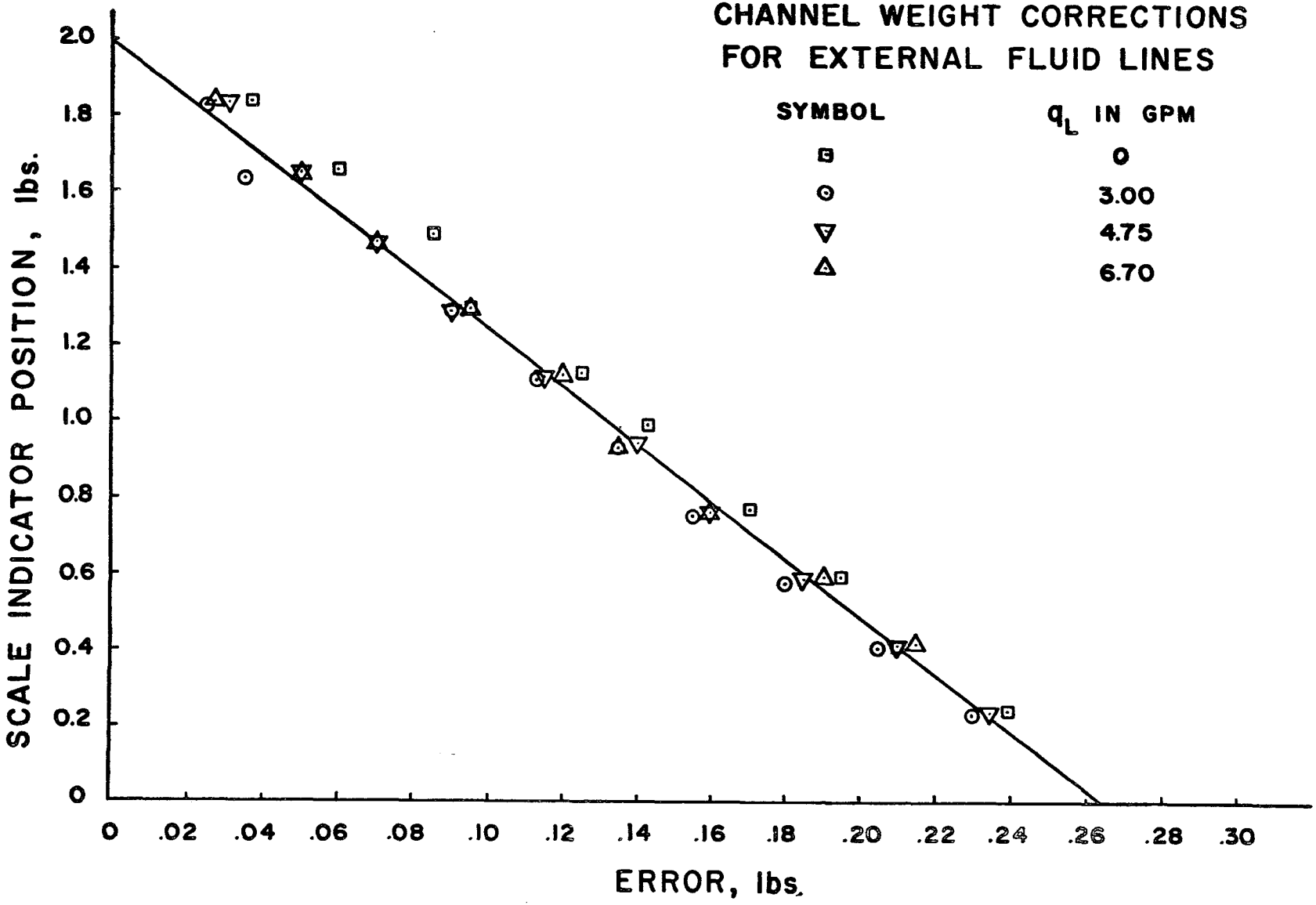

here were a function of the geometric configuration of the inlet and outlet tubes and this changed slightly due to the deflection of the scale, the test were conducted for several positions of the scale indicator. From Figure III-17 it is evident that this effect was negligible. However, a large disturbance of the fluid lines required a new calibration of this momentum effect. Figure III-17 is one calibration curve among the several that were required each time the flow lines were disturbed.

Another calibration that was found to be necessary when the channel was arranged for downward flow was intended to account for the nitrogen trapped in the fluid-gas lines returning the flow back to the fluid reservoir. In many cases, the velocity in this line was not great enough to overcome the bouyant force of the gas. This caused part of this line to be filled with gas, resulting in an erroneous weight measurement. An estimation of the volumes of each phase was difficult due to the irregular shape of the gas-liquid interface. Therefore, a weight measurement was used to determine the relative volumes of each phase at different positions of the interface. More specifically, this exit line was allowed to fill up with gas by forcing nitrogen through the porous bed. Then the gas was turned off. The bed quickly cleared of all

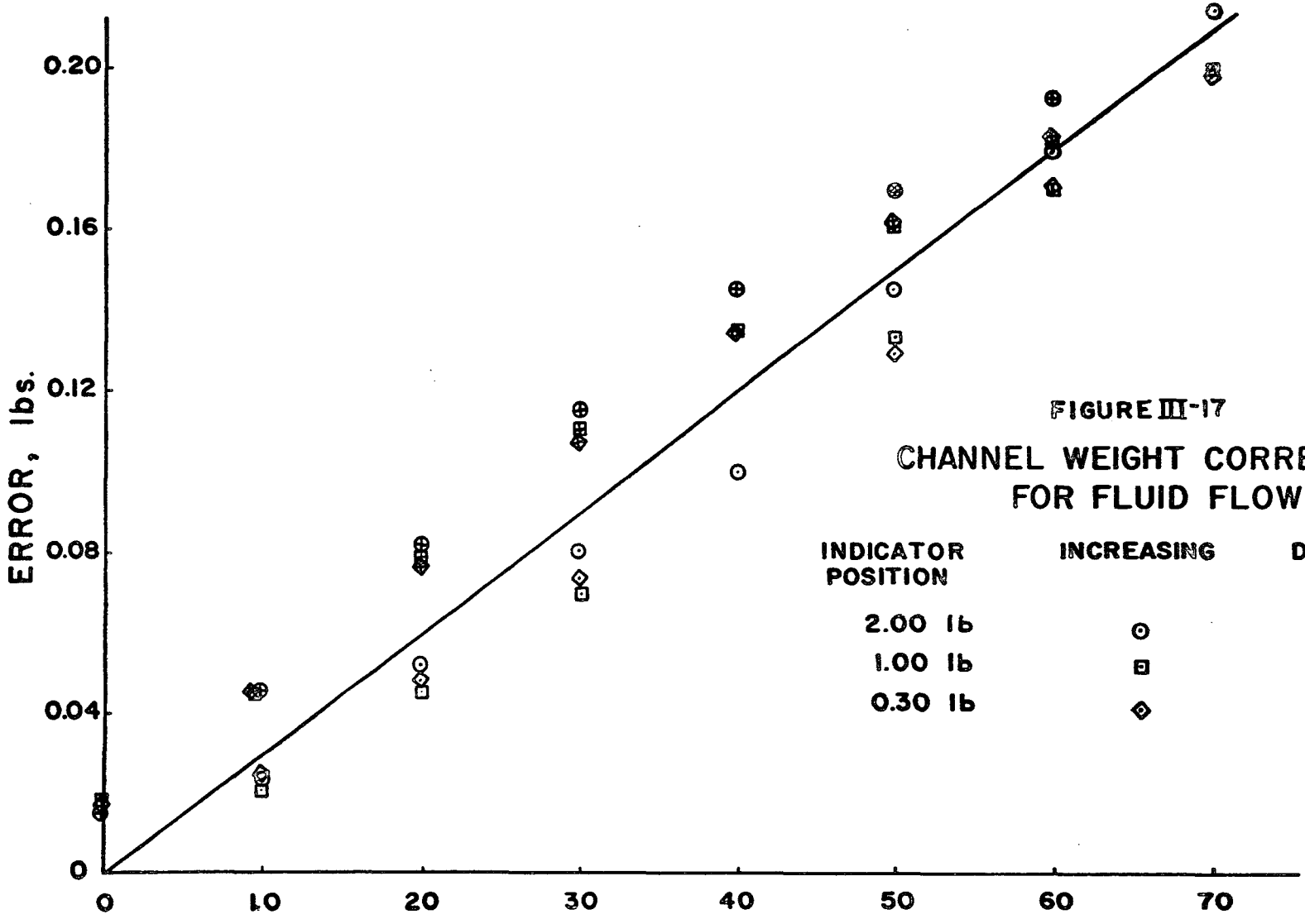

FIGURE III-17

CHANNEL WEIGHT CORRECTIONS FOR FLUID FLOW

gas and any difference in the scale reading was attributed to that gas in the exit line. A flexible scale was affixed to this line and the interface position was recorded for various weight measurements. Figure III-18 is the calibration.

F. Porosity

The porosity Φ of a porous material is defined as the fraction of the bulk volume of the material occupied by voids. Since these voids are in fact the tortuous channels through which all of the flow must occur, an investigation of the magnitude of this quantity is essential to a study of this kind.

The porous materials used in these tests were composed of glass spheres of uniform diameter. Therefore, it seemed that an analytical determination of the porosity was possible. For instance, there exists two extremes in systematic arrangement of the particles which provide on the one hand a maximum possible pore space and on the other a minimum. The tightest packing is called rhombohedral and is formed by placing the fifth sphere in its stable equilibrium position in the center of four other spheres. This is, of course, the most stable packing since further agitation will cause no movement of the spheres and consequently cause no reduction in pore space. The porosity of this arrangement is 25.95% (22)

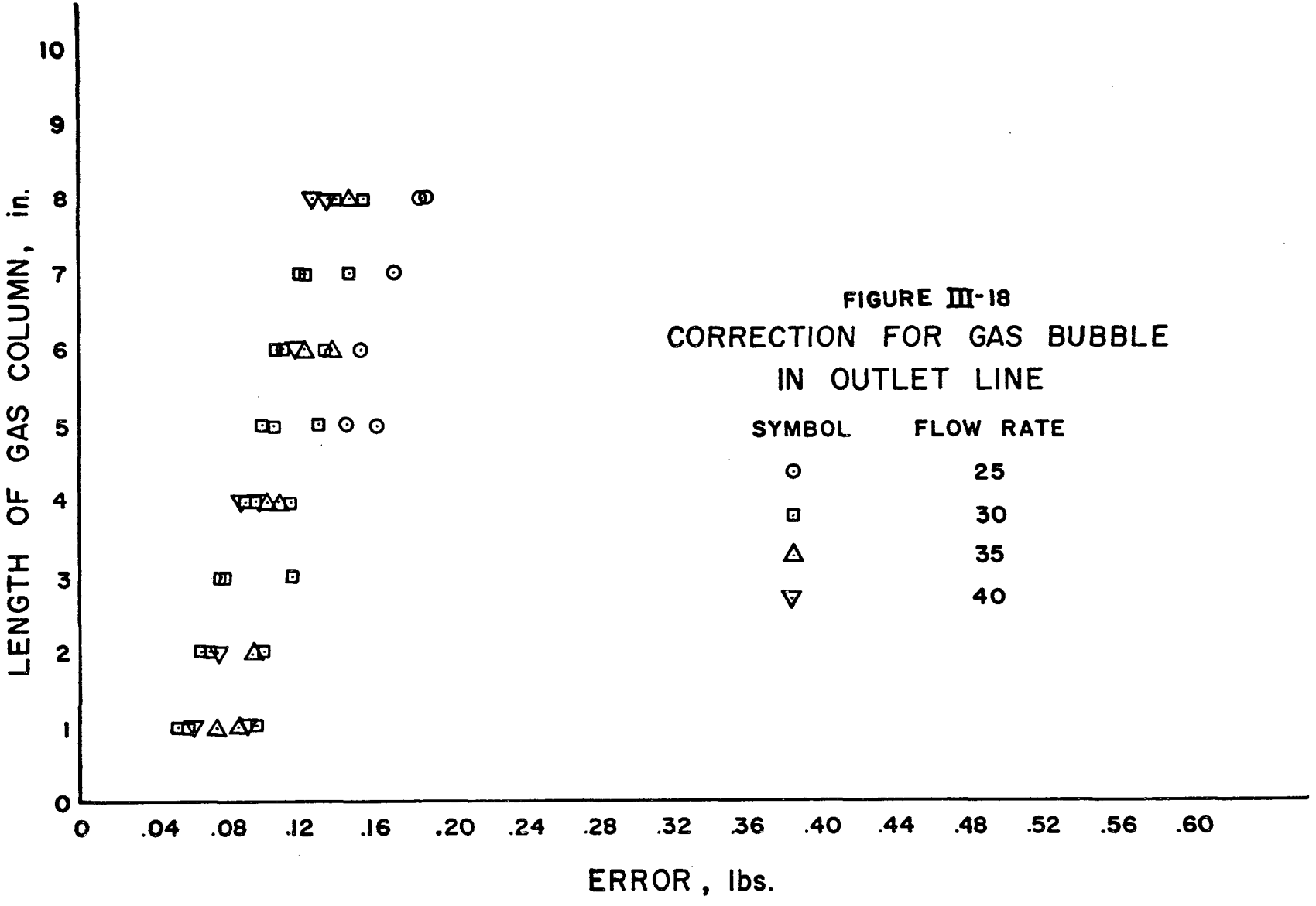

FIGURE III-18

CORRECTION FOR GAS BUBBLE IN OUTLET LINE

independent of the size of the spheres. The loosest packing is called a cubic array and is formed by placing the spheres directly on top of each other. This array, which has a porosity of 47.64% (22) is only stable to forces normal to the cell face and is consequently not expected to exist except under carefully controlled packing conditions. When the packing is random, with some degree of agitation, the arrangement of particles might be expected to approach the rhombohedral array. However, in practice this is not the case for several reasons. First, the distance between the walls of the container is not usually designed to be a multiple of the porous media size, therefore, the pattern is necessarily interrupted at the wall. Second, the particles used to comprise the porous material are not perfectly spherical. Third, friction between the particles cause bridging of groups of particles that are extremely difficult to break down even under severe conditions of agitation (22). Therefore, it has been found experimentally that assemblages of spheres will have porosities averaging between 35% and 40% in spite of careful efforts to induce closer packing (19).

The porosity of media used in these tests was obtained by determining the weight of a container of the media before and after the pores were completely filled with water. The

difference in these two weights represented the weight of water required to fill the pores. When this weight is converted to volume of water required to fill the pores, the following formula was used to compute the porosity Φ.

$$\Phi = \frac{\text{Volume of pores}}{\text{Volume of container}}$$

Since the porosity of a bed is greater in the layers of particles next to the walls of the channel, it is important to account for this effect when measuring the average prosity of a packed bed (See chapter IV on "Edge Effects"). The elimination of this phenomenon is not possible. Therefore, in order that this region of higher porosity be included in the correct percentage of total volume of the channel, one of the actual flow channels (4" x 4" x 24") was used as a measuring container for the porosity measurement. The porosity determined in this manner was found to be 37.1% for the 3 mm beads, 40.5% for the 12.7 mm beads and 37.7% for the .88 mm beads.

At the outset of the tests on these beds, when the fluid was flowing upward through the porous bed, fluidization was observed which caused the bed to pack to a lower porosity even when severe agitation of the bed had failed to do so. Fluidization occurs in a granular bed when the drag and

pressure forces on the solid particles are large enough to move them. When this occurs, the individual granules become disengaged from one another and the bed begins to assume a "quicksand" state. However, as the liquid flow rate was increased the bed again appeared to be rigid except for a six inch portion at the bottom of the bed where the number of solid particles appeared to be greatly reduced and their motion was of a highly turbulent nature. Each time the bed was allowed to go through the process of fluidization and then the flow stopped, the bed was observed to pack down a small amount. After several hundred cycles of this kind, the porosity was calculated to have changed from the above values to 35.2% for the 3 mm bead, 39.6% for the 12.7 mm beads and 34.8% for the .88 mm beads. The bed was refilled periodically as the void space appeared at the top of the channel. The final packing in the case of each bed was found to have undiscernable amounts of fluidization at all flow rates.

G. High Speed Photographs

A visual determination of the size and shape of the bubbles was not possible at high liquid and gas flow rate. Even the initial attempts to stop the motion of the bubbles by photographic means met with failure. For instance, a

Miranda single lens reflex camera was used to photograph the bubbles at a shutter speed of 1/1,000 seconds. However, the bubbles appeared elongated and it was inconclusive as to whether this was the actual shape of the bubble or due to the fact that the camera shutter speed was too slow. Therefore, a 16 mm Fastax high speed camera model WF4T, manufactured by Wollensak Corporation was used to photograph the flow at 5,000 frames per second. Since the camera requires a short time to accelerate up to speed, a MilliMite timing light generator manufactured by Red Lake Laboratories Incorporated was used to place 1,000 marks per second on the edge of the film. These marks were used to determine when the portion of the film was photographed at 5,000 frames per second. The marks also served as a check on the calibration curve that was constructed to predict the speed of the camera for any setting of the Red Lake Laboratories model RL 236-1M variable transformer.

The high speed film data was intended to supply three pieces of information for each of the flow conditions tested, the size and shape of the bubbles and the average velocity of the gaseous phase. This last piece of information was obtained in order to confirm the accuracy of velocity of the gas determined by measuring the gas flow rate, computing

the area allocated to gas flow, by knowing the bed quality, and finally calculating the velocity of the gas.

H. Photodiode Measurement of Bed Quality

Although the bed quality measurements for this series of test can be satisfactorily made using the gravimetric method described in one of the previous sections of this report, it will be useful to future studies of two phase flow at reduced gravity to investigate a method that is not dependent on a gravity field. A visual study of the flow channel under different gas flow rates has indicated that the transparency of the bed is related to the amount of gas present in the bed. For instance, when the bed is filled completely with gas, it is opaque and when it is filled completely with liquid, the bed is transparent. At intermediate stages of bed quality, the transparency is somewhere between these extreme cases listed above. Therefore, if a method of measuring light transmission could be devised which would relate in some repeatable way the amount of light passing through the bed to the amount of gas in the bed, the volumetric quality could be determined under weightless conditions.

Toward this end, a light source was installed along one side of the plexiglas test channel and three photodiodes were

placed on the opposite side of the channel to measure the transmitted light (Figure III-11). The current flowing through the ammeter shown in Figure III-19 was proportional to the light being intercepted by the three photodiodes.

Initially large fluctuations in the readings of the microammeter were experienced as indicated by the experimental scatter in Figure III-20. By observing the gas flow through the bed, it became apparent that the unsteady nature of the photodiode current was in part due to the placement of these sensors. For instance, they were originally spaced one foot apart beginning six inches above the lower liquid reservoir. This allowed the bottom sensor to be influenced in an unsteady fashion by the slugs of gas that had broken through the screen and had not traveled a sufficient distance to become completely dispersed throughout the entire porous bed. This unsteadiness in the photodiode current was eliminated by spacing all three sensors along the upper half of the packed bed where the gas-liquid flow had become, to some extent, a homogeneous mixture.

The experimental results obtained by this improved arrangement are shown in Figure III-21 and reflect the improved correlation between the change in channel weight

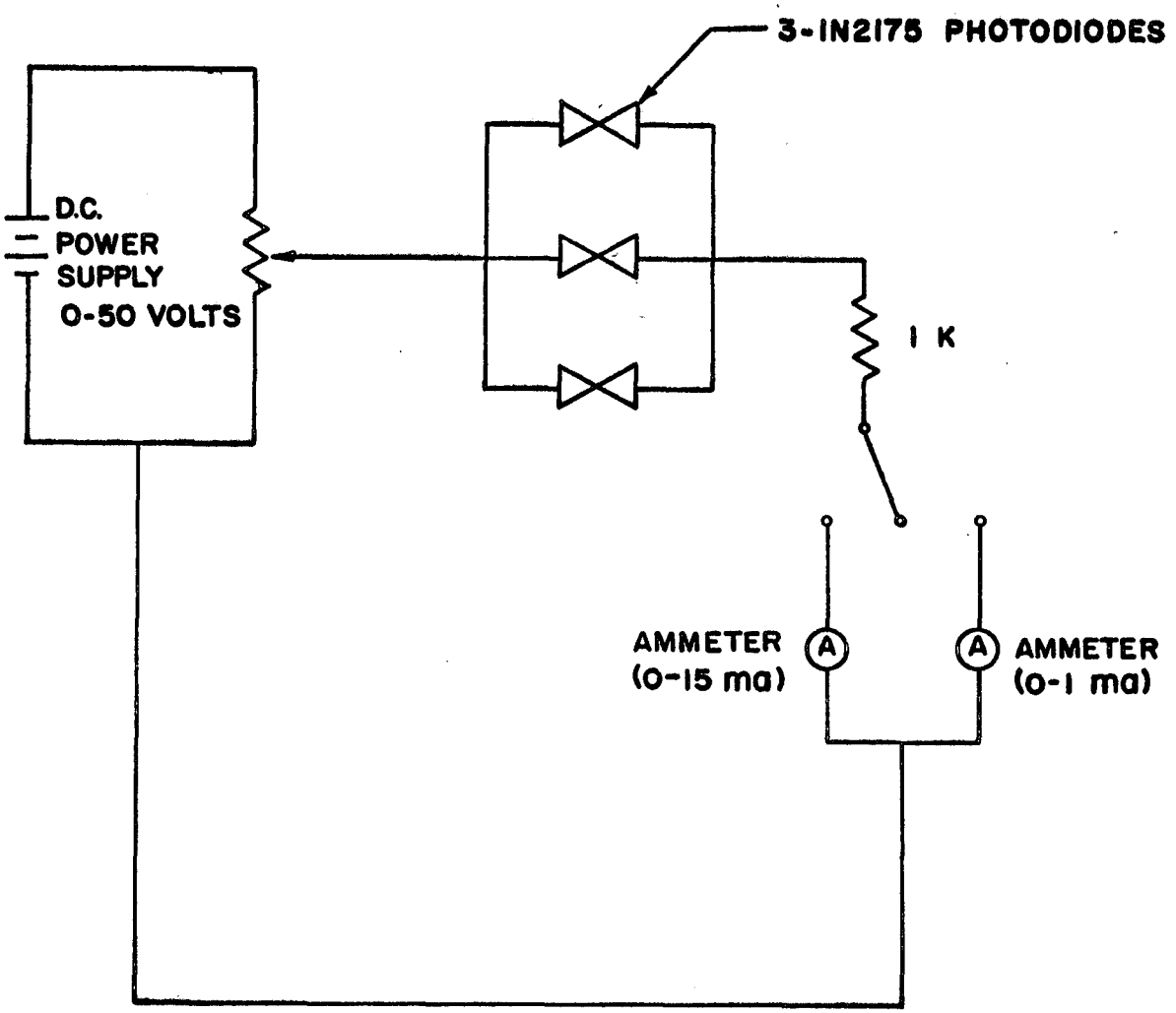

CIRCUIT DIAGRAM FOR LIGHT TRANSMISSION STUDY

FIGURE III-19

FIGURE III-20

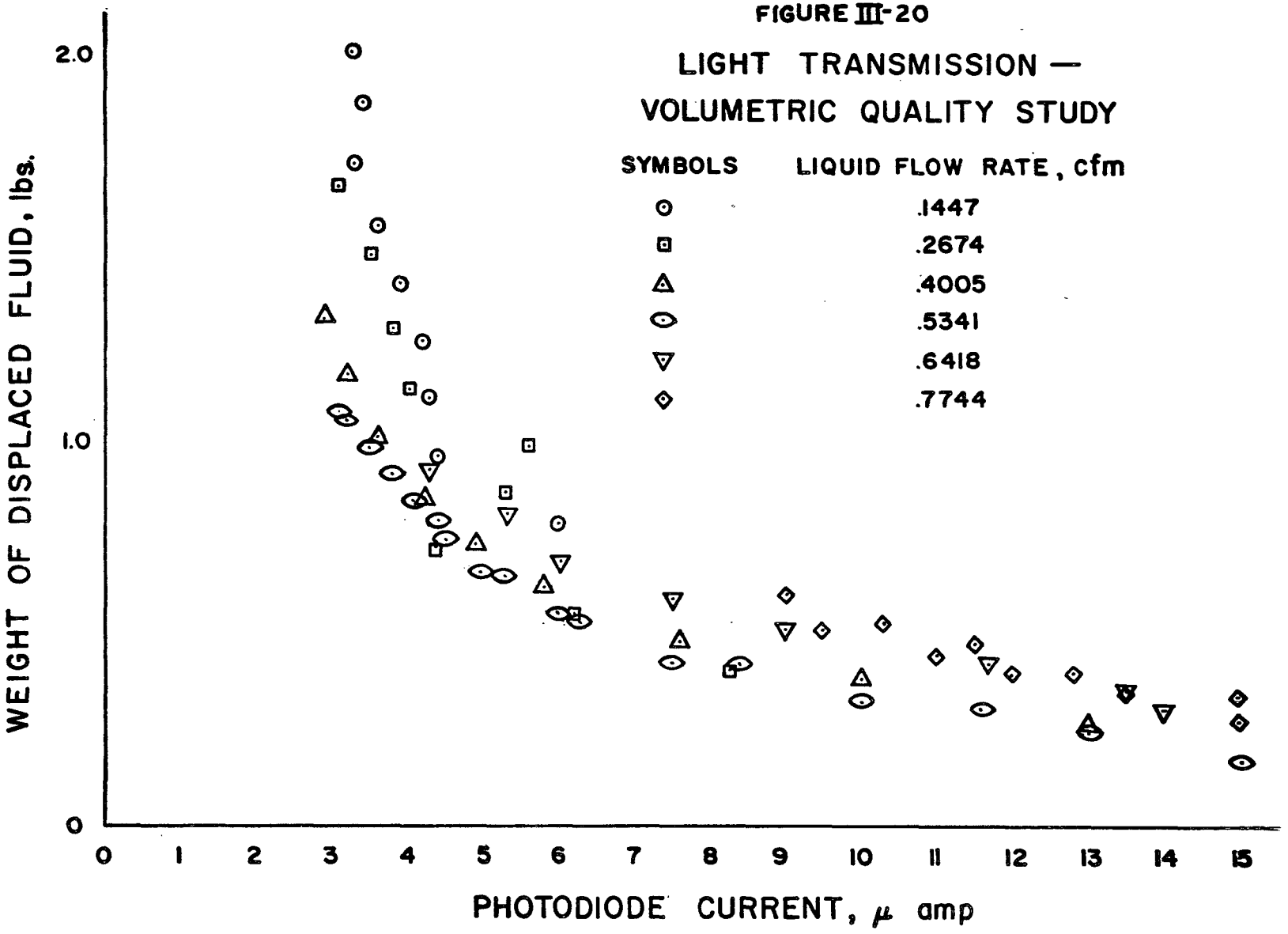

FIGURE III-21

LIGHT TRANSMISSION —

VOLUMETRIC QUALITY STUDY

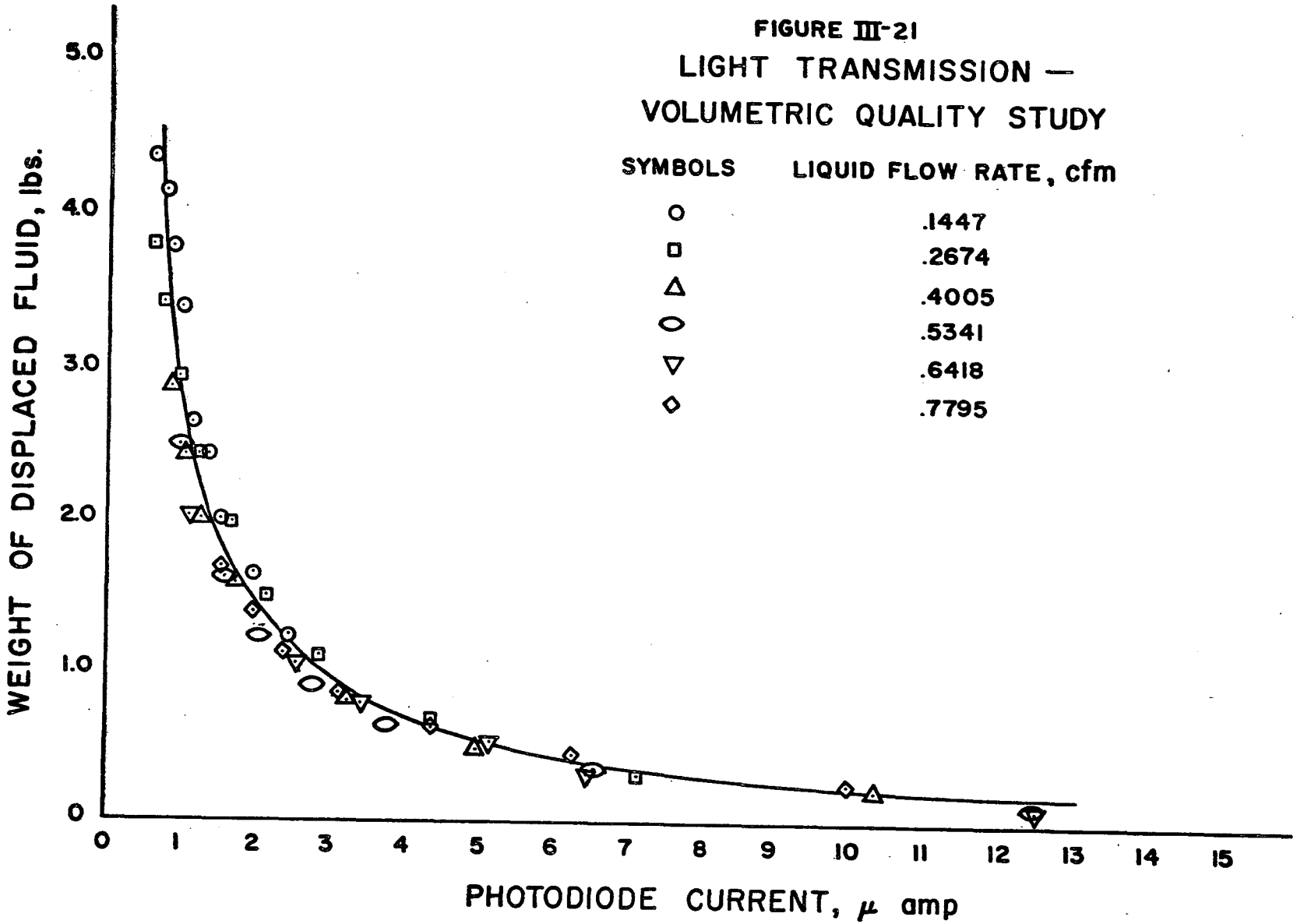

and the photodiode current. The feasibility of this technique also is dependent on the correlation between bed quality (decrease in channel weight) and photodiode current under different flow conditions. For if a unique correlation does not exist as all of the other parameters change, then a more complicated calibration would be required. However, Figure III-21 illustrates a single valued correlation for all flow rates tested, which suggests the possibility that this technique could be refined to measure bed quality in the absence of a gravity field.

IV. ANALYSIS OF RESULTS

In this study three correlation schemes are presented and the advantages of each assessed. First, from a dimensional analysis point of view, the parameters governing the flow are placed into dimensionless groups and their experimental variation presented graphically. Next, the phenomenological description of the flow, expressed mathmatically in equation II-23, is used to determine the dependency of the liquid driving force plus the relative drag term on the liquid Reynolds number. Finally, a modified form of equation II-23 which excludes the Darcy number portion of the correction is used to determine the effect of Gravity-Viscous parameter.

A. Correlation of Data Suggested by Dimensional Analysis

A dimensional analysis, which is presented in the appendix, indicates that under the flow condition studied here the dimensionless liquid driving force, namely the Darcy number, is a function of the volumetric quality Sg, the liquid Reynolds number Re_ℓ, the bed to bead ratio D/d, and the

Grashof number as indicated below

$$Da = \frac{\partial H}{\partial x} \frac{d^2}{\mu_\ell V_\ell} = f\,(Sg,\ Re_\ell\ ,\ D/d,\ Gr) \qquad \text{IV-1}$$

Therefore, the data is presented plotting the liquid driving force or Darcy number versus the liquid Reynolds number for constant values of volumetric quality. Three families of curves are presented for three different values of bed to bead ratio D/d and Grashof number.

The variation in the bed to bead ratio D/d is taken into account by an edge effect correction proposed by Rose and Rizk (28) and is discussed in more detail in section D. The difference in the upward and downward flow results for the three cases studied are primarily due to the relative magnitudes of the viscous, bouyant and inertial forces. The magnitude of the Grashof number indicates the relative size of these effects. Figures IV-1 and IV-2 are the experimental results presented for upward and downward flow respectively through the .88 mm bed which had a Grashof number of 65. The same correlations for the experimental values obtained from the 3 mm bed with a Grashof number of 2700 are graphically presented in Figures IV-3 and IV-4 for upward and downward flow. The results for flow in both directions through the 12.7 mm bed, in which the Grashof number was 202,000, are presented in Figure IV-5.

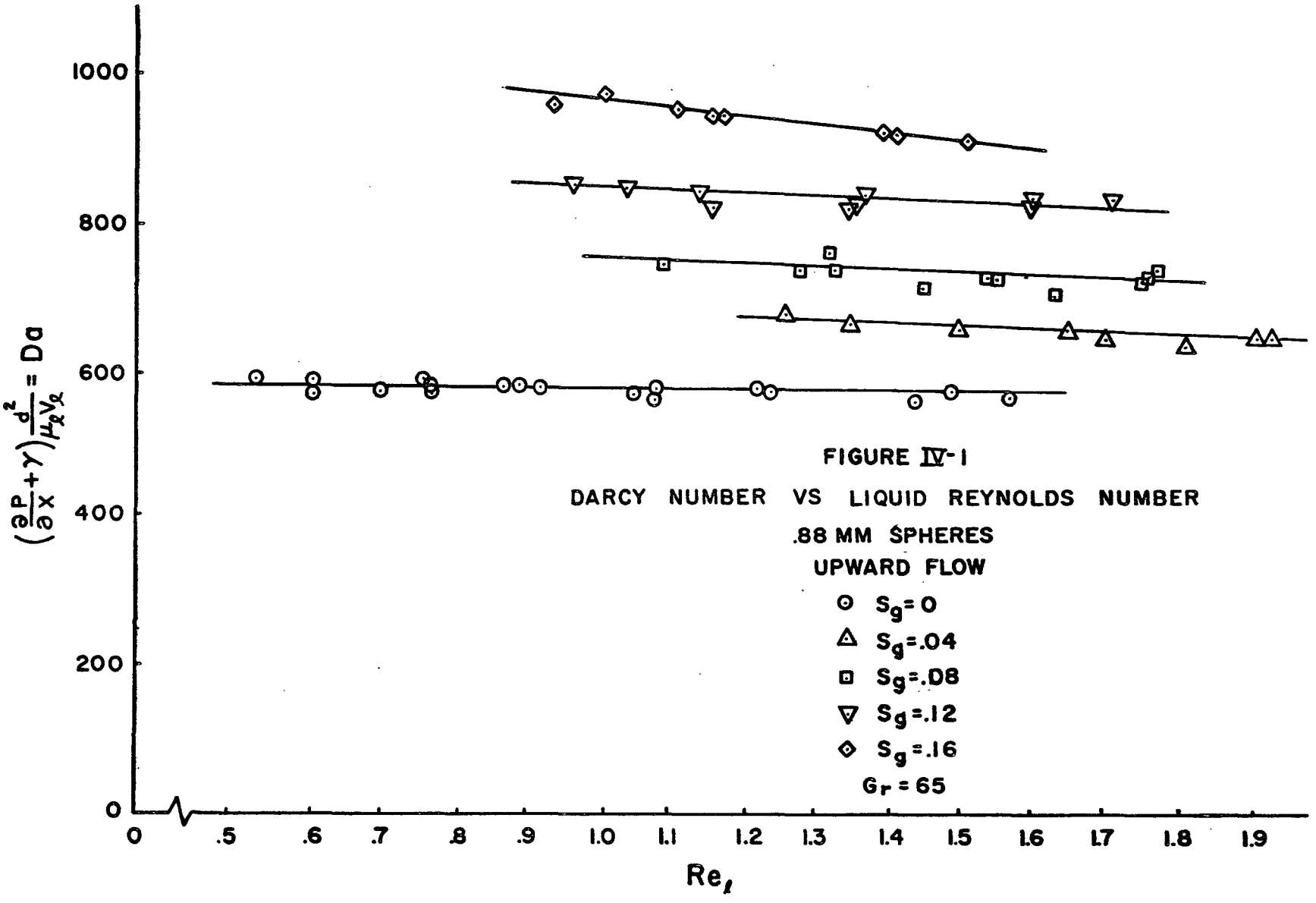
1000
800
600
400
200
0
$\left(\frac{\partial P}{\partial x}+\gamma\right)\frac{d^2}{\mu_\ell V_\ell}=Da$
0
.5
.6
.7
.8
.9
1.0
1.1
1.2
1.3
1.4
1.5
1.6
1.7
1.8
1.9
Re_ℓ
FIGURE IV-1
DARCY NUMBER VS LIQUID REYNOLDS NUMBER
.88 MM SPHERES
UPWARD FLOW
$S_g = 0$
$S_g = .04$
$S_g = .08$
$S_g = .12$
$S_g = .16$
$G_r = 65$

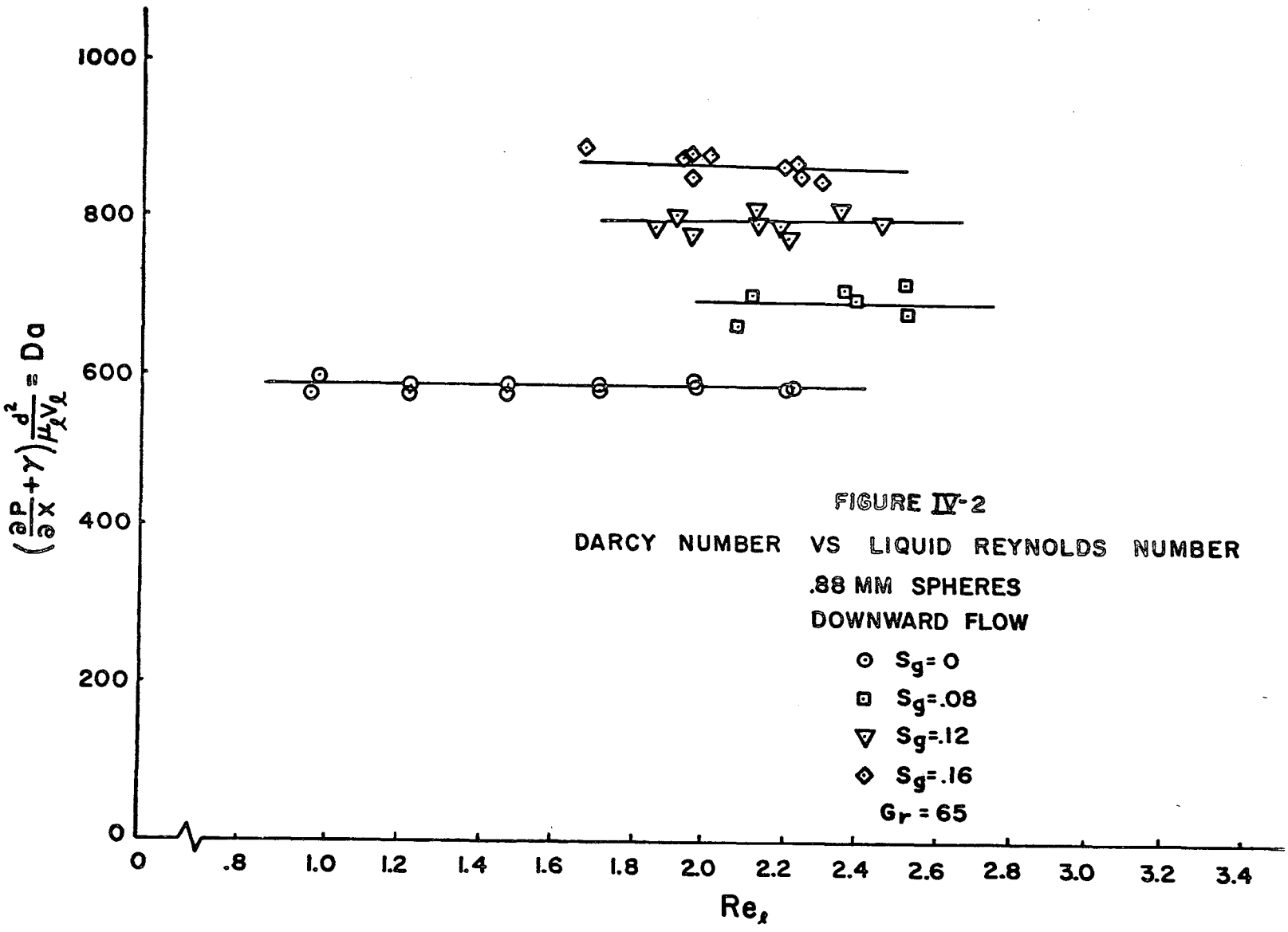

FIGURE IV-2

DARCY NUMBER VS LIQUID REYNOLDS NUMBER

.88 MM SPHERES

DOWNWARD FLOW

⊙ $S_g = 0$

⊡ $S_g = .08$

▽ $S_g = .12$

◇ $S_g = .16$

$G_r = 65$

FIGURE IV-3

DARCY NUMBER VS LIQUID REYNOLDS NUMBER

3 MM SPHERES

UPWARD FLOW

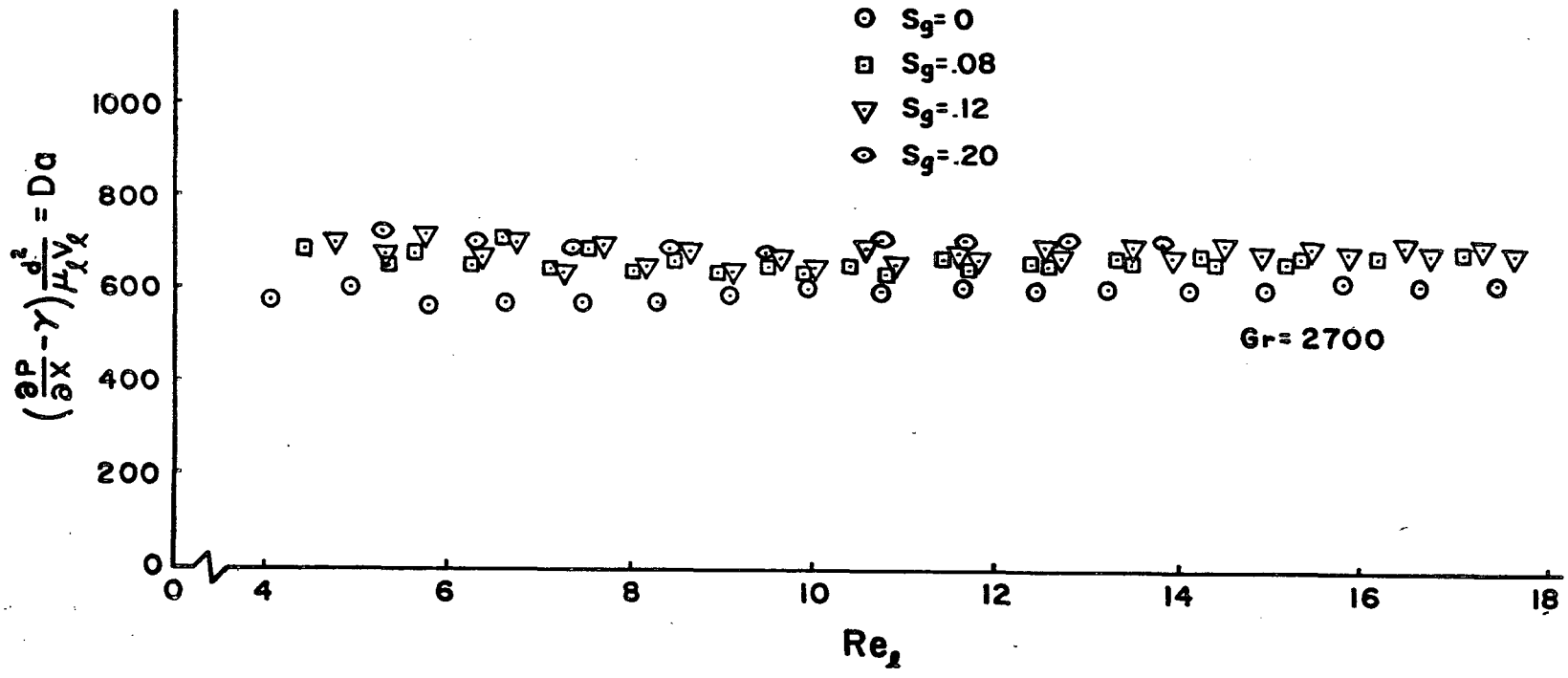

FIGURE IV-4

DARCY NUMBER VS LIQUID REYNOLDS NUMBER

3 MM SPHERES

DOWNWARD FLOW

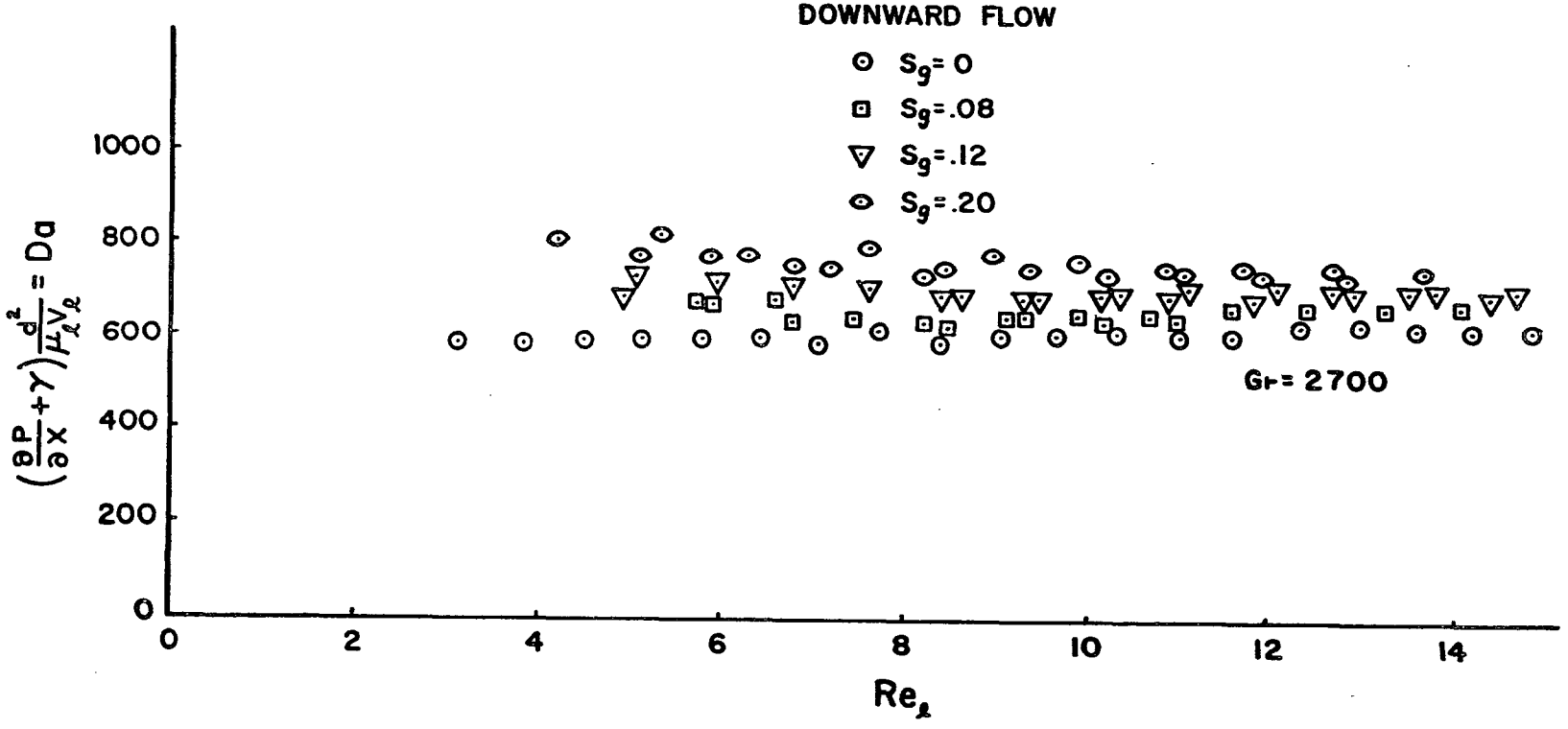

FIGURE IV-5

DARCY NUMBER VS LIQUID REYNOLDS NUMBER

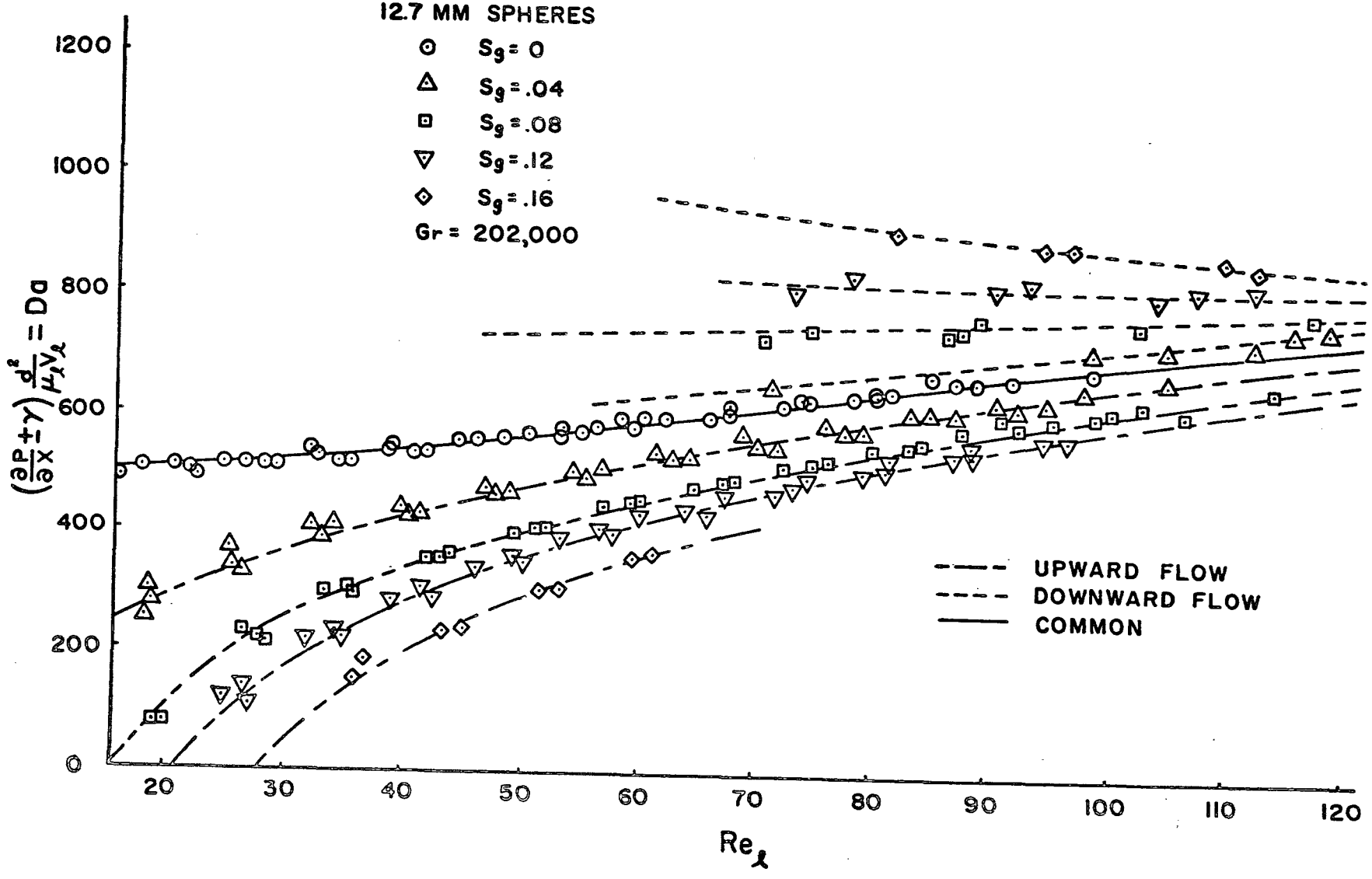

Comparing the results for upward and downward flow through the three beds reveals that the two flow directions yielded common curves for zero volumetric quality for each of the three Grashof numbers. However, as Sg increased they became progressively more dissimilar as the Grashof number got larger. For instance, in the case of the bed with a Grashof number of 65, the results for the two flow directions are the same, within experimental measuring capabilities. However, the data for a Grashof number of 2700 show a significantly closer grouping of the Sg = constant curves for the upward flow than for the downward flow. The greatest contrast in results for upward and downward flow was obtained when the Grashof number was 202,000. In this case as the quality was increased, the upward flow curves fell progressively farther below the zero quality curve, while the downward flow curves were spaced increasingly farther above the zero quality curve. All of the curves except that for zero quality exhibited non-linearity, indicating that an empirical equation relating the Darcy number and the liquid Reynolds number would be a polynomial in powers of Re_ℓ .

First, this initial correlation does not present the data in such a way that flow through beds with other Grashof numbers can be predicted without a series of cross plots. Second, separate

curves and empirical relations are required for upward and downward flow conditions for each Grashof number. Finally, different polynomials in powers of Re_ℓ are required to empirically describe the relationship between the Darcy number and liquid Reynolds number for each volumetric quality.

B. Volumetric Quality Prediction

Considering the ratio of the gas to liquid flow rate as the dependent variable, it has been shown in the appendix that the resulting independent variables are the volumetric quality Sg, the modified Reynolds number Re'_ℓ, the bed to bead ratio D/d and the Grashof number Gr.

$$\frac{q_g}{q_\ell} = f(Sg,\ Re'_\ell,\ D/d,\ Gr) \qquad \text{IV-2}$$

An alternate form of this relation can be written as

$$Sg = f\left(\frac{q_g}{q_\ell},\ Re'_\ell,\ D/d,\ Gr\right) \qquad \text{IV-3}$$

To illustrate the possibility of predicting the volumetric quality when the remaining parameters are known, the ratio of the gas to liquid flow rate is plotted versus the volumetric quality for constant values of modified liquid Reynolds number. These results presented for upward and downward flow in Figures IV-6 and IV-7 were obtained for a bed with a D/d ratio

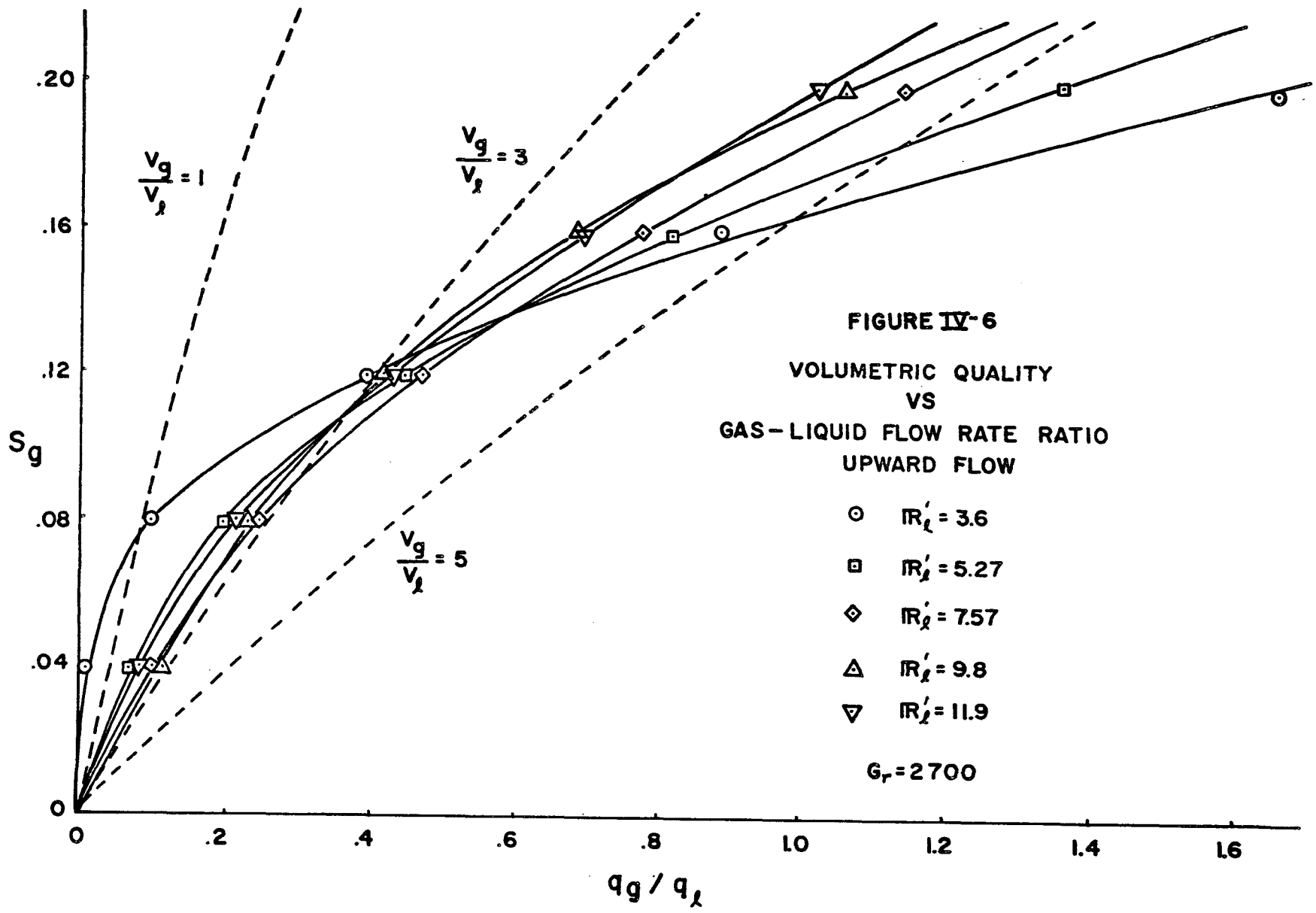
.20
.16
.12
.08
.04
0
S_g
$\frac{V_g}{V_\ell} = 1$
$\frac{V_g}{V_\ell} = 3$
$\frac{V_g}{V_\ell} = 5$
0
.2
.4
.6
.8
1.0
1.2
1.4
1.6
q_g / q_ℓ
FIGURE IV-6
VOLUMETRIC QUALITY
VS
GAS-LIQUID FLOW RATE RATIO
UPWARD FLOW
$IR'_\ell = 3.6$
$IR'_\ell = 5.27$
$IR'_\ell = 7.57$
$IR'_\ell = 9.8$
$IR'_\ell = 11.9$
$G_r = 2700$

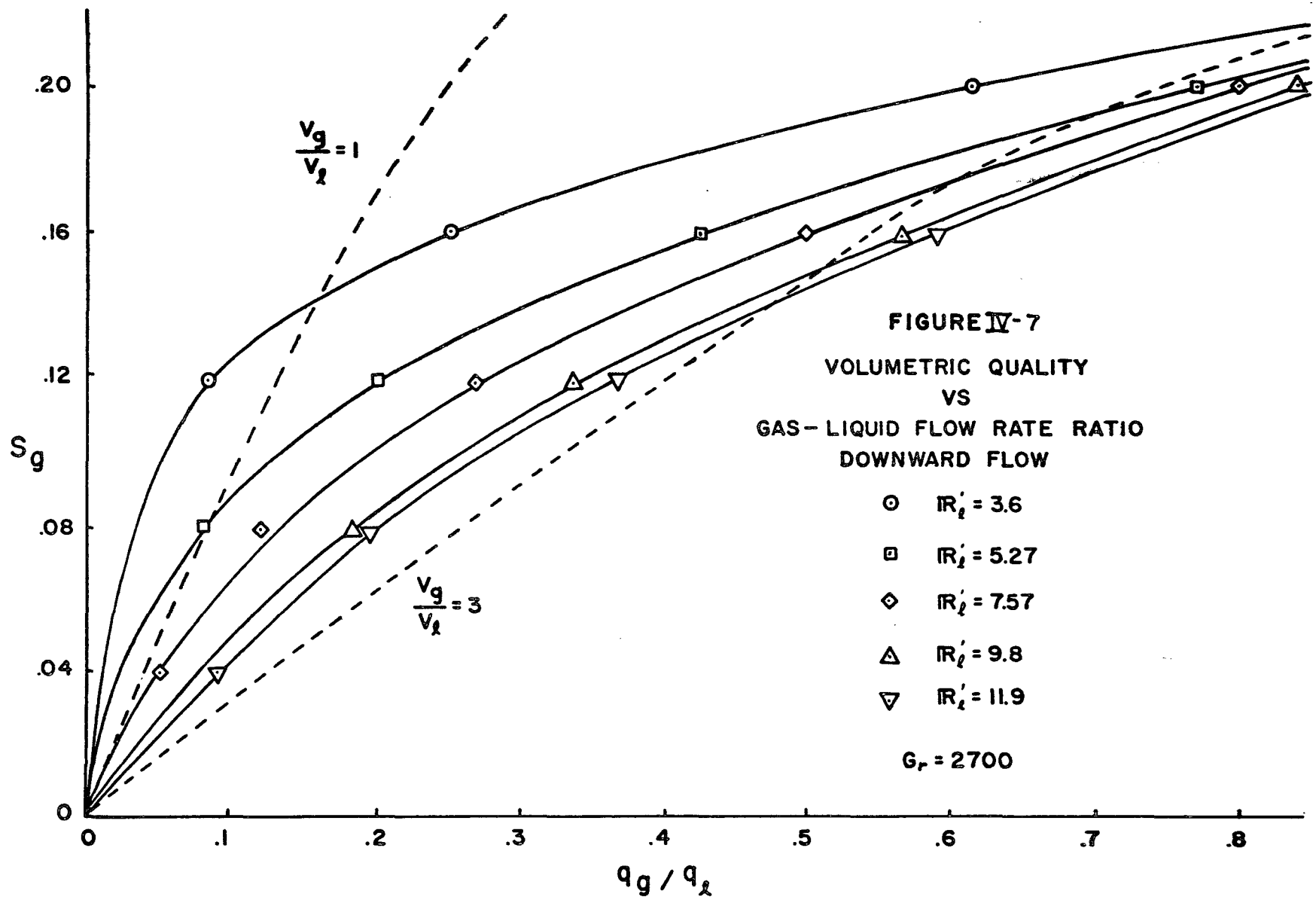
.20
.16
.12
.08
.04
0
S_g
$\frac{V_g}{V_l} = 1$
$\frac{V_g}{V_l} = 3$
0
.1
.2
.3
.4
.5
.6
.7
.8
q_g / q_l
FIGURE IV-7
VOLUMETRIC QUALITY
VS
GAS – LIQUID FLOW RATE RATIO
DOWNWARD FLOW
$IR_l' = 3.6$
$IR_l' = 5.27$
$IR_l' = 7.57$
$IR_l' = 9.8$
$IR_l' = 11.9$
$G_r = 2700$

of 34 and a Grashof number of 2700. The dotted lines in each of these graphs represent the conditions when the bulk velocity of the liquid and gas are as indicated. It should be noted that the velocity of the gas bubbles is considerably larger than the liquid velocity for most of the data points.

C. High Speed Photographic Data

The acquisition of high speed photographic data was performed for two principal purposes. First, it was necessary to determine the characteristics of the flowing gaseous mass under a wide variation of flow conditions. For instance, initially it was not apparent that the gaseous flow was in the form of bubbles. To the naked eye it appeared that it was occurring in continuous streams in the tortuous channels. Second, it was of interest to measure the actual velocity of individual bubbles with the aim of averaging a large number of these velocities and comparing this velocity with the value which was calculated in terms of the gas flow rate, the volumetric quality, the channel area A and the bed porosity φ as indicated below:

$$Vg = \frac{q_g}{A\varphi Sg} \qquad \text{IV-4}$$

The high speed photographs definitely showed that for the present range of flow parameters, the gas flowed in the form

of individual bubbles. In addition, the size of the bubbles were revealed to be of the same order of magnitude as the size of the solid particles comprising the porous bed and their shape was approximately spherical when the bubbles were less than about half the size of the solid particles. For larger bubbles, their shape conformed to the geometry of the particular pore in which the bubble was located. Extensive studies of the photographic data showed that bubbles broke before becoming large enough to occupy more than one pore space (For the present purpose a pore space is defined as the void volume of approximately the size of a solid particle). These studies also revealed the absence of gas-solid interfaces. In other words, each gas bubble was completely surrounded by liquid. This observation formed the initial basis for the neglect of gas to solid drag terms. However, it became apparent that this assumption of negligible solid to gas drag effect is not valid when the relative velocity between the gas and liquid is zero. Therefore, for convenience in the phenomenological description of the flow, the gas bubbles are considered spherical and equal in size to the solid particles. The deviations from actuality are handled by a constant K which was determined experimentally.

The velocity of the gaseous phase was determined in the two ways described above and compared in Figure IV-8, where

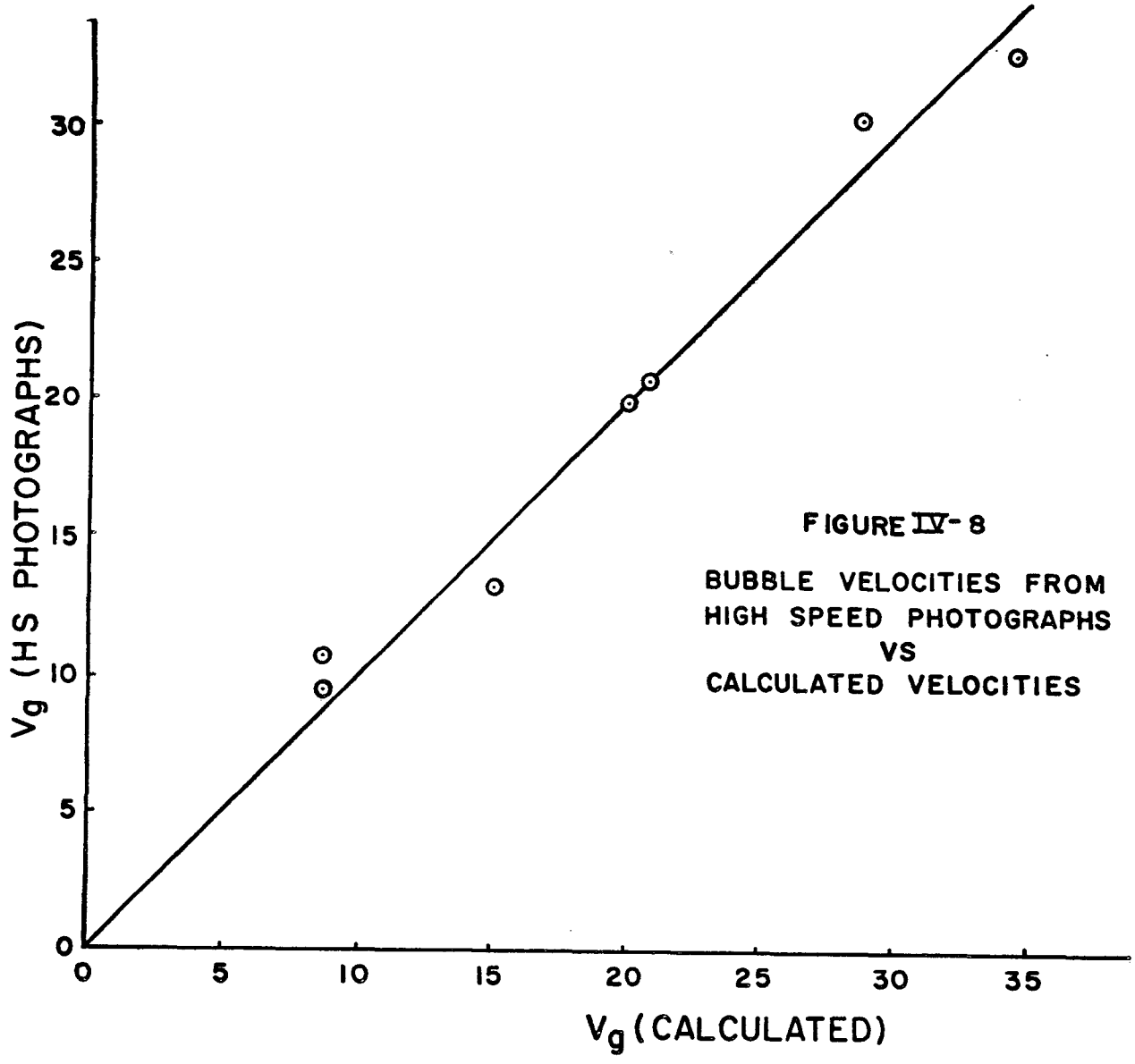

FIGURE IV-8

BUBBLE VELOCITIES FROM HIGH SPEED PHOTOGRAPHS VS CALCULATED VELOCITIES

deviations from the solid line indicate the degree of discrepancy. The agreement illustrated here shows that within experimental error the calculated bulk velocity from equation IV-4 is numerically equal to the average velocity of the individual bubbles as determined from the high speed photographs.

D. Correlation Utilizing the Darcy Number Plus the Gas Bubble Drag Term

The dissimilarity of the data for the three porous beds was hypothesized to be due to the drag force between the liquid and gas bubbles and to the varying degrees of edge effects present in the various packed beds.

In reference to the relative drag effect, it can be observed that in the finer media the bubbles are broken into very small sizes to the point that the gas and the liquid flow at approximately the same velocity. Larger bubbles, however, are driven by the pressure gradient at velocities that can greatly exceed that of the liquid. When the bubbles are traveling faster than the liquid phase, they exert a positive drag force on the liquid.

A suitable prediction of the magnitude of this relative drag force in terms of the other flow parameters permits its inclusion in an equation for the liquid driving force as indicated in equation II-12. When this force is transposed to the left

hand side as in equation II-23 and as repeated here:

$$(\text{Da} + \text{Relative Drag Force} = \alpha_1 + \beta_1 \, \text{Re}_\ell)$$

and the resultant force plotted versus the liquid Reynolds number, common curves for upward and downward flow were expected to result for a given value of volumetric quality. This deduction resulted from the prediction that α_1 and β_1 are functions of the geometry of the porous bed and the volumetric quality and are independent of flow direction.

The data for each of the Grashof numbers were correlated in this manner and the upward and downward flow curves for a given volumetric quality were brought into the expected coalescence. In view of the great disparity between the upward and downward flow, especially in the case where the Grashof number was 202,000, it was felt that this remarkable coalescence was evidence of the basic correctness of the phenomenological description of the flow. As an example of this correlation, the 12% volumetric quality curve is presented in Figure IV-9. The presentation of the complete data in this manner is deferred until the correction for edge effects is made in the next paragraph.

The discontinuities in the data for the three porous beds were due to a phenomenon called edge effects which is a function of D/d. For example, an examination of the cross

DARCY NUMBER PLUS RELATIVE DRAG CORRECTION
VS
LIQUID REYNOLDS NUMBER
BEFORE CORRECTION FOR EDGE EFFECTS
FOR $S_g = .12$

FIGURE IV-9

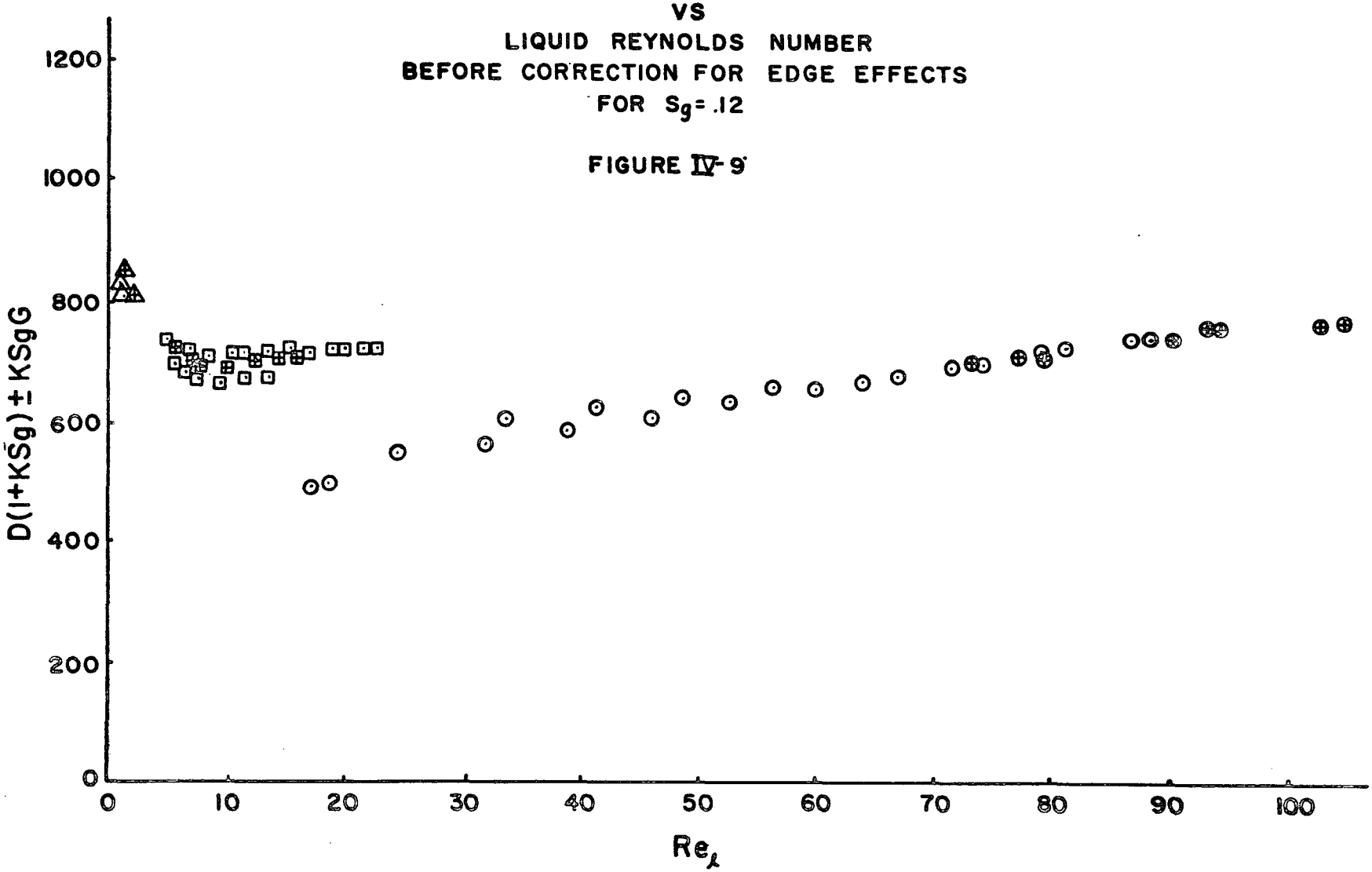

section of a porous bed reveals that the porosity of a bed is greater in the layers next to the wall of the channel than in those nearer the middle of the bed. This appears to be due to two factors. First, the random packing at the interior of the channel has three degrees of freedom while the wall provides a constraint for those particles adjacent to it, yielding for these particles only two degrees of freedom. Second, the wall offers a flat surface for the spherical particles to contact rather than the irregular surface furnished by a layer of particles which allows intermeshing of subsequent layers. The passages in this area of higher porosity are less tortuous than those areas more closely packed, and will thus offer lower resistance to flow than areas having more tortuosity.

Saunders and Ford (29) determined with a pilot tube survey of the exit surface of a porous bed, that the velocity was approximately constant across a bed except in a layer about one particle thickness from the wall. This area was found to have a velocity about 50% greater than other points in the interior. Since this region of relatively low resistance is limited to one particle diameter in depth, the reduction in resistance of the entire bed due to this effect is related to the ratio of bed size D to the size of a particle comprising the porous bed d.

Experimental determinations of this effect have been

obtained by Rose and Rizk (28) for channels with circular cross sections. Their results are depicted graphically in Figure IV-10. These curves indicated that the effect of the wall depends upon the Reynolds number and that experimental data obtained at small values of D/d with wide variations in Reynolds number would be subject to considerable uncertainty if a suitable correction is not made for wall effects. However, when the bed to bead ratio is greater than about 40, the correction may for most purposes be neglected since the wall effect correction is less than the normal uncertainties involved in the data collection.

The experimental data displayed in Figure IV-9 were taken from three beds having different bed to bead ratios. For instance, the bed comprised of .88 mm particles had a D/d ratio of 115. This ratio for the 3 mm bed was 34. For the bed packed with 12.7 mm spheres the bed to bead ratio was 8. This explains why the data points do not coincide in regions of common liquid Reynolds numbers. Therefore, an edge effect correction was applied to all data points except those obtained from the .88 mm bed. In particular, the data obtained from the 12.7 mm bed was corrected by a factor of 1.26, while the 3 mm data required a correction of 1.09. The curves shown in Figures IV-11 and IV-12 exhibit the expected continuity for the experimental points obtained from different beds with common Reynolds

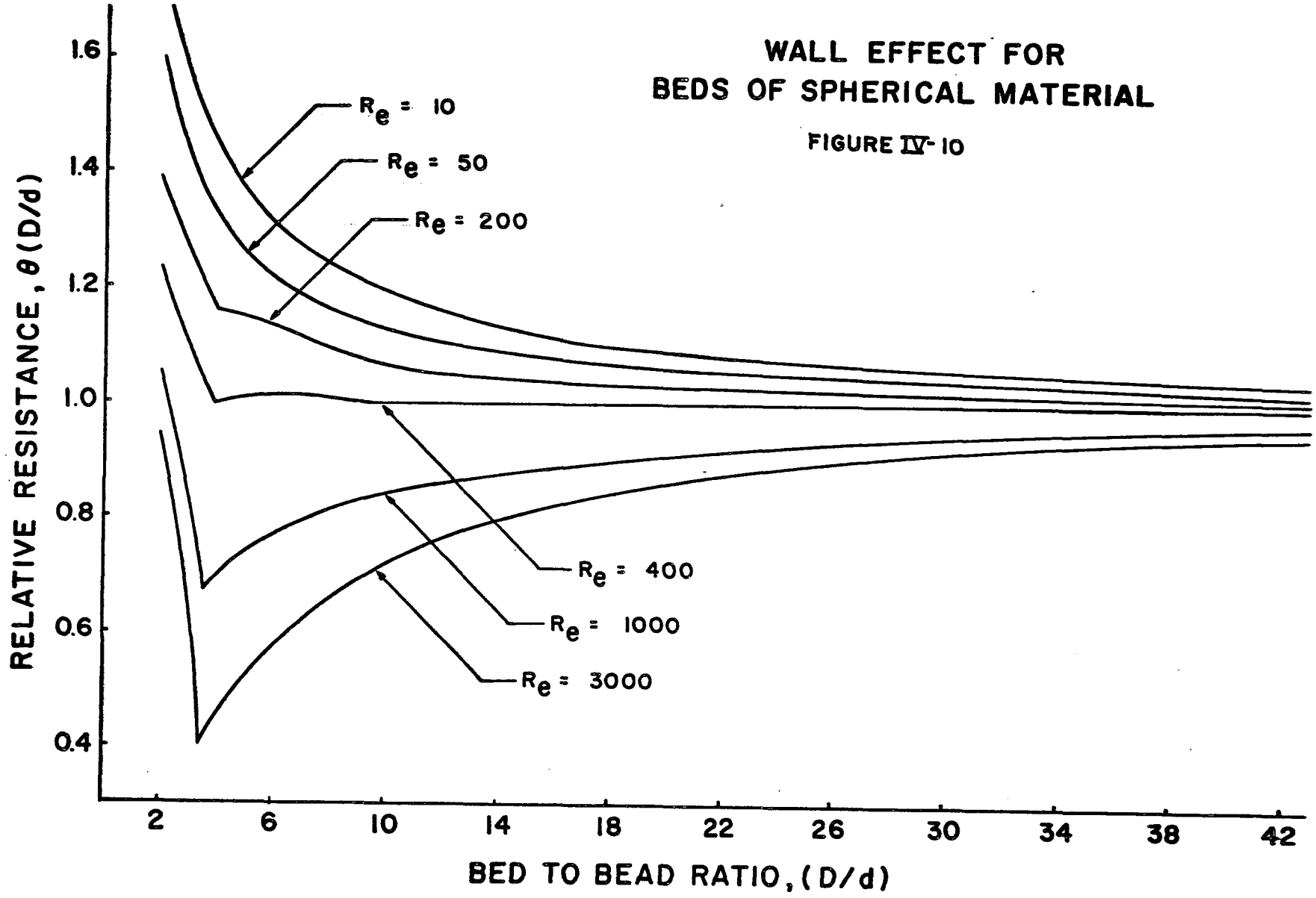
WALL EFFECT FOR
BEDS OF SPHERICAL MATERIAL
FIGURE IV-10
RELATIVE RESISTANCE, θ(D/d)
BED TO BEAD RATIO, (D/d)
Re = 10
Re = 50
Re = 200
Re = 400
Re = 1000
Re = 3000
1.6
1.4
1.2
1.0
0.8
0.6
0.4
2
6
10
14
18
22
26
30
34
38
42

DARCY NUMBER PLUS RELATIVE DRAG CORRECTION
VS
LIQUID REYNOLDS NUMBER
UPWARD FLOW

FIGURE IV-11

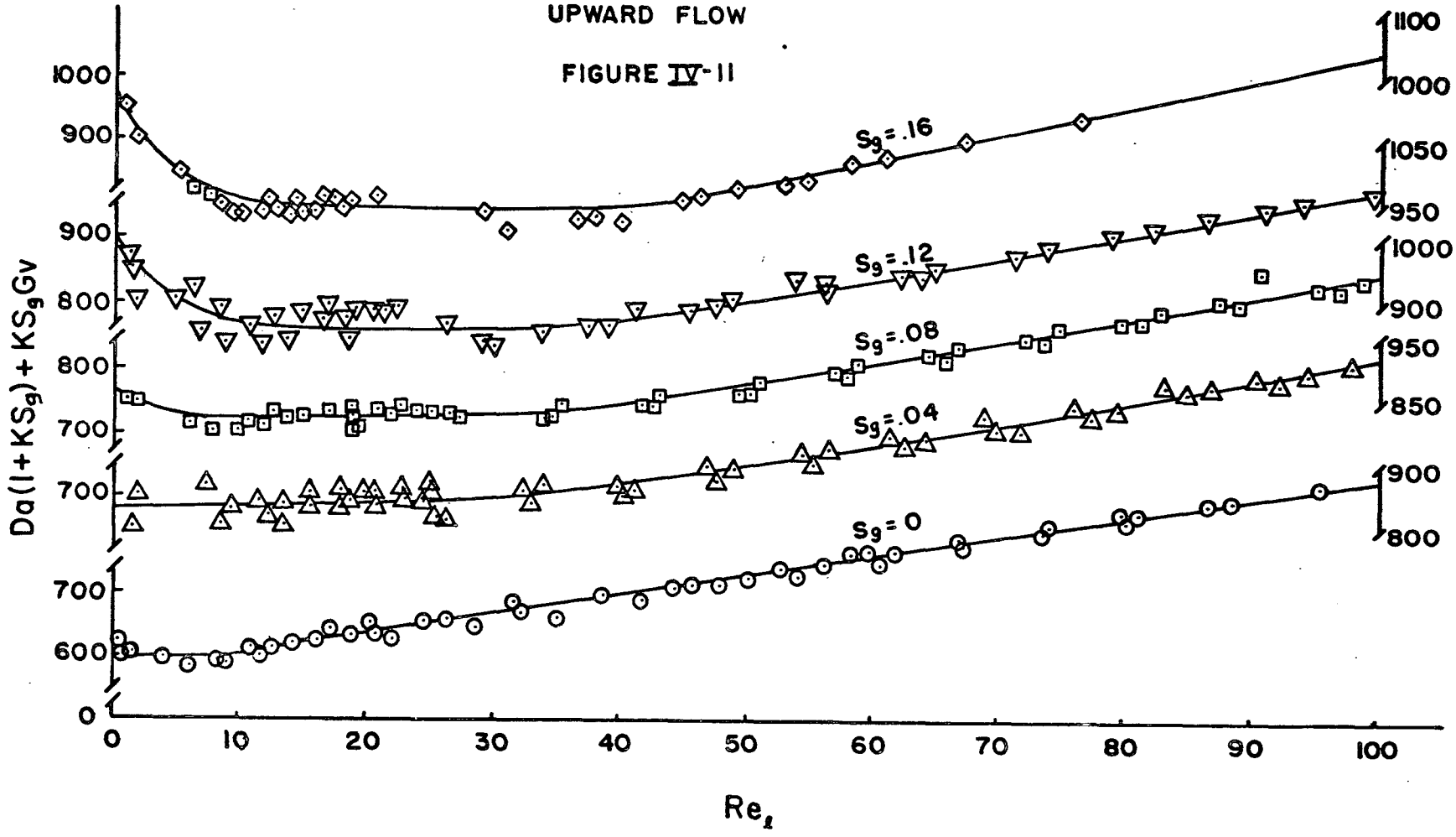

DARCY NUMBER PLUS RELATIVE DRAG CORRECTION
VS
LIQUID REYNOLDS NUMBER
DOWNWARD FLOW
FIGURE IV-12

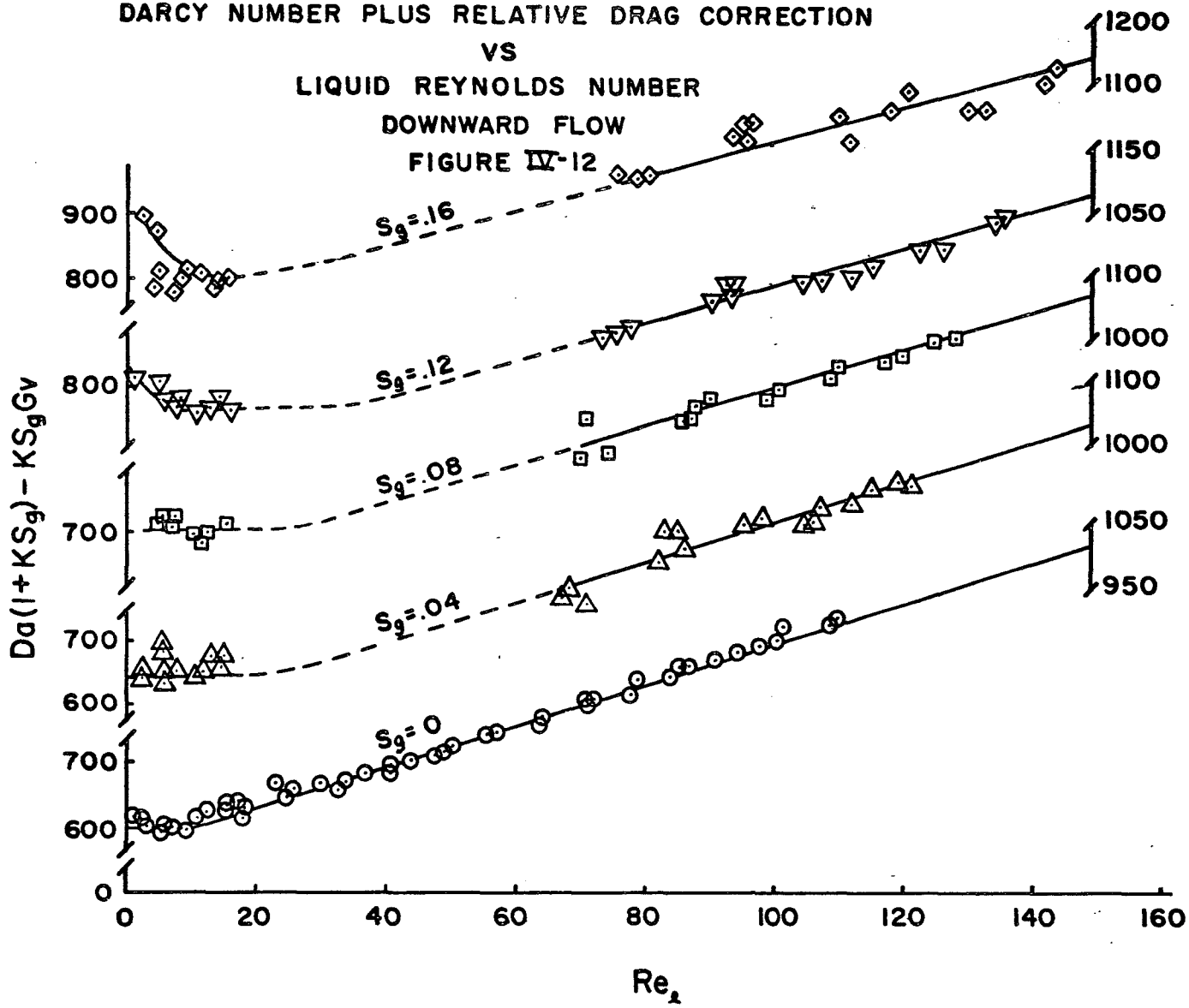

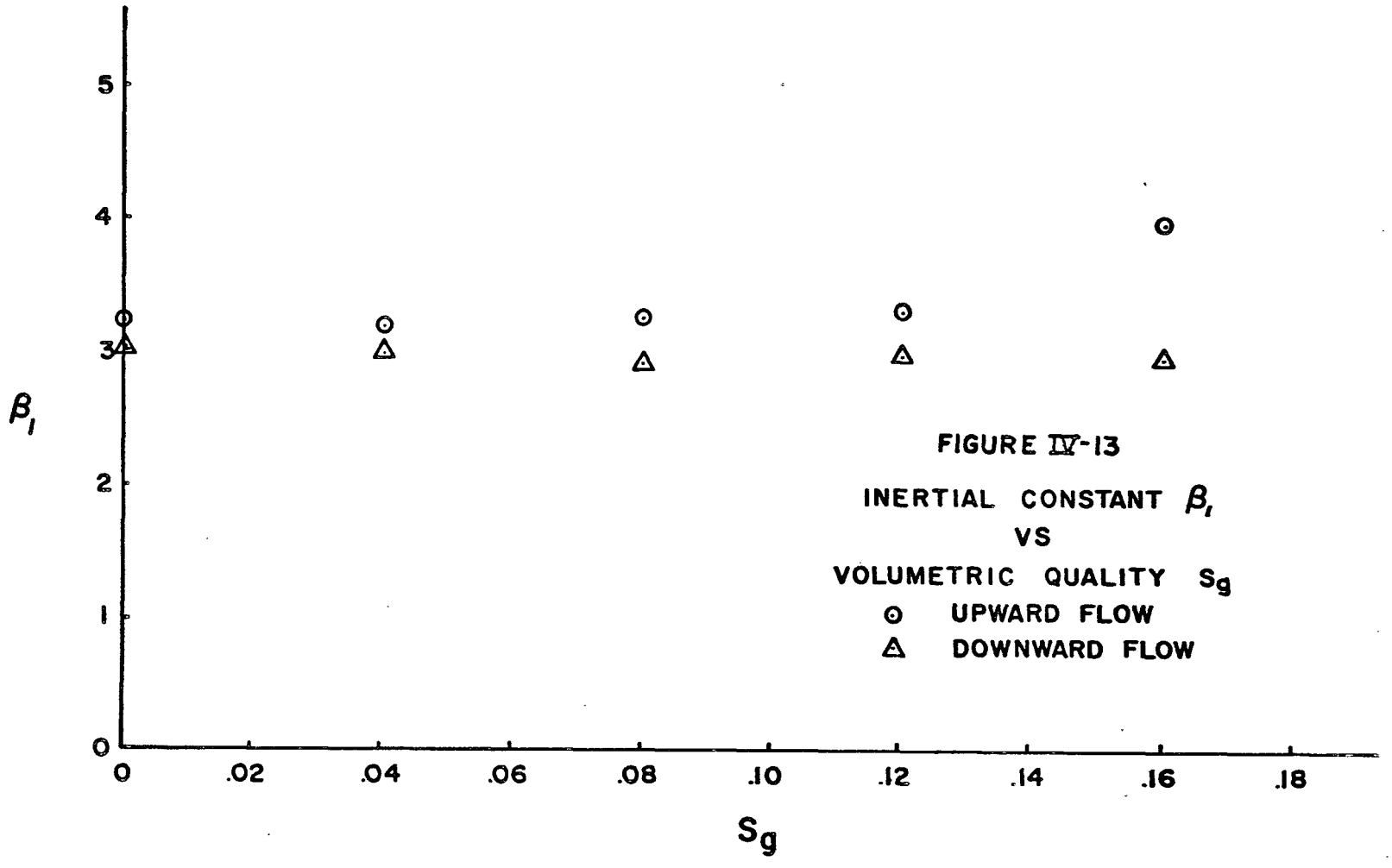

FIGURE IV-13

INERTIAL CONSTANT β_1
VS
VOLUMETRIC QUALITY S_g
⊙ UPWARD FLOW
△ DOWNWARD FLOW

numbers.

The fact that these curves are straight lines for large Reynolds numbers lends credence to the assumption that the liquid-solid drag is as postulated in Chapter II and expressed mathematically by equation II-23. The slope of each curve represents the value of the inertial constant β_1 for various values of volumetric quality, Sg. Figure IV-13 illustrates that the value of β_1 is approximately constant for all of the volumetric qualities obtained in this study. The viscous constant α_1 is numerically equal to the zero intercept of the sloping portion of the curve. The variation of α_1 with volumetric quality is illustrated graphically in Figure IV-14.

As the liquid Reynolds number is decreased, a regime of flow is encountered where the inertial effects are apparently negligible. For example, when the slope of the curves in Figures IV-11 and IV-12 become horizontal, the inertial constant β_1 is zero which implies that the pressure gradient is proportional to the first power of the velocity. This constant of proportionality, which is the ordinate magnitude of the horizontal part of the curves, bears some resemblance to the permeability defined by Darcy's law. In this region the equation governing the flow can be written as

$$Da\,(1+KSg) \pm KSgGv = \alpha \qquad \text{IV-5}$$

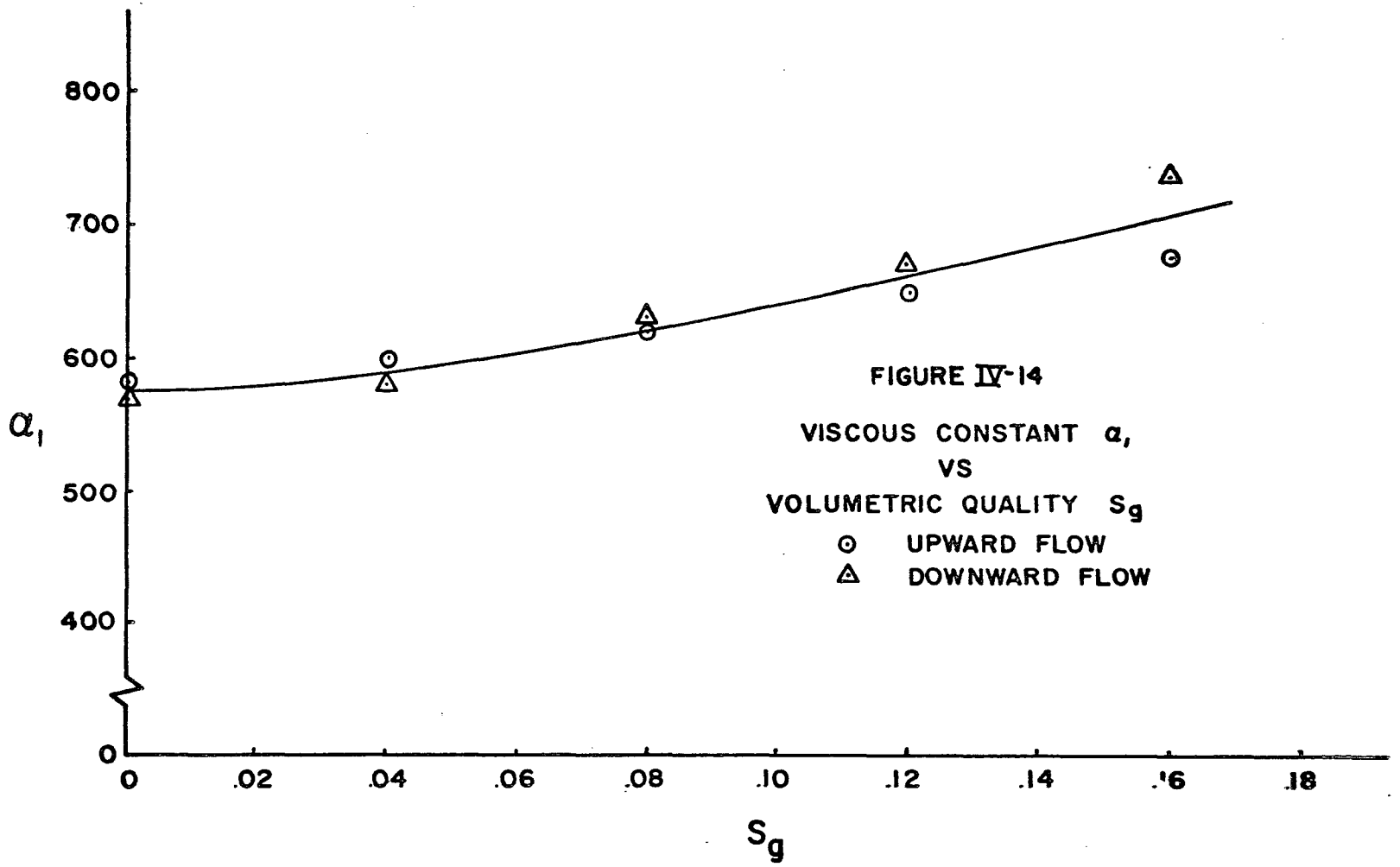

FIGURE IV-14

VISCOUS CONSTANT α_1
VS
VOLUMETRIC QUALITY S_g

⊙ UPWARD FLOW

△ DOWNWARD FLOW

where the value of α is a function of the volumetric quality. This relationship is presented graphically in Figure IV-15. The Reynolds number at the transition from the Darcy type flow to a flow regime which has significant inertial effects can also be seen to be a function of the volumetric quality. For example, the region of Darcy type flow becomes more extensive as the volumetric quality is increased.

At Reynolds numbers less than about two, the horizontal curve is interrupted as the volumetric quality is increased. In this region of flow, the relative velocity between the liquid and gaseous phases is known to be very small so that the contribution of the relative drag term and the drag of the solid particles on the gaseous phase (see equation II-14) are of the same order of magnitude. In which case, the value of the relative drag term is not merely proportional to the sum of the Darcy number plus the gravity-viscous parameter, but must also include the effect of the solid particles on the gaseous phase, which is represented by the second term on the right side of equation II-14. It is noted that this second term has been negligible in the previous correlations. A scheme for determining the contribution of both of these effects when they are the same order of magnitude is not presently available.

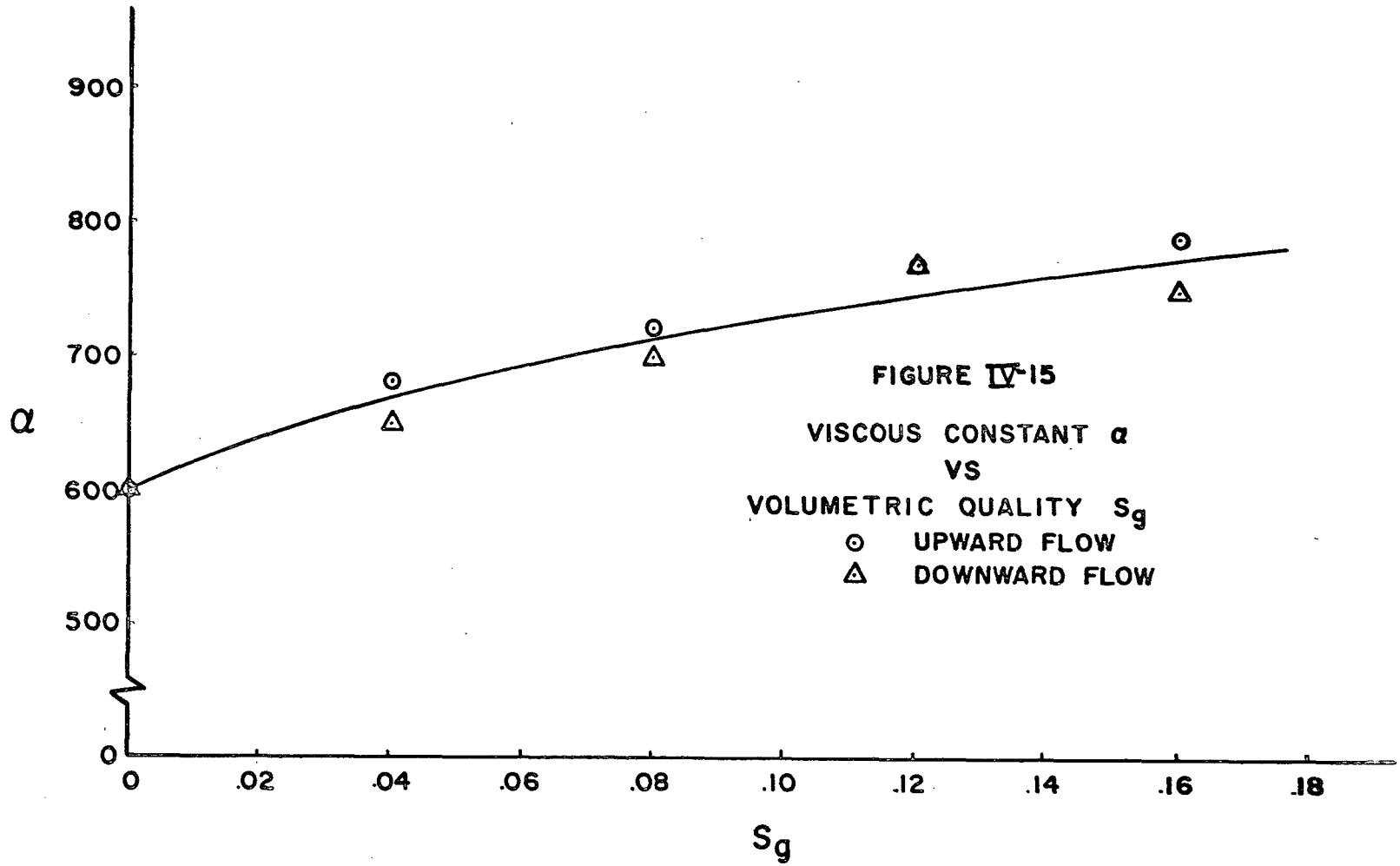

FIGURE IV-15

VISCOUS CONSTANT α
VS
VOLUMETRIC QUALITY S_g
⊙ UPWARD FLOW
△ DOWNWARD FLOW

A very important result of this study has been the elimination of the dissimilarity in the data for upward and downward flow. The fact that the phenomenological description of equation II-23 accounted for the effect of gravity in the two flow direction indicated that this description can also be used to predict the flow of a liquid-gas mixture through a porous bed under reduced gravity conditions.

E. Modified Correlation Excluding Darcy Number Correction

The relative drag term which was added to the liquid driving force to consolidate the data presented in section D was composed to two contributions, the Gravity-Viscous parameter and the Darcy number correction. Specifically, the Gravity-Viscous parameter multiplied by empirical constant K and the volumetric quality Sg was added for upward flow and subtracted for downward flow. The second component which is a function of the Darcy number appears as the KSgDa term in equation II-23. It is interesting to note, however, that the only change in the flow equation (II-23) for upward and downward flow is the sign on the Gravity-Viscous parameter Gv. Therefore, if the Darcy number contribution to the relative drag term is the same for upward and downward flow, the data should also consolidate for both flow directions if only the Gravity-Viscous parameter is

included in the left side of equation II-23. In particular, this equation could be altered to the following form

$$Da \pm KSgGv = a_1 + b_1 Re_\ell \qquad IV-6$$

When the Gravity-Viscous correction, KSgGv, was added to the Darcy number for upward flow and subtracted for downward flow and plotted versus the liquid Reynolds number, the resulting curves did indeed consolidate for both directions of flow. But more significantly, the constants a_1 and b_1 of equation IV-6 can be seen (Figure IV-16) to be independent of volumetric quality for Reynolds numbers larger than 25. For smaller Reynolds numbers b_1 becomes very small and the governing equation can be written as

$$Da \pm KSgGv = a \qquad IV-7$$

In equation IV-7 the value of a is a function of the volumetric quality Sg. This representation is valid for Reynolds numbers between 25 and 2. For Reynolds numbers below 2 the relative permeability correlation proposed by Muskat and Meres (22) and presented in Figure I-1 should be used.

F. Sources of Error

In order to properly evaluate the results of this series

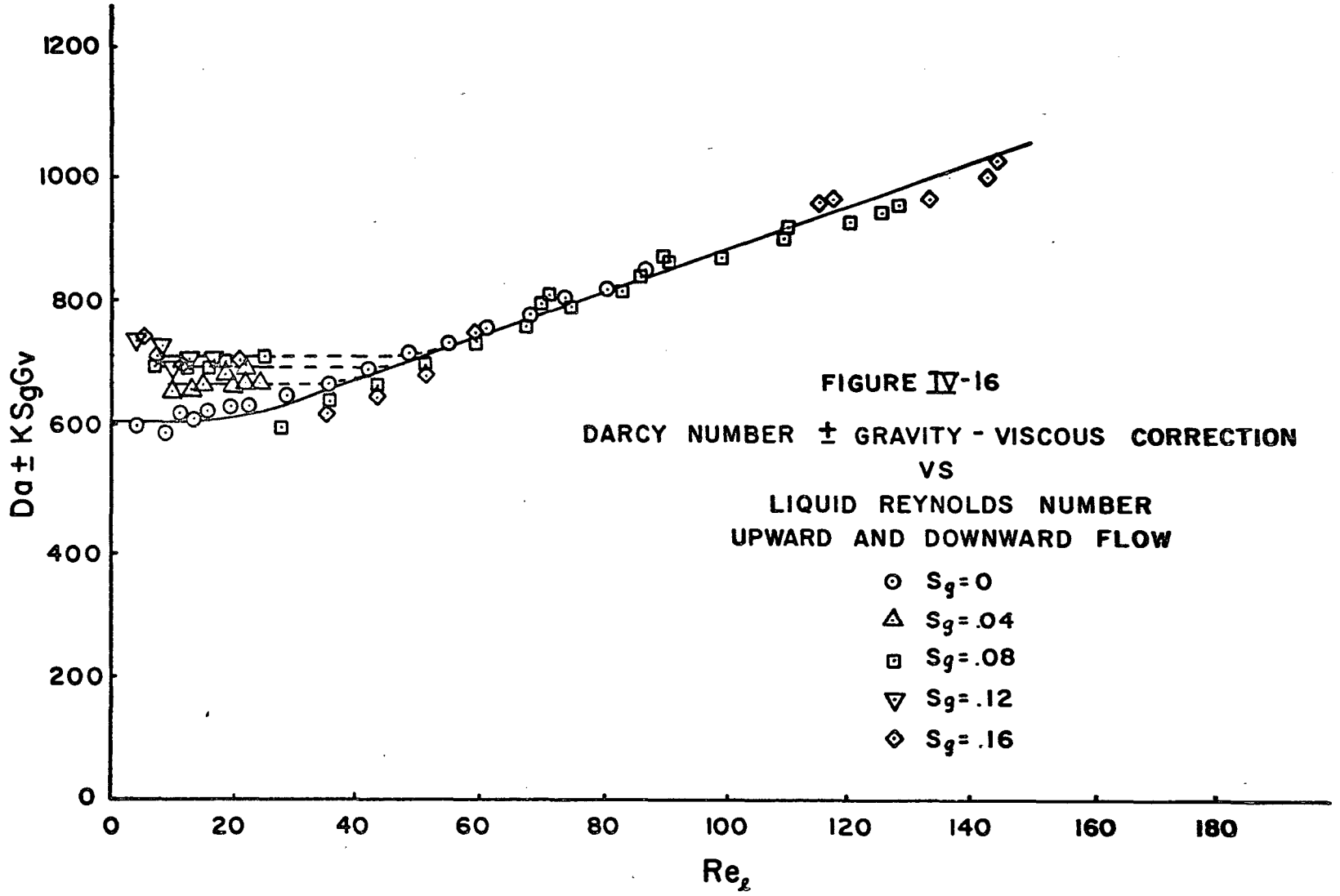

FIGURE IV-16

DARCY NUMBER ± GRAVITY - VISCOUS CORRECTION
VS
LIQUID REYNOLDS NUMBER
UPWARD AND DOWNWARD FLOW

⊙ $S_g = 0$
△ $S_g = .04$
⊡ $S_g = .08$
▽ $S_g = .12$
◇ $S_g = .16$

of tests, it is important to have an awareness of the potential sources of error in the experimental methods. Therefore, the following measurements are discussed in light of the accuracy with which each was made.

1) Pressure Measurements

The pressure gradients for the beds consisting of the two smaller size particles were measured with two bourdon type pressure gauges with an accuracy of 1/4% of full scale. However, the slight amount of unsteadiness experienced under actual test conditions reduced this predicted accuracy to 1/2% of full scale. Therefore, when these gauges were employed at the lower Reynolds number where the pressure drop was of the order of 4 psi, this measurement could be in error by 5%. However, at the higher Reynolds number the pressure drops were in the range of 20 psi reducing the possible error to 1%.

When the channel packed with 12.7 mm particles was tested, the pressure differential was measured with a U tube manometer arrangement that could be read to an accuracy of .2 inches of Cargille fluid. The lowest ratios employed in these tests produced a pressure differential of about 4 inches of Cargille fluid which could be measured with an accuracy of 5%. On the other hand, the highest flow rates yielded a pressure differential of 20 inches of

liquid which could be measured with an accuracy of 1%.

2) Temperature Measurements

Measurements of known temperature standards indicated that the thermocouple-galvanometer arrangement of temperature measurement could be expected to yield an accuracy of one degree fahrenheit. This resulted in a viscosity prediction which varied in accuracy from 1% to 4%.

3) Weight Measurements

The counterbalance arrangement of weighing the channel described in Chapter III could be read with an accuracy of one hundredth of a pound. However, the calibrations that allowed these measurements to be made during actual flow conditions and the small amount of unsteadiness reduced the accuracy of these measurements to 3 hundredths of a pound. This resulted in a potential error of 7% at the lowest volumetric quality and 1 1/2% at the largest quality of 20%.

4) Porosity

Since it was not practical to measure the porosity of the actual bed to be tested, an error resulted in the differences in packing. However, several measurements were made with varying amounts of agitation and it was concluded that this

measurement could be made with an accuracy of 1%. Subsequent pack-down described in Chapter II, however, was measured and the decrease in porosity was calculated which added an additional uncertainity of 1/4%.

5) Liquid Flow Measurements

The rotameters used to measure the liquid flow rate were rated as accurate to 1% of full scale, however, the small unsteadiness with flow increased this uncertainty to 2%. Therefore, the potential error of the lowest flow rates measured with these devices was 10%.

V. CONCLUSIONS AND SUMMARY OF RESULTS

The ultimate goal of this study has been the establishment of relationships that can be used to predict the liquid driving force required to produce the flow of a gas-liquid mixture through a porous bed under varying conditions of gravity.

The results of this investigation have led to the following conclusions:

(1) For the higher Reynolds number range (i.e. for the upward sloping portion of the curves in Figure IV-17) the applicable equation is

$$Da(1+KSg) \pm KSgGv = \alpha_1 + \beta_1 Re_\ell \qquad V-1$$

In equation V-1 α_1 and β_1 are functions of the volumetric quality as shown in Figures IV-13 and IV-14. This expression is valid for both upward and downward flow. It is also postulated that this expression will describe the flow of a liquid gas mixture under an arbitrary gravity condition when suitable values of Gv corresponding to the reduced liquid body force are used.

AVERAGE CURVES
DARCY NUMBER PLUS RELATIVE DRAG CORRECTION
VS
LIQUID REYNOLDS NUMBER

---- DOWNWARD FLOW
—— UPWARD FLOW

FIGURE IV-17

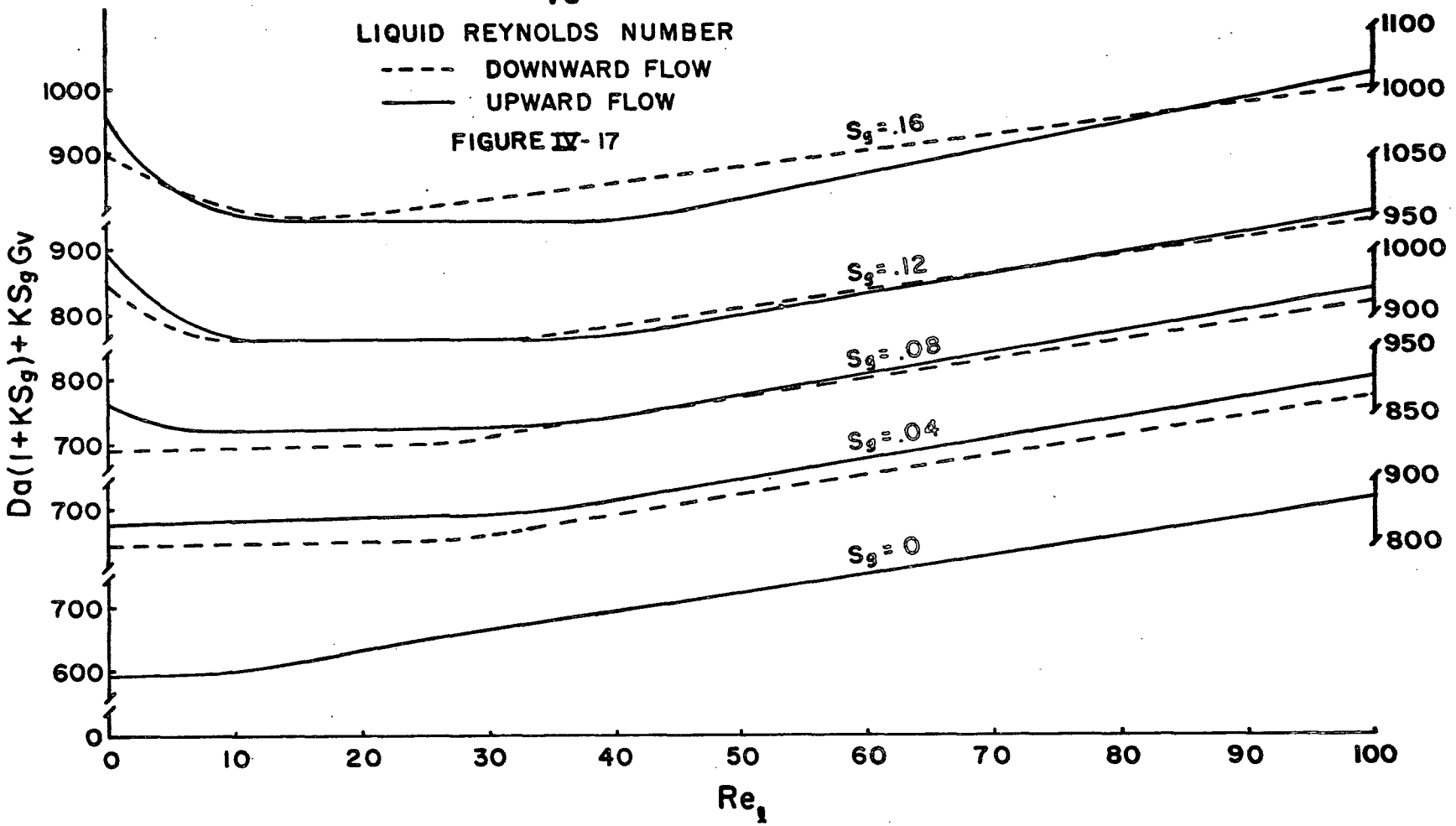

For the range of Reynolds numbers where the curves in Figure IV-11 and IV-12 are horizontal, the following expression is valid:

$$Da(1+KSg) \pm KSgGv = \alpha \qquad V-2$$

(2) For the higher Reynolds number range, the following alternative relation is applicable:

$$Da \pm KSgGv = a_1 + b_1 Re_\ell \qquad V-3$$

This also applies for upward and downward flow and for all values of volumetric quality. Consequently, it is hypothesized that it applies under variable gravity conditions.

When the liquid Reynolds numbers are small enough to yield the horizontal portions of the curves shown in Figure IV-14, and greater than 2 the following expression is valid:

$$Da \pm KSgGv = a \qquad V-4$$

where a is a function of the volumetric quality, but independent of the direction of flow. Therefore, this equation is also hypothesized to be valid for flow under reduced gravity conditions.

Summarizing the results of this study it can be stated that:

(1) The practicality of obtaining visual data for two-phase porous media flow by matching the index of refraction of the liquid phase to that of the solid particles comprising the bed has been established.

(2) The feasibility of measuring volumetric quality by the photodiode measurement of light transmission across the bed has been demonstrated.

(3) For the range of parameters studied in this series of tests, the flow of the gas-liquid mixture has been determined to be of discrete bubble form. Where the size of the bubbles is of the same order of magnitudes as the bed particle size.

(4) By a suitable calibration of the forces exerted by the external fluid lines, the gravimetric method of determining the volumetric quality is possible under actual flow conditions.

Finally, there remains the need for tests conducted under reduced gravity conditions to substantiate the validity of the governing equations proposed in this study.

APPENDIX

DIMENSIONAL ANALYSIS

The gradient of the liquid driving force $\frac{\partial H}{\partial x}$ is chosen as the dependent variable. The independent variables resulting from the steady flow of a liquid-gas mixture through a porous bed are the surface tension σ, the viscosity μ, the velocity V, the density ρ the liquid body force γ, the diameter of a particle of the porous bed d, the width or height of the channel D, the speed of sound C, the porosity of the packed bed φ and the volumetric quality Sg.

The dimensional matrix becomes as shown in Table I where the subscript ℓ refers to the liquid phase and g refers to the gaseous phase.

The matrix of solutions is shown in Table II yielding the dimensionless products.

$$\Pi_1 = \frac{\partial H}{\partial x} \frac{d^2}{\mu_\ell V_\ell} \quad - \quad \text{Darcy number, } D_a \qquad A\text{-}1$$

TABLE I

DIMENSIONAL MATRIX

	a_1	a_2	a_3	a_4	a_5	a_6	a_7	a_8	a_9	a_{10}	a_{11}	a_{12}	a_{13}	a_{14}
	$\frac{\partial H}{\partial x}$	σ	C	Sg	D	γ_ℓ	ρg	Vg	μg	ρ_ℓ	φ	d	V_ℓ	μ_ℓ
M	-1	1	0	0	0	-1	1	0	1	1	0	0	0	1
L	-2	0	1	0	1	-2	-3	1	-1	-3	0	1	1	-1
T	-2	-2	-1	0	0	-2	0	-1	-1	0	0	0	-1	-1

TABLE II

SOLUTION MATRIX

	a_1	a_2	a_3	a_4	a_5	a_6	a_7	a_8	a_9	a_{10}	a_{11}	a_{12}	a_{13}	a_{14}
	$\frac{\partial H}{\partial x}$	σ	ζ	Sg	D	γ	ρg	Vg	μg	ρ_ℓ	φ	d	V_ℓ	μ_ℓ
Π_1	1	0	0	0	0	0	0	0	0	0	0	2	-1	-1
Π_2	0	1	0	0	0	0	0	0	0	0	0	0	-1	-1
Π_3	0	0	1	0	0	0	0	0	0	0	0	0	-1	0
Π_4	0	0	0	1	0	0	0	0	0	0	0	0	0	0
Π_5	0	0	0	0	1	0	0	0	0	0	0	-1	0	0
Π_6	0	0	0	0	0	1	0	0	0	0	0	2	-1	-1
Π_7	0	0	0	0	0	0	1	0	0	0	0	1	1	-1
Π_8	0	0	0	0	0	0	0	1	0	0	0	0	-1	0
Π_9	0	0	0	0	0	0	0	0	1	0	0	0	0	-1
Π_{10}	0	0	0	0	0	0	0	0	0	1	0	1	1	-1
Π_{11}	0	0	0	0	0	0	0	0	0	0	1	0	0	0

$\Pi_2 = \frac{\sigma}{\mu_\ell V_\ell}$	- Surface Tension-Viscous Number, S_T	A-2
$\Pi_3 = \frac{C}{V}$	- (Mach Number, M)$^{-1}$	A-3
$\Pi_4 = Sg$	- Volumetric Quality	A-4
$\Pi_5 = D/d$	- Bed to Bead Ratio	A-5
$\Pi_6 = \frac{\gamma d^2}{\mu_\ell V_\ell}$	- Gravity-Viscous Parameter, Gv	A-6
$\Pi_7 = \frac{\rho_g dV_\ell}{\mu_\ell}$	- Gas-liquid Reynolds Number	A-7
$\Pi_8 = \frac{Vg}{V_\ell}$	- Velocity Ratio	A-8
$\Pi_9 = \frac{\mu g}{\mu_\ell}$	- Viscosity Ratio	A-9
$\Pi_{10} = \frac{\rho_\ell dV_\ell}{\mu_\ell}$	- Liquid Reynolds Number, Re	A-10
$\Pi_{11} = \varphi$	- Porosity	A-11

Since data was obtained for three particle sizes, a dimensionless group was sought which involved only properties of the porous bed and the flowing fluid. Such a parameter would be a constant for any of the three porous beds tested. The only

combination of parameters that would yield such a dimensionless group was obtained by multiplying the Gravity-Viscous parameter times the Reynolds number. This resulted in a parameter which is called the Grashof number Gr that is used in place of the Gravity-Viscous parameter Gv.

$$\Pi_{12} = \Pi_6 \Pi_{10} = Re_\ell Gv = \frac{\gamma_\ell d^3 \rho_\ell}{\mu^2_\ell} = Gr \qquad A\text{-}12$$

The effect of the surface tension forces on the flow was shown in chapter II to be of negligible magnitude. Thus the Surface Tension-Viscous number, which compares the surface tension forces to the viscous, was not considered to be a pertinent parameter. The compressibility effects in these tests were not of the type that lend significance to the Mach number parameter. Therefore, this parameter is excluded from consideration. The viscosity ratio μ_g/μ_ℓ and the porosity φ were essentially constant for these tests and are therefore not included in the list of important dimensionless groups.

In summary, when the dependent variable is the liquid driving force Da, it is found to be related to the volumetric quality Sg, the liquid Reynolds number Re_ℓ, the bed to bead ratio D/d and the Grashof number, that is

$$Da = \frac{\partial H}{\partial x} \frac{d^2}{\mu_\ell V_\ell} = f\,(Sg,\ Re_\ell,\ D/d,\ Gr) \qquad A\text{-}13$$

This is the form used in the presentation of the experimental data in chapter II section A.

An alternative dependent dimensionless parameter of considerable interest is the ratio of gas to liquid flow rate. The independent parameters remain the same except for a change in the definition of the liquid Reynolds number using $\frac{q_g}{\varphi A}$ instead of V_ℓ .

$$\frac{q_g}{q_\ell} = f\,(Sg,\ Re'_\ell\ ,\ D/d,\ Gr) \qquad A\text{-}14$$

LIST OF REFERENCES

1. Adamson, Arthur W. Physical Chemistry of Surfaces. New York: Interscience Publishers, Inc., 1960.

2. Blick, Edward F. "Capillary-Orifice Model for High Speed Flow Through Porous Media," I & EC Process Design and Development, Vol. 5, No. 1, (January, 1966), pp. 90-94.

3. Brownell, Lloyd E. and Katz, Donald L. "Flow of Fluid Through Porous Media-Part II Simultaneous Flow of Two Homogeneous Phases," Chemical Engineering Progress, Vol. 43, No. 11, (November, 1947).

4. Carman, P. C. "Fluid Flow Through Granular Beds," Trans. Institute of Chemical Engineers (London), Vol. 15, 1937, pp. 150-166.

5. Childs, E. C. and Collis-George, N. "The Permeability of Porous Material," Soil Science, 1949, pp. 392-405.

6. D'Arcy, H.P.G. Les fontaines publiques de la ville de Dijon. Paris: Victor Dalmont, 1856.

7. Dupiut, A.J.E.J. Etudes Theoretiques et Pratiques sur le mouvement des Eaux. Paris: Laurent Benoit, 1863.

8. Fatt, I. "The Network Model of Porous Media," Petroleum Transactions AIME, Vol. 207, (1956) pp. 144-181.

9. Forchheimer, P. Hydraulik. Leipzig, Germany: G. B. Teubner, 1914, p. 431.

10. Foreman, J. W., Jr., George, E. W. and Lewis, R.D. "Measurement of Localized Flow Velocities in Gases with a Laser Doppler Flowmeter," Applied Physics, Letters 7, 4, (1965) pp. 77-78.

11. Glaser, M. B. and Mitchell, Litt. "A Physical Model for Mixed Phase Flow Through Beds of Porous Particles," AIChE Journal, Vol. 9, No. 1, pp. 103-106.

12. Hassler, Gerald L., Rice, Raymond R., and Leeman, Erwin H. "Investigation on the Recovery of Oil from Sandstone by Gas Drive," Trans. Am. Inst. Mining Met. Engrs. Vol. 118, (1936) p. 116.

13. Iberall, Arthur S. "Permeability of Glass Wool and other Highly Porous Media," Journal of Research of the National Bureau of Standards, Vol. 45, No. 5, (1950).

14. Kozeny, J. "Uber Kapillare leitung des wassers im boden," Akad. Wiss. Wien. Vol. 136, (1927), p. 303.

15. Lamb, Horace. Hydrodynamics, Cambridge, England: Cambridge University Press, 1924.

16. Landau and Lifshitz. Fluid Mechanics, London: Pergamon Press, 1959.

17. Langhaar, Henry L. Energy Methods in Applied Mechanics, New York: John Wiley and Sons, Inc., 1962, p. 36.

18. Lapple, C. E. and Shepherd, C. B. "Drag on a Sphere," Ind. Eng. Chem. Vol. 32, (1940), p. 605.

19. Leva, Max and Grummer, Milton. "Pressure Drop Through Packed Tubes Part III-Prediction of Voids in Packed Tubes," Chemical Engineering Progress, Vol. 43, No. 12, (December, 1947), pp. 713-718.

20. Leverett, M. C. "Flow of Oil-water through Unconsolidated Sands," Trans. AIME, Vol. 132, (1939), p. 149.

21. Muskat, M. The Flow of Homogeneous Fluids through Porous Media. New York: McGraw-Hill Book Co., 1937.

22. Muskat, Morris and Meres, Milan W. "The Flow of Heterogeneous Fluids through Porous Media," Physics, Vol. 7, (1936), pp. 346-363.

23. Morcom, A. R. "Fluid Flow through Granular Materials," Proc. Inst. Chem. Eng., Vol. 24, pp. 30-43.

24. O'Brien, M. P. and Gosline, J. E. "Drag Coefficient of Bubble in Oil," Ind. Eng. Chem., Vol. 27, (1935), p. 1436.

25. Prager, Stephen. "Viscous Flow through Porous Media," The Physics of Fluids, Vol. 4, No. 12, (December, 1961), pp. 1477-1482.

26. Purcell, W. R. "Capillary Pressures-Their Measurements Using Mercury and the Calculation of Permeability Therefrom," Petroleum Transaction AIME, Vol. 186, (February, 1949), pp. 39-48.

27. Rose, H. E. "Further Researches in Fluid Flow through Beds of Granular Material," Proc. Inst'n Mech. Engrs. Vol. 160, (1949), pp. 493-503.

28. Rose, H. E. and Rizk, A.M.A. "Edge Effects in Porous Beds," Proc. Inst'n Mech. Engrs., Vol. 160 (1949), p. 493.

29. Saunders, O. A. and Ford, H. "Velocity Profile of a Porous Bed," Journal Iron, Steel Institute, Vol. 141, (1940) p. 291.

30. Scheidegger, A. E. Physics of Flow through Porous Media, Toronto: University of Toronto Press, 1960, p. 92.

31. Smith, W. O. "Capillary flow through an Ideal Uniform Soil," Physics, Vol. 3, (September, 1932), pp. 139-146.

32. Welch, N. and Tomme, R. "Measurement of Velocities in Liquids with a Laser Doppler Flowmeter," NASA TMX-53703.

33. Wyckoff, R. D. and Botset, H. G. "The Flow of Gas-Liquid Mixtures through Unconsolidated Sands," Physics, Vol. 7, (1936), pp. 325-345.

34. Wyllie, M. R. J. and Gardner, G. H. F. "The Generalized Kozeny-Carman Equation," World Oil, (April, 1958), pp. 210-228.